LARGE DEPTH COMPLETION MODEL FROM SPARSE OBSERVATIONS

Zhu Yu[1*] **Zhengyi Zhao**[2] **Runmin Zhang**[1] **Lingteng Qiu**[2] **Kejie Qiu**[2]
Yisheng He[2] **Siyu Zhu**[3] **Zilong Dong**[2†] **Si-Yuan Cao**[4,5,6†] **Hui-Liang Shen**[1]
[1]Zhejiang University [2]Tongyi Lab, Alibaba Group [3]Fudan University
[4]Ningbo Innovation Center, Zhejiang University [5]NingboTech University
[6]Jinhua Institute of Zhejiang University
{yu_zhu, cao_siyuan}@zju.edu.cn
Project Page: https://pkqbajng.github.io/ldcm/

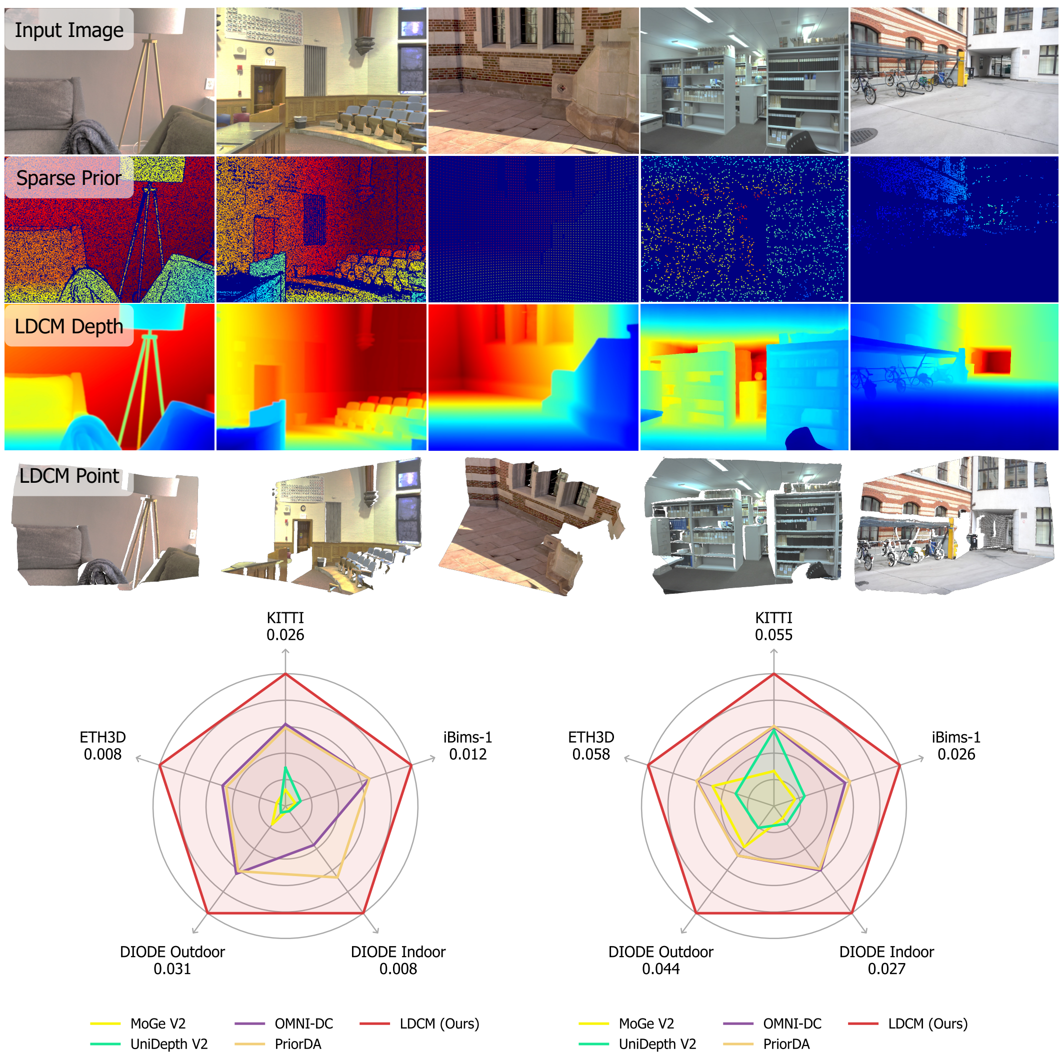

(a) Depth Completion (b) Point Map Estimation

Figure 1: We present LDCM, a simple and effective model for depth completion. Without complex module design, LDCM achieves state-of-the-art performance in zero-shot depth completion and metric point map estimation. On the leaderboard, larger areas indicate lower relative error (REL). LDCM ranks first across diverse datasets.

[*]Internship at Tongyi Lab
[†]Corresponding author

ABSTRACT

This work presents the Large Depth Completion Model (LDCM), a simple, effective, and robust framework for single-view metric depth estimation with sparse observations. Without relying on complex architectural designs, LDCM generates metric-accurate dense depth maps use a transformer. It outperforms existing approaches across diverse datasets and sparse observations. We achieve this from two key perspectives: (1) leveraging existing monocular foundation models to improve the quality of sparse depth inputs, and (2) reformulating training objectives to better capture geometric structure and metric consistency. Specifically, a Poisson-based depth initialization strategy is firstly introduced to generate a uniform coarse dense depth map from diverse sparse observations, providing a strong structural prior for the network. Regarding the training objective, we replace the conventional depth head with a point map head that regresses per-pixel 3D coordinates in camera space, enabling the model to directly learn the underlying 3D scene structure instead of performing pixel-wise depth map restoration. Moreover, this design eliminates the need for camera intrinsic parameters, allowing LDCM to naturally produce metric-scaled 3D point maps. Extensive experiments demonstrate that LDCM consistently outperforms state-of-the-art methods across multiple benchmarks and varying sparsity levels in both depth completion and point map estimation, showcasing its effectiveness and strong generalization to unseen data distributions.

1 INTRODUCTION

Dense depth maps are essential for applications in robotics Wang et al. (2024c), autonomous driving An et al. (2022), and augmented reality Krajancich et al. (2020). However, capturing dense and accurate depth data requires expensive active sensors such as LiDAR or structured light cameras, which are often limited by cost and hardware constraints. Thus, depth completion, which estimates a dense depth map from low-cost sparse depth observations and a corresponding RGB image, provides a cost-effective and efficient alternative.

While prior approaches Cheng et al. (2018; 2019); Yan et al. (2022; 2025a); Park et al. (2020); Yu et al. (2023); Zhou et al. (2023) perform well on in-domain datasets such as NYUv2 Silberman et al. (2012) and KITTI Uhrig et al. (2017), they often fail to generalize to unseen environments and irregular sparse depth maps (e.g., Structure-from-Motion points with non-uniform density and large missing regions), limiting their real-world applicability. Driven by the success of foundation models trained on large-scale datasets Yang et al. (2024a;b); Yin et al. (2023); Hu et al. (2024), recent works Zuo et al. (2024); Wang et al. (2023a; 2025g; 2024a; 2025a) have focused on architectural innovations and training with larger, more diverse data to improve robustness under domain shifts and varying sparsity. More recently, inspired by advances in natural language models Achiam et al. (2023); Yang et al. (2025), prompt-based approaches Lin et al. (2025); Viola et al. (2024); Liu et al. (2024); Park et al. (2024); Wang et al. (2025g) treat the sparse depth map as a conditioning signal for transformer-based Yang et al. (2024a;b) or diffusion-based Ke et al. (2024); Viola et al. (2024); Liu et al. (2024) depth foundation models, guiding the prediction toward metric-scale geometry. Despite their promising results, these methods fundamentally address depth completion as a depth restoration task, where the model learns to interpolate or denoise depth values conditioned on the sparse observation. This paradigm prioritizes local smoothness and texture-aware completion but lacks explicit 3D geometric reasoning, leading to unsatisfactory performance under severe domain shifts and highly irregular sparse depth maps.

In this work, we introduce the Large Depth Completion Model (LDCM), which produces dense, metric-accurate depth maps even from highly sparse and irregular observations. We achieve this by enhancing the input preprocessing pipeline and reformulating the training objective. To address the challenge of sparse and irregular depth maps, we leverage a monocular depth foundation model Yang et al. (2024a;b) to enrich the geometric prior. Specifically, we construct a dense gradient field by combining sparse depth map with relative depth cues predicted by the foundation model. We demonstrate that this hybrid gradient field serves as an proxy for solving a Poisson-based optimization problem, enabling the reconstruction of an initial coarse depth map that preserves fine geometric structures and exhibits metric-consistent depth values. Regarding the training objective, we replace the conventional depth regression head with a point map regression head, inspired by recent advances in 3D reconstruction Wang et al. (2024b); Leroy et al. (2024); Wang et al. (2025b); Fang et al. (2025). This reformulation explicitly encourages the network to predict metric-scale 3D coordinates, rather than focusing on pixel-wise restoration. The final depth map is obtained by extracting the z-component of the predicted point map, leading to more geometrically faithful and globally consistent predictions. Moreover, benefiting from this design, LDCM naturally predicts 3D point maps without requiring camera intrinsics, facilitating robust deployment in uncalibrated environments.

We perform extensive experiments to evaluate LDCM across six diverse benchmarks. The results demonstrate that our model surpasses all previous state-of-the-art methods in both depth completion and point map estimation, achieving top rankings across all tasks and metrics, as displayed in Fig. 1. Our contribution can be summarized as follows:

- We propose the Large Depth Completion Model (LDCM), which replaces the conventional depth regression head with a point map regression head to directly predict metric-scale 3D coordinates from a monocular image and sparse observations. This formulation facilitates more effective learning of metric-consistent 3D structures, leading to superior performance in dense depth completion.
- We introduce a Poisson-based coarse depth completion strategy that leverages relative depth cues from a monocular depth foundation model and sparse observations. This strategy generates high-quality initial depth maps, providing a geometrically faithful structural prior for subsequent feature learning.
- We demonstrate through extensive experiments that LDCM outperforms previous state-of-the-art methods in both depth completion and metric point map estimation across diverse benchmarks and varying sparsity levels, showcasing its robust generalization to unseen data.

2 Related Work

Depth Completion. Depth completion aims to infer a dense depth map from a monocular image and a sparse depth map, which can be readily obtained from sources such as Structure-from-Motion Schops et al. (2017) or low-cost depth cameras Silberman et al. (2012). Recent deep learning-based approaches have achieved significant progress by proposing numerous spatial propagation network variants Liu et al. (2017); Cheng et al. (2018; 2019); Park et al. (2020); Lin et al. (2022) or exploiting visual structural guidance from images for guided restoration. To better exploit the 3D geometric information in sparse inputs, several 2D-3D joint depth completion approaches have also been proposed Yu et al. (2023); Yan et al. (2024; 2025b); Zhou et al. (2023). Despite achieving impressive performance on single-domain datasets (e.g., NYUv2 Silberman et al. (2012) and KITTI Uhrig et al. (2017)), these methods often struggle with cross-domain generalization, particularly when deployed in unseen environments and varying sparse observations.

Inspired by the success of foundation models Kirillov et al. (2023); Oquab et al. (2023); Yang et al. (2024a;b); Yin et al. (2023); Hu et al. (2024); Wang et al. (2025a) trained on large-scale datasets, recent works Zuo et al. (2024); Wang et al. (2023a; 2024a; 2025g) have focused on architectural innovations and training with larger, more diverse datasets to improve generalization. More recently, drawing inspiration from large language models Achiam et al. (2023); Yang et al. (2025), prompt-based approaches Lin et al. (2025); Viola et al. (2024); Park et al. (2024); Jeong et al. (2025) have emerged that treat auxiliary priors as prompts to condition depth foundation models, effectively guiding predictions toward metric-scale outputs. PromptDA Lin et al. (2025) introduces a compact prompt fusion architecture specifically designed for the DPT head Ranftl et al. (2021), enabling the integration of low-resolution depth cues. TestPromptDC Jeong et al. (2025) presents a test-time prompt tuning method that adapts foundation models during inference without modifying their parameters, achieving sensor-specific depth scale adaptation while preserving foundational knowledge. MarigoldDC Viola et al. (2024) prompts the sparse depth to a diffusion-based Ke et al. (2024) foundation model. However, these methods fundamentally address depth completion as a depth restoration task, where the model learns to interpolate or denoise depth values conditioned on sparse inputs. The performance remains unsatisfactory under severe domain shifts and highly irregular sparse depth maps. In this work, we introduce a Poisson-based depth initialization module to effectively maximize the potential of depth foundation models to generate a coarse dense depth map, which serves as a strong structural prior for the following geometric feature learning. Besides, we reformulate the training objective as point maps, providing a more structurally faithful supervision for the network.

Monocular Depth Estimation. A variety of monocular depth estimation foundation models Yang et al. (2024a;b); Piccinelli et al. (2024; 2025); Yin et al. (2023); Ke et al. (2024); Wang et al. (2025d;c) have been proposed. These models learn rich, generalizable priors from large-scale data and serve as strong backbones for downstream tasks such as stereo matching Wen et al. (2025); Jiang et al. (2025a); Cheng et al. (2025), depth super-resolution Yan et al. (2025c), depth completion Park et al. (2024); Lin et al. (2025); Liu et al. (2024); Viola et al. (2024); Wang et al. (2025g), and autonomous driving Yu et al. (2024); Li et al. (2025); Yu et al. (2025); Li et al. (2023a); An et al. (2022). For instance, FoundationStereo Wen et al. (2025) introduces a side-tuning feature adapter that leverages monocular priors to bridge the sim-to-real domain gap. DuCos Yan et al. (2025c) treats foundation model outputs as structural priors for depth super-resolution (DSR) and seamlessly integrates them into a Lagrangian duality framework. PriorDA Wang et al. (2025g) employs a local weighted linear regression (LWLR) module Xu et al. (2022) to align the scale of relative depth with sparse observations, where the result is then refined by a structure-aware network to produce dense depth map. However, this local alignment strategy often fails under highly sparse observations. In contrast, we propose a novel Poisson-based initialization strategy to better exploit the potential of foundation models by enforcing gradient consistency constraints, yielding a significantly more geometrically coherent coarse depth map.

Geometry Estimation Foundation Models. Point map Wang et al. (2024b; 2025b;e); Fang et al. (2025); Gao et al. (2025); Jang et al. (2025) representation has demonstrated strong potential for holistic scene understanding. Unlike depth maps, which indeedly encode 2.5D geometry tied to camera intrinsics, point maps explicitly model 3D structure. Several approaches Yin et al. (2021); Piccinelli et al. (2024; 2025) decouple this task into depth prediction and camera parameter estimation. In contrast, DUSt3R Wang et al. (2024b) bypasses explicit camera modeling by directly regressing a scale-invariant point map in an end-to-end fashion, with its successor Mast3R Leroy et al. (2024) enabling metric-scale reconstruction. VGGT Wang et al. (2025b) introduces a feed-forward neural network capable of 3D reconstruction from one, a few, or even hundreds of input views of a scene. AnySplat Jiang et al. (2025b) extends VGGT Wang et al. (2025b) to support novel view synthesis from uncalibrated image collections. To facilitate single-view geometry learning, MoGe Wang et al. (2025e;f) predicts an affine-invariant point map and recovers metric scale using a global scaling factor derived from contextual cues. More recently, several approaches Liu et al. (2025); Keetha et al. (2025); Jang et al. (2025) have introduced additional priors to enhance geometry estimation. Notably, Pow3R Jang et al. (2025) extends the DUSt3R Wang et al. (2024b) paradigm by incorporating complementary modalities; however, it remains limited to relative geometry. In this work, we introduce point map representations for depth completion, enabling the model to directly learn the underlying 3D scene structure and produce metric quantities. Our concurrent work, MapAnything Keetha et al. (2025), also estimates metric 3D geometry from images and additional priors.

3 METHOD

3.1 OVERALL FRAMEWORK

The framework of the proposed LDCM is illustrated in Fig. 2. Given an RGB image $\mathbf{I} \in \mathbb{R}^{H\times W\times 3}$ and a sparse depth map $\mathbf{S} \in \mathbb{R}^{H\times W}$, LDCM predicts a metric point map $\mathbf{P} \in \mathbb{R}^{H\times W\times 3}$ in camera space, from which the dense depth map is derived by extracting the z-channel component. The framework consists of two main stages. In the first stage, we harness the power of monocular depth foundation model to generate an initial coarse depth map $\mathbf{C} \in \mathbb{R}^{H\times W}$ via Poisson reconstruction. In the second stage, a ViT-based Dosovitskiy et al. (2020) depth completion network takes the image $\mathbf{I}$ and the coarse depth $\mathbf{C}$ as input to predict the final metric 3D point map $\mathbf{P}$. The details of each stage are elaborated in the following sections.

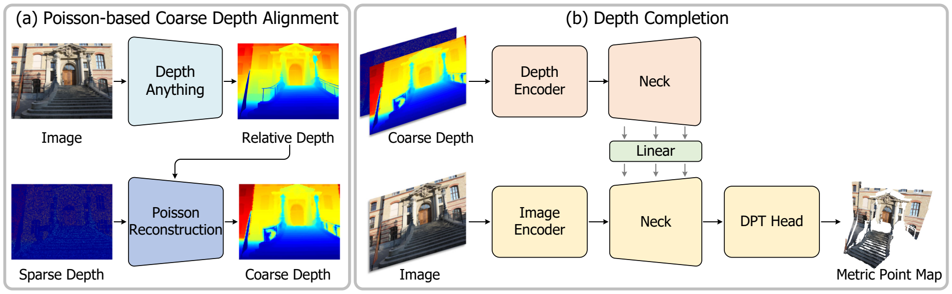

Figure 2: Schematics and detailed architecture of LDCM. Given a single image and sparse depth map, LDCM begins with a Poisson-based coarse depth alignment strategy. This process leverages a pretrained depth foundation model to generate an initial coarse depth map through gradient-domain optimization. This coarse depth, together with the input image, is then fed into the following point map prediction network to regress a dense, metric-scale 3D point map.

3.2 Coarse Depth Alignment

Different types of sparse depth priors exhibit distinct spatial distributions, ranging from random points and Structure-from-Motion keypoints to LiDAR-like structured sparsity, posing significant challenges for generalization. A straightforward approach involves direct interpolation of the sparse depth map Liu et al. (2024); however, it often introduces severe artifacts due to the absence of strong geometric priors. With the advent of depth foundation models Ranftl et al. (2020; 2021), which capture scene-level structure from large-scale training, leveraging them to provide robust geometric guidance has emerged as a promising direction.

To integrate sparse observations with foundation model predictions, we evaluate several coarse alignment strategies, including global affine alignment, local weighted linear regression (LWLR), and Poisson-based optimization. While the former two offer simple parametric alignment, they exhibit critical limitations. Global affine alignment assumes a uniform scale and shift across the entire image, making it unable to recover per-pixel metric values. LWLR improves spatial adaptivity by fitting local models, but its performance is highly sensitive to the distribution and density of sparse depth maps. In contrast, Poisson-based optimization formulates the alignment as a gradient-field reconstruction problem, demonstrating superior geometric coherence and metric accuracy across diverse sparse observations. Therefore, we adopt Poisson reconstruction in the first stage of LDCM to generate the coarse depth map $\mathbf{C}$.

Specifically, given a sparse depth input $\mathbf{S}$ and relative depth cues $\mathbf{D}_r$ from a foundation model, we aim to generate a coarse dense depth map $\mathbf{C}$ that aligns with the geometric structure of $\mathbf{D}_r$, while preserving the observed values in $\mathbf{S}$. The problem can be formulated as minimizing the following optimzation function:

$$\mathbf{C} = \arg\min_{\mathbf{D}} \left(\sum_i \|\nabla \log \mathbf{D}_i - \mathbf{G}_i\|^2 + \lambda \sum_{i \in \Omega} (\mathbf{D}_i - \mathbf{S}_i)^2 \right), \tag{1}$$

where $\mathbf{G}$ is a target log-gradient field that encodes structural fidelity and metric consistency, Ω denotes the set of valid sparse depth points, and λ balances two terms. A naive choice is $\mathbf{G} = \nabla \log \mathbf{D}_r$, but this ignores the unknown scale and shift of relative depth and may lead to misaligned gradients in metric space. Instead, we construct a more informed target by incorporating metric priors from sparse observations. Let (α, β) be the global affine transformation that best aligns $\mathbf{D}_r$ with $\mathbf{S}$:

$$(\alpha, \beta) = \arg\min_{\alpha', \beta'} \sum_{i \in \Omega} \left(\mathbf{S}_i - \alpha' \cdot (\mathbf{D}_r)_i - \beta'\right)^2, \tag{2}$$

and define $\gamma = \beta/\alpha$. We then set:

$$\mathbf{G} = \nabla \log(\mathbf{D}_r + \gamma). \tag{3}$$

This choice is motivated by the fact that during training, the relative depth ground truth $\mathbf{D}_r$ is derived from the metric ground truth $\mathbf{D}^*$ via an affine transformation: $\mathbf{D}_r = (\mathbf{D}^* - \beta)/\alpha$. While this ideal relationship may not strictly hold for the predicted $\mathbf{D}_r$ during inference, introducing a shift γ helps align its gradient structure with the metric space. Empirically, $\nabla \log(\mathbf{D}_r + \gamma)$ serves as a robust proxy for the target log-gradient field, preserving fine geometric details while being anchored to the metric scale through sparse inputs. Thus, the final formulation becomes:

$$\mathbf{C} = \arg\min_{\mathbf{D}} \left(\sum_i \|\nabla \log \mathbf{D}_i - \nabla \log(\mathbf{D}_r + \gamma)_i\|^2 + \lambda \sum_{i \in \Omega} (\mathbf{D}_i - \mathbf{S}_i)^2 \right), \tag{4}$$

which can be solved through the conjugate gradient method Hestenes et al. (1952). In this formulation, each sparse point anchors the global energy, and due to the nature of gradient-domain reconstruction, its influence propagates across the entire image via the structural constraints encoded in the gradient field.

3.3 Depth Completion Network

The architecture is illustrated in Fig. 2(b). We employ dual encoders to extract features from the coarse depth map $\mathbf{C}$ and the RGB image, respectively. Features are fused using the prompt fusion block Lin et al. (2025). For the final output, instead of regressing a depth map, we replace the standard depth regression head with a point map head that directly predicts per-pixel 3D coordinates $\mathbf{P}$. This enables the model to learn the underlying 3D scene structure holistically, rather than performing pixel-wise depth restoration. Ablation studies demonstrate that this design leads to better accuracy. Moreover, thanks to this end-to-end formulation, the model naturally produces metric 3D point maps, facilitating robust deployment in uncalibrated environments.

3.4 Training

Training Losses. We train the LDCM using three complementary losses on the predicted 3D point map $\mathbf{P}$, with the ground-truth metric point map denoted as $\hat{\mathbf{P}}$.

$$\mathcal{L} = \mathcal{L}_{\text{global}} + \lambda_{\text{local}} \mathcal{L}_{\text{local}} + \lambda_{\text{normal}} \mathcal{L}_{\text{normal}}, \tag{5}$$

where the individual terms are defined as follows. The global point map loss enforces overall structural consistency:

$$\mathcal{L}_{\text{global}} = \sum_{i \in \mathcal{M}} \frac{1}{\hat{\mathbf{D}}_i} \|\mathbf{P}_i - \hat{\mathbf{P}}_i\|_1, \tag{6}$$

where $\mathcal{M}$ denotes the region of valid ground-truth. The local point map loss captures fine-grained geometry by operating in 3D neighborhoods. Following Wang et al. (2025e), we sample anchor points and define spherical regions $\mathcal{S}_j$ in 3D space:

$$\mathcal{L}_{\text{local}} = \sum_{j \in \mathcal{H}_a} \sum_{i \in \mathcal{S}_j} \frac{1}{\hat{\mathbf{D}}_i} \|\mathbf{P}_i - \hat{\mathbf{P}}_i\|_1. \tag{7}$$

This encourages local coherence independent of image perspective. The normal loss promotes surface smoothness and alignment:

$$\mathcal{L}_{\text{normal}} = \sum_{i \in \mathcal{M}} \arccos \left(\frac{\mathbf{N}_i^\top \hat{\mathbf{N}}_i}{\|\mathbf{N}_i\| \|\hat{\mathbf{N}}_i\|} \right), \tag{8}$$

where $\mathbf{N}_i$ and $\hat{\mathbf{N}}_i$ are surface normals estimated from $\mathbf{P}$ and $\hat{\mathbf{P}}$, respectively.

Implementation Details. We train the LDCM on 11 public RGB-D datasets Roberts et al. (2021); Wang et al. (2020; 2019); Zheng et al. (2023); Gómez et al. (2025); Wrenninge & Unger (2018); Li et al. (2023b); LightwheelAI & contributors (2024); Huang et al. (2018); Ros et al. (2016); Yeshwanth et al. (2023), approximately 2.7 million samples. The combined data covers diverse indoor and outdoor scenes; further details are provided in the *suppl. material*.

LDCM uses a ViT-B Dosovitskiy et al. (2020) pretrained with DINOv2 Oquab et al. (2023) as the image encoder. For coarse depth alignment, we use DepthAnythingV2-S Yang et al. (2024b) as the foundation model. Training runs for 200 K iterations using the AdamW optimizer Loshchilov &

Table 1: **Quantitative comparison of depth completion methods on benchmark datasets.** All methods are evaluated under zero-shot settings. Methods marked with † produce relative depth, and metric depth is recovered by optimizing global scale and shift via least squares regression using the *same* sparse depth prior. Methods marked with ‡ use dataset-specific configurations for indoor and outdoor scenes, respectively. The best and second-best results are highlighted.

Method	KITTI					iBims-1					DIODE Indoor				
	RMSE↓	MAE↓	REL↓	δ_1 ↑	Rk.↓	RMSE↓	MAE↓	REL↓	δ_1 ↑	Rk.↓	RMSE↓	MAE↓	REL↓	δ_1 ↑	Rk.↓
DepthPro	4.149	2.763	0.178	0.731	13.432	0.605	0.503	0.156	0.829	13.750	0.837	0.702	0.193	0.668	14.114
UniDepth V1	3.335	2.010	0.118	0.938	8.636	1.166	1.082	0.370	0.236	16.000	0.939	0.840	0.158	0.779	13.523
UniDepth V2	3.150	1.598	0.090	0.960	6.500	0.446	0.321	0.100	0.935	11.932	0.811	0.678	0.165	0.681	13.023
DepthAnythingV2†	4.007	1.890	0.092	0.916	9.091	0.349	0.179	0.043	0.975	8.295	0.386	0.189	0.045	0.976	7.295
VGGT†	4.219	2.518	0.158	0.783	12.909	0.348	0.194	0.053	0.957	10.318	0.425	0.294	0.096	0.920	10.773
MoGe V1†	3.050	1.821	0.125	0.887	8.568	0.238	0.120	0.035	0.981	6.045	0.272	0.175	0.064	0.950	7.386
MoGe V2	4.617	3.366	0.213	0.458	15.182	0.633	0.540	0.156	0.707	14.500	1.064	0.938	0.235	0.433	15.841
G2-MonoDepth‡	2.638	0.964	0.054	0.949	5.295	0.227	0.094	0.028	0.973	5.409	0.298	0.198	0.067	0.879	6.341
OMNI-DC	2.302	0.760	0.042	0.963	3.045	0.192	0.063	0.018	0.982	2.932	0.141	0.064	0.022	0.968	2.932
PriorDA	2.364	0.861	0.044	0.971	4.159	0.176	0.065	0.018	0.990	3.477	0.093	0.037	0.012	0.994	3.023
SPNet‡	2.365	0.757	0.041	0.966	3.000	0.189	0.059	0.016	0.987	2.659	0.157	0.078	0.028	0.954	3.273
PromptDA	3.040	1.261	0.067	0.946	6.545	0.249	0.116	0.033	0.975	6.091	0.203	0.115	0.037	0.965	6.068
WorldMirror†	4.439	2.432	0.142	0.824	11.818	0.352	0.192	0.051	0.963	9.205	0.386	0.243	0.084	0.941	9.364
MapAnything	12.974	6.784	0.350	0.588	15.750	0.968	0.374	0.104	0.909	13.295	0.909	0.458	0.104	0.899	11.000
Pow3R†	3.515	2.096	0.141	0.832	10.750	0.338	0.183	0.049	0.965	9.091	0.353	0.240	0.078	0.943	9.000
LDCM (Ours)	1.911	0.537	0.026	0.983	1.068	0.161	0.044	0.012	0.991	1.659	0.084	0.025	0.008	0.993	1.545

Method	DIODE Outdoor					ETH3D					Average				
	RMSE↓	MAE↓	REL↓	δ_1 ↑	Rk.↓	RMSE↓	MAE↓	REL↓	δ_1 ↑	Rk.↓	RMSE↓	MAE↓	REL↓	δ_1 ↑	Rk.↓
DepthPro	9.539	7.635	0.403	0.177	14.636	3.199	2.562	0.302	0.477	15.023	3.666	2.833	0.246	0.576	14.191
UniDepth V1	5.782	3.841	0.189	0.661	11.795	3.482	3.170	0.579	0.116	15.728	2.941	2.189	0.283	0.546	13.136
UniDepth V2	11.145	8.936	0.515	0.526	15.250	1.630	1.169	0.200	0.726	13.387	3.436	2.540	0.214	0.766	12.018
DepthAnythingV2†	5.940	2.777	0.124	0.869	8.659	2.091	0.424	0.049	0.979	9.477	2.555	1.092	0.071	0.943	8.563
VGGT†	4.898	2.893	0.237	0.772	10.591	0.540	0.317	0.060	0.949	9.103	2.086	1.243	0.121	0.876	10.739
MoGe V1†	10.576	8.340	0.406	0.599	14.250	1.651	0.550	0.082	0.943	8.750	3.157	2.201	0.142	0.872	9.000
MoGe V2	4.807	3.352	0.182	0.680	10.477	0.847	0.619	0.114	0.839	11.784	2.394	1.763	0.180	0.623	13.557
G2-MonoDepth‡	2.393	0.875	0.062	0.938	4.682	0.428	0.177	0.034	0.969	5.603	1.197	0.462	0.049	0.942	5.466
OMNI-DC	2.322	0.726	0.049	0.955	3.341	0.290	0.100	0.016	0.987	2.932	1.049	0.343	0.029	0.971	3.036
PriorDA	2.310	0.858	0.051	0.957	3.932	0.274	0.105	0.017	0.990	3.443	1.043	0.385	0.028	0.980	3.607
SPNet‡	2.111	0.658	0.048	0.959	2.114	0.419	0.119	0.019	0.986	3.625	1.048	0.334	0.030	0.970	2.934
PromptDA	3.604	1.561	0.087	0.912	6.182	0.644	0.276	0.041	0.967	7.102	1.548	0.666	0.053	0.953	6.398
WorldMirror†	4.464	2.317	0.151	0.828	8.045	0.524	0.302	0.051	0.962	7.761	2.033	1.097	0.096	0.904	9.239
MapAnything	7.675	3.891	0.219	0.731	11.318	1.952	0.711	0.108	0.904	12.523	4.896	2.444	0.177	0.806	12.777
Pow3R†	3.682	2.068	0.169	0.840	7.568	0.480	0.273	0.048	0.964	7.545	1.674	0.972	0.097	0.909	8.791
LDCM (Ours)	1.969	0.529	0.031	0.970	1.568	0.187	0.048	0.008	0.997	1.148	0.862	0.237	0.017	0.987	1.398

Hutter (2017) with a cosine learning rate schedule and linear warmup over the first 5% of iterations. The peak learning rates are 1×10^{-5} for the encoder and 1×10^{-4} for all other layers. We use a global batch size of 128, with mini-batches sampling an approximately equal number of images from each dataset. During training, images are resized such that their aspect ratios range uniformly from $1 : 2$ to $2 : 1$, and total pixel counts fall between $250\,\text{K}$ and $500\,\text{K}$. Data augmentation includes random cropping, color jittering, Gaussian blur, JPEG compression-decompression, and perspective-aware cropping to align the principal point with the image center. Sparse depth inputs are synthetically generated by subsampling dense ground-truth depth maps with varying patterns, following the protocol of OMNI-DC Zuo et al. (2024). The training is conducted on 16 H20 GPUs and takes approximately six days to complete.

4 Experiments

4.1 Quantitative Evaluations

We evaluate the zero-shot performance of LDCM and compare it with several state-of-the-art approaches for depth completion Wang et al. (2023a); Zuo et al. (2024); Wang et al. (2024a); Lin et al. (2025); Wang et al. (2025g), monocular depth estimation Yang et al. (2024a;b); Wang et al. (2025b); Bochkovskiy et al. (2025), and monocular point map estimation Piccinelli et al. (2024; 2025); Wang et al. (2025e;f); Liu et al. (2025); Jang et al. (2025); Keetha et al. (2025). Additional details on the compared approaches and evaluation protocols are provided in the *suppl. material*. As demonstrated in the experiments, LDCM achieves superior performance across multiple benchmarks.

Depth completion. We evaluate depth completion on KITTI Uhrig et al. (2017), ETH3D Schops et al. (2017), iBims-1 Koch et al. (2018), and DIODE Vasiljevic et al. (2019), covering both indoor and outdoor scenarios. To assess robustness under diverse sparse sampling patterns, we synthesize sparse depth inputs using the following strategies:

- **Noisy random sampling**: uniformly sampled points at varying densities (e.g., 1%, 3%, 5%, 10%), with mild noise simulation;
- **Keypoint-based sampling**: depth values extracted at SIFT or ORB keypoints;
- **LiDAR-simulated sampling**: synthetic LiDAR scans with varying numbers of vertical beams (e.g., 64, 32, 16 lines).

On KITTI, the simulation is applied to raw single-frame LiDAR measurements Zuo et al. (2024); Wang et al. (2023b). For all other datasets, they are generated from dense ground-truth depth maps. We evaluate the predicted depth maps using standard metrics: Root Mean Squared Error (RMSE), Mean Absolute Error (MAE), Relative Error (REL), and the accuracy threshold δ_1. For methods that produce relative depth maps Wang et al. (2025b); Yang et al. (2024b); Wang et al. (2025e), we recover the global scale and shift via least squares regression using the sparse depth prior. Table 1 reports the average RMSE, MAE, REL, and δ_1 across all synthetic patterns per dataset, along with the mean ranking over competing methods. As shown in the table, LDCM achieves state-of-the-art performance. Notably, it maintains high accuracy even under extreme sparsity, demonstrating strong robustness and generalization across diverse sparse input configurations.

Table 2: **Quantitative comparison of point map estimation methods on benchmark datasets.** All methods are evaluated under zero-shot settings. The best and second-best results are highlighted.

Method	KITTI					iBims-1					DIODE Indoor				
	MAE^p ↓	RMSE^p ↓	REL^p ↓	δ_1^p ↑	Rk.↓	MAE^p ↓	RMSE^p ↓	REL^p ↓	δ_1^p ↑	Rk.↓	MAE^p ↓	RMSE^p ↓	REL^p ↓	δ_1^p ↑	Rk.↓
UniDepth V1	2.207	3.540	0.120	0.954	6.773	1.154	1.239	0.370	0.239	9.000	0.911	1.017	0.159	0.779	7.318
UniDepth V2	1.813	3.540	0.096	0.961	5.409	0.365	0.489	0.107	0.932	6.909	0.730	0.872	0.164	0.694	7.273
MoGe V2	3.536	4.899	0.208	0.484	9.000	0.574	0.667	0.156	0.740	8.000	1.048	1.185	0.242	0.410	8.955
G2-MonoDepth	1.669	3.118	0.098	0.946	4.841	0.186	0.287	0.052	0.972	4.750	0.305	0.401	0.087	0.875	4.841
OMNI-DC	1.542	2.828	0.092	0.960	3.409	0.164	0.256	0.046	0.980	3.341	0.174	0.241	0.045	0.967	2.977
PriorDA	1.573	2.836	0.091	0.965	4.341	0.159	0.240	0.043	0.989	3.500	0.140	0.190	0.034	0.994	2.909
SPNet	1.507	2.881	0.089	0.964	3.068	0.152	0.239	0.042	0.988	2.455	0.172	0.236	0.046	0.963	2.636
PromptDA	1.933	3.612	0.110	0.938	6.659	0.199	0.309	0.054	0.975	5.545	0.204	0.301	0.056	0.963	5.523
‘ LDCM (Ours)	**1.027**	**2.308**	**0.055**	**0.982**	**1.045**	**0.092**	**0.194**	**0.026**	**0.992**	**1.000**	**0.127**	**0.179**	**0.027**	**0.992**	**1.159**

Method	DIODE Outdoor					ETH3D					Average				
	MAE^p ↓	RMSE^p ↓	REL^p ↓	δ_1^p ↑	Rk.↓	MAE^p ↓	RMSE^p ↓	REL^p ↓	δ_1^p ↑	Rk.↓	MAE^p ↓	RMSE^p ↓	REL^p ↓	δ_1^p ↑	Rk.↓
UniDepth V1	4.653	5.100	0.461	0.145	9.000	3.541	3.875	0.551	0.106	9.000	2.493	2.954	0.332	0.445	8.218
UniDepth V2	1.879	2.844	0.216	0.712	8.000	1.252	1.785	0.191	0.769	8.000	1.208	1.906	0.155	0.814	7.118
MoGe V2	0.931	1.206	0.115	0.890	5.977	0.716	0.913	0.119	0.865	6.409	1.361	1.774	0.168	0.678	7.668
G2-MonoDepth	0.794	1.129	0.109	0.891	4.864	0.603	0.826	0.105	0.911	5.160	0.711	1.152	0.090	0.919	4.891
OMNI-DC	0.714	0.946	0.095	0.915	2.795	0.550	0.710	0.095	0.929	3.284	0.629	0.996	0.075	0.950	3.161
PriorDA	0.698	0.908	0.095	0.919	3.295	0.538	0.682	0.094	0.936	3.352	0.622	0.971	0.071	0.961	3.479
SPNet	0.733	1.243	0.100	0.914	3.932	0.557	0.859	0.096	0.931	3.796	0.624	1.092	0.075	0.952	3.177
PromptDA	0.824	1.422	0.100	0.911	5.591	0.592	0.950	0.093	0.932	4.159	0.750	1.319	0.083	0.944	5.495
LDCM (Ours)	**0.427**	**0.580**	**0.044**	**0.995**	**1.000**	**0.347**	**0.456**	**0.058**	**0.996**	**1.000**	**0.404**	**0.743**	**0.042**	**0.991**	**1.041**

Point map estimation. We adopt the same benchmarks used for depth completion to evaluate monocular point map estimation. The predicted point maps are evaluated using point-wise metrics: RMSE^p, MAE^p, REL^p and δ_1^p. Table 2 reports the average performance across all synthetic patterns per dataset for each metric. For depth completion methods, we use the camera intrinsics from UniDepth V2 Piccinelli et al. (2025) to back-project the completed depth maps into 3D point maps. As shown in the table, LDCM consistently outperforms all competing methods, achieving the best results across all datasets and metrics.

Affine-invariant point map estimation. We adopt the same benchmarks to evaluate monocular affine-invariant point map estimation. Following MoGe Wang et al. (2025e), we resolve the scale and shift of the predicted point map using the proposed ROE solver to align it with the ground truth. Table 3 reports the average performance in terms of REL^p and δ_1^p. As shown in the table, our method achieves superior performance compared to baseline approaches and outperforms state-of-the-art relative geometry estimation methods, including VGGT Wang et al. (2025b) and WorldMirror Liu et al. (2025). This demonstrates that our model preserves—rather than compromises—the accuracy of relative geometry estimation.

4.2 Ablation Study

We conduct ablation studies to evaluate the effectiveness of the Poisson-based coarse depth alignment strategy and the training objectives. For simplicity, we adopt LiDAR-simulated sparse patterns (64, 32, 16, and 8 lines) on outdoor datasets, and keypoint-based sampling on indoor datasets.

Table 3: **Quantitative comparison of affine-invariant point map estimation methods on benchmark datasets.** All methods are evaluated under zero-shot settings. The best and second-best results are highlighted.

Method	KITTI			iBims-1			DIODE Indoor		
	$REL^p \downarrow$	$\delta_1^p \uparrow$	Rk.↓	$REL^p \downarrow$	$\delta_1^p \uparrow$	Rk.↓	$REL^p \downarrow$	$\delta_1^p \uparrow$	Rk.↓
VGGT	0.147	0.823	4.500	0.048	0.967	3.909	0.107	0.926	4.636
MoGe V2	0.056	0.968	1.909	0.046	0.972	2.455	0.052	0.972	1.955
WorldMirror	0.108	0.886	3.136	0.044	0.965	2.864	0.073	0.953	3.091
MapAnything	0.366	0.344	6.000	0.233	0.611	6.000	0.172	0.758	6.000
Pow3R	0.152	0.850	4.318	0.064	0.965	4.318	0.108	0.947	4.273
LDCM (Ours)	0.039	0.983	1.091	0.017	0.992	1.000	0.014	0.995	1.000

Method	DIODE Outdoor			ETH3D			Average		
	$REL^p \downarrow$	$\delta_1^p \uparrow$	Rk.↓	$REL^p \downarrow$	$\delta_1^p \uparrow$	Rk.↓	$REL^p \downarrow$	$\delta_1^p \uparrow$	Rk.↓
VGGT	0.215	0.700	5.000	0.053	0.978	3.591	0.114	0.879	4.327
MoGe V2	0.124	0.841	2.000	0.044	0.980	2.637	0.064	0.947	2.191
WorldMirror	0.155	0.788	3.045	0.049	0.976	3.023	0.086	0.914	3.032
MapAnything	0.302	0.501	6.000	0.265	0.549	6.000	0.268	0.553	6.000
Pow3R	0.197	0.750	3.955	0.074	0.982	3.796	0.119	0.899	4.132
LDCM (Ours)	0.077	0.949	1.000	0.039	0.994	1.728	0.037	0.983	1.164

Table 4: ablation study on the coarse depth alignment strategy. We report the relative error (REL) for coarse depth and final prediction. The best and second-best results are highlighted.

Configuration	Corse Depth (REL ↓)					Estimated Depth (REL ↓)				
	KITTI	iBims-1	DIODE	ETH3D	Average	KITTI	iBims-1	DIODE	ETH3D	Average
Sparse	-	-	-	-	-	0.021	0.029	0.040	0.026	0.029
Global alignment	0.095	0.075	0.102	0.078	0.087	0.020	0.019	0.035	0.023	0.024
LWLR	0.078	0.108	0.108	0.061	0.088	0.019	0.022	0.036	0.021	0.025
Poisson w/o global alignment	0.069	0.208	0.174	0.138	0.147	-	-	-	-	-
Poisson	0.033	0.073	0.088	0.044	0.059	0.019	0.018	0.033	0.019	0.022

Coarse Depth Alignment Strategy. We ablate various coarse depth alignment strategies for robust geometric guidance. First, we assess the accuracy of the generated coarse depth maps. As shown on the left side of Table 4, Poisson-based alignment achieves the best performance, demonstrating its effectiveness. Notably, global alignment is essential—its omission leads to a significant performance drop. By comparison, LWLR performs worse than even simple global alignment under extreme sparsity, highlighting its sensitivity to sparse and irregular inputs. A qualitative ablation example is provided in Fig. 3, where the Poisson-based method not only achieves the highest accuracy but also best preserves geometric structure. On the right side of Table 4, we use these coarse depth maps as inputs to our completion model; again, the Poisson-based variant yields the best results.

Table 5: Ablation study on the output representation. We report the relative error (REL) for depth completion and REL^p for point map estimation. The best and second-best results are highlighted.

Configuration	Depth Completion (REL ↓)					Point Map Estimation (REL^p ↓)				
	KITTI	iBims-1	DIODE	ETH3D	Average	KITTI	iBims-1	DIODE	ETH3D	Average
SI-Log Depth	0.023	0.023	0.037	0.021	0.026	-	-	-	-	-
SI-Log Depth + Ray map	0.022	0.022	0.038	0.021	0.026	0.073	0.050	0.084	0.097	0.067
Point Map	0.019	0.018	0.033	0.019	0.022	0.047	0.032	0.070	0.059	0.045

Output Representation. We ablate the output representation by replacing the point map with either a conventional depth map or the concatenation of depth and dense ray maps (depth + ray map). As shown in Table 5, both alternatives lead to performance degradation, demonstrating that the point map provides more effective 3D structural guidance than depth-based representations.

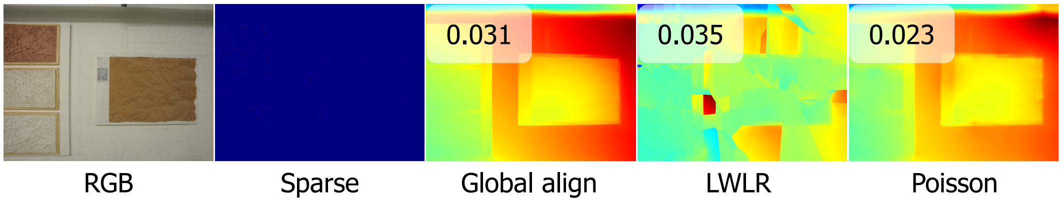

Figure 3: Qualitative comparison between three coarse alignment stragies. We report the relative error for each result.

4.3 Depth completion results on standard benchmarks

Table 6: **Quantitative comparison of depth completion methods on real-pattern benchmark datasets.** All methods are evaluated under zero-shot settings. Methods marked with † produce relative depth, and metric depth is recovered by optimizing global scale and shift via least squares regression using the same sparse depth prior. Methods marked with ‡ use dataset-specific configurations for indoor and outdoor scenes, respectively. The best and second-best results are highlighted.

Method	NYUv2					VOID					ETH3D				
	RMSE↓	MAE↓	REL↓	δ_1 ↑	Rk.↓	RMSE↓	MAE↓	REL↓	δ_1 ↑	Rk.↓	RMSE↓	MAE↓	REL↓	δ_1 ↑	Rk.↓
DepthPro	0.332	0.253	0.096	0.929	15.000	0.759	0.396	0.189	0.726	14.833	3.199	2.562	0.302	0.477	14.750
UniDepth V1	0.213	0.148	0.056	0.981	10.375	0.651	0.267	0.107	0.902	12.083	3.482	3.170	0.579	0.116	15.625
UniDepth V2	0.293	0.218	0.085	0.948	14.000	0.651	0.269	0.115	0.900	13.000	1.630	1.169	0.200	0.726	13.000
DepthAnythingV2†	0.220	0.128	0.045	0.977	11.250	0.605	0.214	0.063	0.958	8.250	1.915	0.493	0.063	0.963	6.500
VGGT†	0.168	0.087	0.033	0.985	7.000	0.572	0.196	0.064	0.952	6.750	0.650	0.432	0.095	0.906	6.375
MoGe V1†	0.180	0.093	0.037	0.979	8.750	0.577	0.200	0.064	0.952	7.500	2.877	0.450	0.108	0.924	6.500
MoGe V2	0.261	0.186	0.070	0.963	13.000	0.779	0.421	0.202	0.557	15.833	0.847	0.619	0.114	0.839	9.375
G2-MonoDepth‡	0.166	0.071	0.026	0.985	7.125	0.607	0.195	0.055	0.942	7.500	1.425	0.525	0.136	0.886	10.375
OMNI-DC	0.147	0.053	0.020	0.987	4.375	0.574	0.168	0.040	0.962	4.167	0.822	0.317	0.079	0.925	4.625
PriorDA	0.122	0.047	0.017	0.993	2.750	0.571	0.171	0.039	0.968	3.333	0.671	0.260	0.061	0.962	2.500
SPNet‡	0.127	0.047	0.017	0.992	2.500	0.578	0.178	0.054	0.959	5.250	1.299	0.372	0.092	0.943	6.625
PromptDA	0.162	0.079	0.028	0.989	6.000	0.565	0.182	0.049	0.965	4.000	0.911	0.483	0.090	0.896	6.875
WorldMirror†	0.217	0.121	0.042	0.979	10.125	0.596	0.208	0.067	0.946	9.833	0.898	0.668	0.153	0.836	9.250
MapAnything	0.724	0.327	0.132	0.885	16.000	0.782	0.282	0.110	0.900	13.750	2.283	0.874	0.150	0.863	12.375
Pow3R†	0.155	0.081	0.031	0.988	5.625	0.571	0.196	0.067	0.949	7.333	0.881	0.656	0.154	0.833	9.875
LDCM (Ours)	**0.113**	**0.037**	**0.013**	**0.994**	**1.000**	**0.536**	**0.145**	**0.028**	**0.977**	**1.000**	**0.445**	**0.154**	**0.035**	**0.978**	**1.250**

To further evaluate zero-shot depth completion under real-world sparse patterns, we follow prior work in evaluating methods on the NYUv2 Silberman et al. (2012), VOID Wong et al. (2020), and ETH3D Schops et al. (2017) datasets. For NYUv2, we adopt the sampling protocol from OMNI-DC Zuo et al. (2024), extracting 500 and 100 sparse depth points per image, respectively. For VOID, we use the provided sparse depth maps derived from a visual-inertial odometry system, which come in three sparsity levels: 1500, 500, and 150 points per frame. For ETH3D, we project the sparse 3D points from COLMAP SfM reconstructions into the image plane to generate sparse depth maps. Table 6 reports the quantitative results on each dataset. As shown in the table, LDCM significantly outperforms all comparison methods, ranking first on all the datasets.

5 Conclusion

We have presented the Large Depth Completion Model (LDCM), a simple yet powerful framework for metric depth estimation from sparse observations. LDCM is both effective and robust, leveraging a Poisson-based alignment strategy to maximize the potential of existing monocular foundation models by preprocessing input sparse observations into strong geometric priors for subsequent feature learning. Furthermore, LDCM replaces the conventional depth map representation with a point map representation, enabling direct learning of the underlying 3D structure rather than per-pixel depth restoration. Our method achieves superior zero-shot performance across multiple benchmarks, demonstrating robustness under varying sparse observation patterns. Moreover, the point map design allows LDCM to naturally output metric-scaled 3D geometry without requiring camera intrinsics, facilitating reliable deployment in uncalibrated environments. We believe LDCM marks a significant advancement in depth completion and can serve as a robust foundational model for downstream 3D vision tasks.

Acknowledgments

This work was supported in part by the National Natural Science Foundation of China under grant 62301484, in part by the Jinhua Science and Technology Bureau Project under grant 2026-1-022, in part by the Young Talent Fund of Zhejiang Association for Science and Technology under grant ZJSKXQT2026135, and in part by the Ningbo Natural Science Foundation of China under grant 2024J454.

Ethics Statement

Our study focuses on depth completion, a core problem in the field of computer vision. The experimental evaluation is based exclusively on public datasets that have been curated without inclusion of any personally identifiable or sensitive content. We assert that this research has been carried out in accordance with the code of ethics.

Reproducibility Statement

To facilitate verification and extension of our work, we include the implementation code in the supplementary materials. Furthermore, we provide key training and evaluation procedures in the paper, and will make the complete code and trained models publicly available after publication to support full experimental reproducibility.

References

Josh Achiam, Steven Adler, Sandhini Agarwal, Lama Ahmad, Ilge Akkaya, Florencia Leoni Aleman, Diogo Almeida, Janko Altenschmidt, Sam Altman, Shyamal Anadkat, et al. Gpt-4 technical report. *arXiv preprint arXiv:2303.08774*, 2023.

Dong An, Yuankai Qi, Yangguang Li, Yan Huang, Liang Wang, Tieniu Tan, and Jing Shao. Bevbert: Multimodal map pre-training for language-guided navigation. *arXiv preprint arXiv:2212.04385*, 2022.

Alexey Bochkovskiy, Amaël Delaunoy, Hugo Germain, Marcel Santos, Yichao Zhou, Stephan Richter, and Vladlen Koltun. Depth pro: Sharp monocular metric depth in less than a second. In *International Conference on Learning Representations*, 2025.

Junda Cheng, Longliang Liu, Gangwei Xu, Xianqi Wang, Zhaoxing Zhang, Yong Deng, Jinliang Zang, Yurui Chen, Zhipeng Cai, and Xin Yang. Monster: Marry monodepth to stereo unleashes power. In *Proceedings of the Computer Vision and Pattern Recognition Conference*, pp. 6273–6282, 2025.

Xinjing Cheng, Peng Wang, and Ruigang Yang. Depth estimation via affinity learned with convolutional spatial propagation network. In *Proceedings of the European Conference on Computer Vision*, pp. 103–119, 2018.

Xinjing Cheng, Peng Wang, and Ruigang Yang. Learning depth with convolutional spatial propagation network. *IEEE Transactions on Pattern Analysis and Machine Intelligence*, 42(10):2361–2379, 2019.

Alexey Dosovitskiy, Lucas Beyer, Alexander Kolesnikov, Dirk Weissenborn, Xiaohua Zhai, Thomas Unterthiner, Mostafa Dehghani, Matthias Minderer, G Heigold, S Gelly, et al. An image is worth 16x16 words: Transformers for image recognition at scale. In *International Conference on Learning Representations*, 2020.

Xianze Fang, Jingnan Gao, Zhe Wang, Zhuo Chen, Xingyu Ren, Jiangjing Lyu, Qiaomu Ren, Zhonglei Yang, Xiaokang Yang, Yichao Yan, et al. Dens3r: A foundation model for 3d geometry prediction. *arXiv preprint arXiv:2507.16290*, 2025.

Jingnan Gao, Zhe Wang, Xianze Fang, Xingyu Ren, Zhuo Chen, Shengqi Liu, Yuhao Cheng, Jiangjing Lyu, Xiaokang Yang, and Yichao Yan. More: 3d visual geometry reconstruction meets mixture-of-experts. *arXiv preprint arXiv:2510.27234*, 2025.

Andreas Geiger, Philip Lenz, and Raquel Urtasun. Are we ready for autonomous driving? the kitti vision benchmark suite. In *Proceedings of the IEEE/CVF Conference on Computer Vision and Pattern Recognition*, pp. 3354–3361, 2012.

Jose L Gómez, Manuel Silva, Antonio Seoane, Agnès Borrás, Mario Noriega, Germán Ros, Jose A Iglesias-Guitian, and Antonio M López. All for one, and one for all: Urbansyn dataset, the third musketeer of synthetic driving scenes. *Neurocomputing*, 637:130038, 2025.

Magnus R Hestenes, Eduard Stiefel, et al. Methods of conjugate gradients for solving linear systems. *Journal of research of the National Bureau of Standards*, 49(6):409–436, 1952.

Mu Hu, Wei Yin, Chi Zhang, Zhipeng Cai, Xiaoxiao Long, Hao Chen, Kaixuan Wang, Gang Yu, Chunhua Shen, and Shaojie Shen. Metric3d v2: A versatile monocular geometric foundation model for zero-shot metric depth and surface normal estimation. *IEEE Transactions on Pattern Analysis and Machine Intelligence*, 2024.

Po-Han Huang, Kevin Matzen, Johannes Kopf, Narendra Ahuja, and Jia-Bin Huang. Deepmvs: Learning multi-view stereopsis. In *Proceedings of the IEEE/CVF Conference on Computer Vision and Pattern Recognition*, pp. 2821–2830, 2018.

Wonbong Jang, Philippe Weinzaepfel, Vincent Leroy, Lourdes Agapito, and Jerome Revaud. Pow3r: Empowering unconstrained 3d reconstruction with camera and scene priors. In *Proceedings of the Computer Vision and Pattern Recognition Conference*, pp. 1071–1081, 2025.

Chanhwi Jeong, Inhwan Bae, Jin-Hwi Park, and Hae-Gon Jeon. Test-time prompt tuning for zero-shot depth completion. In *Proceedings of the IEEE/CVF International Conference on Computer Vision*, pp. 9443–9454, 2025.

Hualie Jiang, Zhiqiang Lou, Laiyan Ding, Rui Xu, Minglang Tan, Wenjie Jiang, and Rui Huang. Defom-stereo: Depth foundation model based stereo matching. In *Proceedings of the Computer Vision and Pattern Recognition Conference*, pp. 21857–21867, 2025a.

Lihan Jiang, Yucheng Mao, Linning Xu, Tao Lu, Kerui Ren, Yichen Jin, Xudong Xu, Mulin Yu, Jiangmiao Pang, Feng Zhao, et al. Anysplat: Feed-forward 3d gaussian splatting from unconstrained views. *arXiv preprint arXiv:2505.23716*, 2025b.

Bingxin Ke, Anton Obukhov, Shengyu Huang, Nando Metzger, Rodrigo Caye Daudt, and Konrad Schindler. Repurposing diffusion-based image generators for monocular depth estimation. In *Proceedings of the IEEE/CVF Conference on Computer Vision and Pattern Recognition*, pp. 9492–9502, 2024.

Nikhil Keetha, Norman Müller, Johannes Schönberger, Lorenzo Porzi, Yuchen Zhang, Tobias Fischer, Arno Knapitsch, Duncan Zauss, Ethan Weber, Nelson Antunes, Jonathon Luiten, Manuel Lopez-Antequera, Samuel Rota Bulò, Christian Richardt, Deva Ramanan, Sebastian Scherer, and Peter Kontschieder. MapAnything: Universal feed-forward metric 3D reconstruction, 2025. arXiv preprint arXiv:2509.13414.

Alexander Kirillov, Eric Mintun, Nikhila Ravi, Hanzi Mao, Chloe Rolland, Laura Gustafson, Tete Xiao, Spencer Whitehead, Alexander C Berg, Wan-Yen Lo, et al. Segment anything. In *Proceedings of the IEEE/CVF international conference on computer vision*, pp. 4015–4026, 2023.

Tobias Koch, Lukas Liebel, Friedrich Fraundorfer, and Marco Korner. Evaluation of cnn-based single-image depth estimation methods. In *Proceedings of the European Conference on Computer Vision Workshops*, pp. 0–0, 2018.

Brooke Krajancich, Petr Kellnhofer, and Gordon Wetzstein. Optimizing depth perception in virtual and augmented reality through gaze-contingent stereo rendering. *ACM transactions on graphics*, 39(6):1–10, 2020.

Vincent Leroy, Yohann Cabon, and Jérôme Revaud. Grounding image matching in 3d with mast3r. In *Proceedings of the European Conference on Computer Vision*, pp. 71–91, 2024.

Wuyang Li, Zhu Yu, and Alexandre Alahi. Voxdet: Rethinking 3d semantic occupancy prediction as dense object detection. *Advances in Neural Information Processing Systems*, 38, 2025.

Yiming Li, Zhiding Yu, Christopher Choy, Chaowei Xiao, Jose M Alvarez, Sanja Fidler, Chen Feng, and Anima Anandkumar. Voxformer: Sparse voxel transformer for camera-based 3d semantic scene completion. In *Proceedings of the IEEE/CVF Conference on Computer Vision and Pattern Recognition*, pp. 9087–9098, 2023a.

Yixuan Li, Lihan Jiang, Linning Xu, Yuanbo Xiangli, Zhenzhi Wang, Dahua Lin, and Bo Dai. Matrixcity: A large-scale city dataset for city-scale neural rendering and beyond. In *Proceedings of the IEEE/CVF International Conference on Computer Vision*, pp. 3205–3215, 2023b.

LightwheelAI and LightwheelOcc contributors. Lightwheelocc: A 3d occupancy synthetic dataset in autonomous driving. https://github.com/OpenDriveLab/LightwheelOcc, 2024.

Haotong Lin, Sida Peng, Jingxiao Chen, Songyou Peng, Jiaming Sun, Minghuan Liu, Hujun Bao, Jiashi Feng, Xiaowei Zhou, and Bingyi Kang. Prompting depth anything for 4k resolution accurate metric depth estimation. In *Proceedings of the Computer Vision and Pattern Recognition Conference*, pp. 17070–17080, 2025.

Yuankai Lin, Tao Cheng, Qi Zhong, Wending Zhou, and Hua Yang. Dynamic spatial propagation network for depth completion. In *Proceedings of the AAAI Conference on Artificial Intelligence*, volume 36, pp. 1638–1646, 2022.

Sifei Liu, Shalini De Mello, Jinwei Gu, Guangyu Zhong, Ming-Hsuan Yang, and Jan Kautz. Learning affinity via spatial propagation networks. *Advances in Neural Information Processing Systems*, 30, 2017.

Yifan Liu, Zhiyuan Min, Zhenwei Wang, Junta Wu, Tengfei Wang, Yixuan Yuan, Yawei Luo, and Chunchao Guo. Worldmirror: Universal 3d world reconstruction with any-prior prompting. *arXiv preprint arXiv:2510.10726*, 2025.

Zhiheng Liu, Ka Leong Cheng, Qiuyu Wang, Shuzhe Wang, Hao Ouyang, Bin Tan, Kai Zhu, Yujun Shen, Qifeng Chen, and Ping Luo. Depthlab: From partial to complete. *arXiv preprint arXiv:2412.18153*, 2024.

Ilya Loshchilov and Frank Hutter. Decoupled weight decay regularization. *arXiv preprint arXiv:1711.05101*, 2017.

Maxime Oquab, Timothée Darcet, Théo Moutakanni, Huy Vo, Marc Szafraniec, Vasil Khalidov, Pierre Fernandez, Daniel Haziza, Francisco Massa, Alaaeldin El-Nouby, et al. Dinov2: Learning robust visual features without supervision. *arXiv preprint arXiv:2304.07193*, 2023.

Jin-Hwi Park, Chanhwi Jeong, Junoh Lee, and Hae-Gon Jeon. Depth prompting for sensor-agnostic depth estimation. In *Proceedings of the IEEE/CVF Conference on Computer Vision and Pattern Recognition*, pp. 9859–9869, 2024.

Jinsun Park, Kyungdon Joo, Zhe Hu, Chi-Kuei Liu, and In So Kweon. Non-local spatial propagation network for depth completion. In *Proceedings of the European conference on computer vision*, pp. 120–136, 2020.

Luigi Piccinelli, Yung-Hsu Yang, Christos Sakaridis, Mattia Segu, Siyuan Li, Luc Van Gool, and Fisher Yu. Unidepth: Universal monocular metric depth estimation. In *Proceedings of the IEEE/CVF Conference on Computer Vision and Pattern Recognition*, pp. 10106–10116, 2024.

Luigi Piccinelli, Christos Sakaridis, Yung-Hsu Yang, Mattia Segu, Siyuan Li, Wim Abbeloos, and Luc Van Gool. Unidepthv2: Universal monocular metric depth estimation made simpler. *arXiv preprint arXiv:2502.20110*, 2025.

René Ranftl, Katrin Lasinger, David Hafner, Konrad Schindler, and Vladlen Koltun. Towards robust monocular depth estimation: Mixing datasets for zero-shot cross-dataset transfer. *IEEE Transactions on Pattern Analysis and Machine Intelligence*, 44(3):1623–1637, 2020.

René Ranftl, Alexey Bochkovskiy, and Vladlen Koltun. Vision transformers for dense prediction. In *Proceedings of the IEEE/CVF International Conference on Computer Vision*, pp. 12179–12188, 2021.

Mike Roberts, Jason Ramapuram, Anurag Ranjan, Atulit Kumar, Miguel Angel Bautista, Nathan Paczan, Russ Webb, and Joshua M Susskind. Hypersim: A photorealistic synthetic dataset for holistic indoor scene understanding. In *Proceedings of the IEEE/CVF International Conference on Computer Vision*, pp. 10912–10922, 2021.

German Ros, Laura Sellart, Joanna Materzynska, David Vazquez, and Antonio M Lopez. The synthia dataset: A large collection of synthetic images for semantic segmentation of urban scenes. In *Proceedings of the IEEE/CVF Conference on Computer Vision and Pattern Recognition*, pp. 3234–3243, 2016.

Thomas Schops, Johannes L Schonberger, Silvano Galliani, Torsten Sattler, Konrad Schindler, Marc Pollefeys, and Andreas Geiger. A multi-view stereo benchmark with high-resolution images and multi-camera videos. In *Proceedings of the IEEE/CVF Conference on Computer Vision and Pattern Recognition*, pp. 3260–3269, 2017.

Nathan Silberman, Derek Hoiem, Pushmeet Kohli, and Rob Fergus. Indoor segmentation and support inference from rgbd images. In *Proceedings of the European Conference on Computer Vision*, pp. 746–760, 2012.

Jonas Uhrig, Nick Schneider, Lukas Schneider, Uwe Franke, Thomas Brox, and Andreas Geiger. Sparsity invariant cnns. In *International Conference on 3D Vision*, pp. 11–20, 2017.

Igor Vasiljevic, Nick Kolkin, Shanyi Zhang, Ruotian Luo, Haochen Wang, Falcon Z Dai, Andrea F Daniele, Mohammadreza Mostajabi, Steven Basart, Matthew R Walter, et al. Diode: A dense indoor and outdoor depth dataset. *arXiv preprint arXiv:1908.00463*, 2019.

Massimiliano Viola, Kevin Qu, Nando Metzger, Bingxin Ke, Alexander Becker, Konrad Schindler, and Anton Obukhov. Marigold-dc: Zero-shot monocular depth completion with guided diffusion. *arXiv preprint arXiv:2412.13389*, 2024.

Haotian Wang, Meng Yang, and Nanning Zheng. G2-monodepth: A general framework of generalized depth inference from monocular rgb+ x data. *IEEE Transactions on Pattern Analysis and Machine Intelligence*, 46(5):3753–3771, 2023a.

Haotian Wang, Meng Yang, Xinhu Zheng, and Gang Hua. Scale propagation network for generalizable depth completion. *IEEE Transactions on Pattern Analysis and Machine Intelligence*, 2024a.

Haotian Wang, Aoran Xiao, Xiaoqin Zhang, Meng Yang, and Shijian Lu. Pacgdc: Label-efficient generalizable depth completion with projection ambiguity and consistency. *arXiv preprint arXiv:2507.07374*, 2025a.

Jianyuan Wang, Minghao Chen, Nikita Karaev, Andrea Vedaldi, Christian Rupprecht, and David Novotny. Vggt: Visual geometry grounded transformer. In *Proceedings of the Computer Vision and Pattern Recognition Conference*, pp. 5294–5306, 2025b.

Jiyuan Wang, Chunyu Lin, Cheng Guan, Lang Nie, Jing He, Haodong Li, Kang Liao, and Yao Zhao. Jasmine: Harnessing diffusion prior for self-supervised depth estimation. *arXiv preprint arXiv:2503.15905*, 2025c.

JiYuan Wang, Chunyu Lin, Lei Sun, Rongying Liu, Lang Nie, Mingxing Li, Kang Liao, Xiangxiang Chu, and Yao Zhao. From editor to dense geometry estimator. *arXiv preprint arXiv:2509.04338*, 2025d.

Qiang Wang, Shizhen Zheng, Qingsong Yan, Fei Deng, Kaiyong Zhao, and Xiaowen Chu. Irs: A large naturalistic indoor robotics stereo dataset to train deep models for disparity and surface normal estimation. *arXiv preprint arXiv:1912.09678*, 2019.

Ruicheng Wang, Sicheng Xu, Cassie Dai, Jianfeng Xiang, Yu Deng, Xin Tong, and Jiaolong Yang. Moge: Unlocking accurate monocular geometry estimation for open-domain images with optimal training supervision. In *Proceedings of the Computer Vision and Pattern Recognition Conference*, pp. 5261–5271, 2025e.

Ruicheng Wang, Sicheng Xu, Yue Dong, Yu Deng, Jianfeng Xiang, Zelong Lv, Guangzhong Sun, Xin Tong, and Jiaolong Yang. Moge-2: Accurate monocular geometry with metric scale and sharp details. *arXiv preprint arXiv:2507.02546*, 2025f.

Shuzhe Wang, Vincent Leroy, Yohann Cabon, Boris Chidlovskii, and Jerome Revaud. Dust3r: Geometric 3d vision made easy. In *Proceedings of the IEEE/CVF Conference on Computer Vision and Pattern Recognition*, pp. 20697–20709, 2024b.

Tai Wang, Xiaohan Mao, Chenming Zhu, Runsen Xu, Ruiyuan Lyu, Peisen Li, Xiao Chen, Wenwei Zhang, Kai Chen, Tianfan Xue, et al. Embodiedscan: A holistic multi-modal 3d perception suite towards embodied ai. In *Proceedings of the IEEE/CVF Conference on Computer Vision and Pattern Recognition*, pp. 19757–19767, 2024c.

Wenshan Wang, Delong Zhu, Xiangwei Wang, Yaoyu Hu, Yuheng Qiu, Chen Wang, Yafei Hu, Ashish Kapoor, and Sebastian Scherer. Tartanair: A dataset to push the limits of visual slam. In *2020 IEEE/RSJ International Conference on Intelligent Robots and Systems*, pp. 4909–4916, 2020.

Yufei Wang, Bo Li, Ge Zhang, Qi Liu, Tao Gao, and Yuchao Dai. Lrru: Long-short range recurrent updating networks for depth completion. In *Proceedings of the IEEE/CVF International Conference on Computer Vision*, pp. 9422–9432, 2023b.

Zehan Wang, Siyu Chen, Lihe Yang, Jialei Wang, Ziang Zhang, Hengshuang Zhao, and Zhou Zhao. Depth anything with any prior. *arXiv preprint arXiv:2505.10565*, 2025g.

Bowen Wen, Matthew Trepte, Joseph Aribido, Jan Kautz, Orazio Gallo, and Stan Birchfield. Foundationstereo: Zero-shot stereo matching. In *Proceedings of the Computer Vision and Pattern Recognition Conference*, pp. 5249–5260, 2025.

Alex Wong, Xiaohan Fei, Stephanie Tsuei, and Stefano Soatto. Unsupervised depth completion from visual inertial odometry. *IEEE Robotics and Automation Letters*, 5(2):1899–1906, 2020.

Magnus Wrenninge and Jonas Unger. Synscapes: A photorealistic synthetic dataset for street scene parsing. *arXiv preprint arXiv:1810.08705*, 2018.

Guangkai Xu, Wei Yin, Hao Chen, Chunhua Shen, Kai Cheng, Feng Wu, and Feng Zhao. Towards 3d scene reconstruction from locally scale-aligned monocular video depth. *arXiv preprint arXiv:2202.01470*, 2022.

Zhiqiang Yan, Kun Wang, Xiang Li, Zhenyu Zhang, Jun Li, and Jian Yang. Rignet: Repetitive image guided network for depth completion. In *Proceedings of the European Conference on Computer Vision*, pp. 214–230. Springer, 2022.

Zhiqiang Yan, Yuankai Lin, Kun Wang, Yupeng Zheng, Yufei Wang, Zhenyu Zhang, Jun Li, and Jian Yang. Tri-perspective view decomposition for geometry-aware depth completion. In *Proceedings of the IEEE/CVF Conference on Computer Vision and Pattern Recognition*, pp. 4874–4884, 2024.

Zhiqiang Yan, Xiang Li, Le Hui, Zhenyu Zhang, Jun Li, and Jian Yang. Rignet++: Semantic assisted repetitive image guided network for depth completion: Z. yan et al. *International Journal of Computer Vision*, pp. 1–23, 2025a.

Zhiqiang Yan, Kun Wang, Xiang Li, Guangwei Gao, Jun Li, and Jian Yang. Tri-perspective view decomposition for geometry aware depth completion and super-resolution. *IEEE Transactions on Pattern Analysis and Machine Intelligence*, 2025b.

Zhiqiang Yan, Zhengxue Wang, Haoye Dong, Jun Li, Jian Yang, and Gim Hee Lee. Ducos: Duality constrained depth super-resolution via foundation model. *arXiv preprint arXiv:2503.04171*, 2025c.

An Yang, Anfeng Li, Baosong Yang, Beichen Zhang, Binyuan Hui, Bo Zheng, Bowen Yu, Chang Gao, Chengen Huang, Chenxu Lv, et al. Qwen3 technical report. *arXiv preprint arXiv:2505.09388*, 2025.

Guorun Yang, Xiao Song, Chaoqin Huang, Zhidong Deng, Jianping Shi, and Bolei Zhou. Drivingstereo: A large-scale dataset for stereo matching in autonomous driving scenarios. In *Proceedings of the IEEE/CVF Conference on Computer Vision and Pattern Recognition*, pp. 899–908, 2019.

Lihe Yang, Bingyi Kang, Zilong Huang, Xiaogang Xu, Jiashi Feng, and Hengshuang Zhao. Depth anything: Unleashing the power of large-scale unlabeled data. In *Proceedings of the IEEE/CVF conference on computer vision and pattern recognition*, pp. 10371–10381, 2024a.

Lihe Yang, Bingyi Kang, Zilong Huang, Zhen Zhao, Xiaogang Xu, Jiashi Feng, and Hengshuang Zhao. Depth anything v2. *Advances in Neural Information Processing Systems*, 37:21875–21911, 2024b.

Chandan Yeshwanth, Yueh-Cheng Liu, Matthias Nießner, and Angela Dai. Scannet++: A high-fidelity dataset of 3d indoor scenes. In *Proceedings of the IEEE/CVF International Conference on Computer Vision*, pp. 12–22, 2023.

Wei Yin, Jianming Zhang, Oliver Wang, Simon Niklaus, Long Mai, Simon Chen, and Chunhua Shen. Learning to recover 3d scene shape from a single image. In *Proceedings of the IEEE/CVF conference on computer vision and pattern recognition*, pp. 204–213, 2021.

Wei Yin, Chi Zhang, Hao Chen, Zhipeng Cai, Gang Yu, Kaixuan Wang, Xiaozhi Chen, and Chunhua Shen. Metric3d: Towards zero-shot metric 3d prediction from a single image. In *Proceedings of the IEEE/CVF International Conference on Computer Vision*, pp. 9043–9053, 2023.

Zhu Yu, Zehua Sheng, Zili Zhou, Lun Luo, Si-Yuan Cao, Hong Gu, Huaqi Zhang, and Hui-Liang Shen. Aggregating feature point cloud for depth completion. In *Proceedings of the IEEE/CVF International Conference on Computer Vision*, pp. 8732–8743, 2023.

Zhu Yu, Runmin Zhang, Jiacheng Ying, Junchen Yu, Xiaohai Hu, Lun Luo, Si-Yuan Cao, and Hui-Liang Shen. Context and geometry aware voxel transformer for semantic scene completion. *Advances in Neural Information Processing Systems*, 37:1531–1555, 2024.

Zhu Yu, Bowen Pang, Lizhe Liu, Runmin Zhang, Qiang Li, Si-Yuan Cao, Maochun Luo, Mingxia Chen, Sheng Yang, and Hui-Liang Shen. Language driven occupancy prediction. In *Proceedings of the IEEE/CVF International Conference on Computer Vision*, pp. 7548–7558, 2025.

Yang Zheng, Adam W Harley, Bokui Shen, Gordon Wetzstein, and Leonidas J Guibas. Pointodyssey: A large-scale synthetic dataset for long-term point tracking. In *Proceedings of the IEEE/CVF International Conference on Computer Vision*, pp. 19855–19865, 2023.

Wending Zhou, Xu Yan, Yinghong Liao, Yuankai Lin, Jin Huang, Gangming Zhao, Shuguang Cui, and Zhen Li. Bev@dc: Bird's-eye view assisted training for depth completion. In *Proceedings of the IEEE/CVF Conference on Computer Vision and Pattern Recognition*, pp. 9233–9242, 2023.

Yiming Zuo, Willow Yang, Zeyu Ma, and Jia Deng. Omni-dc: Highly robust depth completion with multiresolution depth integration. *arXiv preprint arXiv:2411.19278*, 2024.

APPENDIX

A DATASETS

A.1 TRAINING DATASETS

We collected 11 open-source RGB-D datasets to train LDCM, comprising 10 synthetic and 1 real-world dataset. An overview of the training datasets is provided in Table 7, spanning four distinct domains: indoor, outdoor, in-the-wild, and driving scenarios. The combined training set contains approximately 2.6 million images. The number of RGB-D pairs in each dataset may slightly differ from the originally released versions, as we manually excluded some invalid frames.

Table 7: An overview of the training datasets.

Dataset	Domain	Statistic	Type
Hypersim Roberts et al. (2021)	Indoor	75K	Synthetic
TartanAir Wang et al. (2020)	In-the-wild	306K	Synthetic
IRS Wang et al. (2019)	Indoor	101K	Synthetic
PointOdyssey Zheng et al. (2023)	Indoor	303K	Synthetic
UrbanSyn Gómez et al. (2025)	Outdoor/Driving	7K	Synthetic
Synscapes Wrenninge & Unger (2018)	Outdoor/Driving	25K	Synthetic
MatrixCity Li et al. (2023b)	Outdoor/Driving	424K	Synthetic
LightwheelOcc LightwheelAI & contributors (2024)	Outdoor/Driving	204K	Synthetic
MVS-Synth Huang et al. (2018)	Outdoor/Driving	12K	Synthetic
Synthia Ros et al. (2016)	Outdoor/Driving	140K	Synthetic
ScanNet++ Yeshwanth et al. (2023)	Indoor	1M	Real
Total	-	2.6M	-

A.2 EVALUATION DATASETS

We use six datasets that are excluded from the training set for to compare the performance between LDCM and previous state-of-the-art methods. Below, we provide details for each dataset.

NYUv2 Dataset. The NYUv2 dataset Silberman et al. (2012) is an indoor dataset captured using a Microsoft Kinect sensor, containing RGB and depth sequences from 464 indoor scenes. The official test split contains 654 samples. Following Marigold Ke et al. (2024), we crop the images to a resolution of 426×560 for consistent input dimensions.

KITTI Dataset. The KITTI Depth dataset Geiger et al. (2012); Uhrig et al. (2017) is a large-scale outdoor dataset collected from a moving vehicle. The official validation split consists of 1,000 samples. Depth maps are acquired using an HDL-64 LiDAR sensor, with raw depth maps containing fewer than 6% valid pixels. The provided ground truth is generated by fusing multiple consecutive LiDAR scans, resulting in a denser depth map with approximately 14% valid pixels. For depth completion, input images are center-cropped to the bottom region of 252×1216 to exclude the sky and regions with unreliable depth due to the limited vertical field of view of the LiDAR.

DIODE Dataset. The DIODE dataset Vasiljevic et al. (2019) contains thousands of high-resolution RGB images with accurate, dense, and long-range depth measurements, captured using a FARO Focus S350 laser scanner. The official validation split includes 3 indoor and 3 outdoor scenes, comprising 325 and 446 samples, respectively. To reduce noise at occlusion boundaries, we filter out depth values where the maximum relative difference to any neighboring pixel exceeds 5% (indoor) and 15% (outdoor). Input images are resized to 480×640.

iBims-1 Dataset. The iBims-1 dataset Koch et al. (2018) is an indoor benchmark captured in diverse environments, providing high-resolution RGB images and highly accurate depth maps derived from laser scans. The official evaluation split contains 100 samples, with images at a native resolution of 480×640.

VOID Dataset. The VOID dataset Wong et al. (2020) is an indoor dataset captured using the Intel RealSense D435i camera. The official validation split consists of 800 samples, each paired with sparse depth maps at three sparsity levels (approximately 1500, 500, and 150 valid pixels) and RGB images at a resolution of 480×640. These varying sparsity levels allow for robust evaluation under different input conditions.

ETH3D Dataset. The ETH3D dataset Schops et al. (2017) consists of multi-view stereo images and dense depth maps captured using a high-precision laser scanner and DSLR cameras, covering diverse viewpoints and scene types. The official validation set contains 13 scenes with a total of 454 image pairs. The original image resolution is 4032×6048. Input images are resized to 480×640.

B Evaluation Details

B.1 Comparison Methods

We compare LDCM against a comprehensive set of state-of-the-art approaches: Depth-Pro[1] Bochkovskiy et al. (2025), UniDepth V1 & V2[2] Piccinelli et al. (2024; 2025), Depth Anything V2[3] Yang et al. (2024b), VGGT[4] Wang et al. (2025b), MoGe V1 & V2[5] Wang et al. (2025e;f), G2-MonoDepth[6] Wang et al. (2023a), OMNI-DC[7] Zuo et al. (2024), PriorDA[8] Wang et al. (2025g), SPNet[9] Wang et al. (2024a), PromptDA[10] Lin et al. (2025), Marigold-DC[11] Viola et al. (2024), DepthLab[12] Liu et al. (2024), Pow3R[13] Jang et al. (2025), MapAnything[14] Keetha et al. (2025), WorldMirror[15] Liu et al. (2025), spanning the key tasks of monocular depth estimation, monocular geometry estimation, depth completion. All methods are evaluated using their publicly available implementations and pre-trained checkpoints. Notably, G2-MonoDepth Wang et al. (2023a) and SPNet Wang et al. (2024a) employ different configurations for indoor and outdoor scenarios, while LDCM and the remaining methods do not use scenario-specific hyperparameters. PromptDA Lin et al. (2025) is specifically designed to leverage dense, low-resolution priors; therefore, we apply Poisson surface reconstruction to the input sparse depth map to obtain a dense prior before inference. Pow3R Jang et al. (2025) and WorldMirror Liu et al. (2025) produce relative geometry, even when sparse depth priors are provided.

B.2 Evaluation Protocol

To clarity the notations in this section:

- $\mathbf{P}$ and $\hat{\mathbf{P}}$ are the predicted and ground truth points, respectively.
- $\mathbf{D}$ and $\hat{\mathbf{D}}$ are the predicted and ground truth depths, which are the z-coordinate of corresponding points.
- $\mathcal{M}$ is the mask of valid ground truth.

Depth Completion. In the manuscript, we use four standard metrics for depth completion evaluation, including RMSE, MAE, REL, δ_1. Formally, they are defined as follows:

[1] https://github.com/apple/ml-depth-pro.
[2] https://github.com/lpiccinelli-eth/UniDepth.
[3] https://github.com/DepthAnything/Depth-Anything-V2.
[4] https://github.com/facebookresearch/vggt.
[5] https://github.com/microsoft/MoGe.
[6] https://github.com/Wang-xjtu/G2-MonoDepth.
[7] https://github.com/princeton-vl/OMNI-DC.
[8] https://github.com/SpatialVision/Prior-Depth-Anything.
[9] https://github.com/Wang-xjtu/SPNet.
[10] https://github.com/DepthAnything/PromptDA.
[11] https://github.com/prs-eth/Marigold-DC.
[12] https://github.com/ant-research/DepthLab.
[13] https://github.com/naver/pow3r.
[14] https://github.com/facebookresearch/map-anything.
[15] https://github.com/Tencent-Hunyuan/HunyuanWorld-Mirror.

- Root mean square error (RMSE) (RMSE):

$$\sqrt{\frac{1}{|\mathcal{M}|}\sum_{i\in\mathcal{M}}(\hat{\mathbf{D}}_i-\mathbf{D}_i)^2} \tag{9}$$

- Mean absolute error (MAE):

$$\frac{1}{|\mathcal{M}|}\sum_{i\in\mathcal{M}}\left|\hat{\mathbf{D}}_i-\mathbf{D}_i\right| \tag{10}$$

- Mean relative error (REL):

$$\frac{1}{|\mathcal{M}|}\sum_{i\in\mathcal{M}}\frac{\left|\hat{\mathbf{D}}_i-\mathbf{D}_i\right|}{\hat{\mathbf{D}}_i} \tag{11}$$

- Thresholded accuracy (δ_1):

$$\frac{1}{|\mathcal{M}|}\sum_{i\in\mathcal{M}}\max\left(\frac{\hat{\mathbf{D}}_i}{\mathbf{D}_i},\frac{\mathbf{D}_i}{\hat{\mathbf{D}}_i}\right)<1.25 \tag{12}$$

For models that produce relative depth maps $\mathbf{D}_r$, we first follow Equation 2 to compute (α,β), and then the metric depth maps are recoverd by:

$$\mathbf{D}=\alpha\cdot\mathbf{D}_r+\beta. \tag{13}$$

Point Map Estimation. For evaluating the reconstructed 3D point map, we adopt analogous metrics based on Euclidean distances between predicted and ground truth points. The metrics include RMSE^p, MAE^p, REL^p, and δ_1^p, defined as:

- Point-wise Root Mean Square Error (RMSE^p):

$$\sqrt{\frac{1}{|\mathcal{M}|}\sum_{i\in\mathcal{M}}\left\|\hat{\mathbf{P}}_i-\mathbf{P}_i\right\|^2} \tag{14}$$

- Point-wise Mean Absolute Error (MAE^p):

$$\frac{1}{|\mathcal{M}|}\sum_{i\in\mathcal{M}}\left\|\hat{\mathbf{P}}_i-\mathbf{P}_i\right\| \tag{15}$$

- Point-wise Mean Relative Error (REL^p):

$$\frac{1}{|\mathcal{M}|}\sum_{i\in\mathcal{M}}\frac{\left\|\hat{\mathbf{P}}_i-\mathbf{P}_i\right\|}{\|\mathbf{P}_i\|} \tag{16}$$

- Point-wise Thresholded Accuracy (δ_1^p):

$$\frac{1}{|\mathcal{M}|}\sum_{i\in\mathcal{M}}\left\|\hat{\mathbf{P}}_i-\mathbf{P}_i\right\|<0.25\cdot\min\left(\|\mathbf{P}_i\|,\|\hat{\mathbf{P}}_i\|\right) \tag{17}$$

Affine-invariant Point Map Estimation. To evaluate the affine-invariant point, we first compute the scale α_p and shift β_p using the following equation, which recovers the affine transformation applied to the predicted point map. This equation can be solved efficiently using the ROE solver proposed by MoGe Wang et al. (2025e).

$$(\alpha_p,\beta_p)=\arg\min_{\alpha_p,\beta_p}\sum_{i\in\mathcal{M}}\left(\hat{\mathbf{P}}_i-\alpha_p\cdot\mathbf{P}_i-\beta_p\right)^2, \tag{18}$$

C More Quantitative Results

From Table 12 to Table 29, we provide detailed quantitative results under different types of sparse observations.

Table 8: **Quantitative comparison of depth completion with diffusion-based methods on benchmark datasets.** The **best** results are in **bold**.

Method	VOID-1500-Points				VOID-500-Points				VOID-150-Points			
	RMSE↓	MAE↓	REL↓	δ_1 ↑	RMSE↓	MAE↓	REL↓	δ_1 ↑	RMSE↓	MAE↓	REL↓	δ_1 ↑
DepthLab	0.577	0.162	0.034	0.969	0.572	0.183	0.053	0.941	0.688	0.249	0.083	0.901
Marigold-DC	0.553	0.154	0.031	0.975	0.536	0.162	0.043	0.965	0.626	0.199	0.053	0.955
LDCM (Ours)	**0.528**	**0.135**	**0.021**	**0.981**	**0.501**	**0.134**	**0.027**	**0.978**	**0.580**	**0.167**	**0.035**	**0.972**
Method	NYUv2-500-Points				NYUv2-100-Points				KITTI-64-Lines			
	RMSE↓	MAE↓	REL↓	δ_1 ↑	RMSE↓	MAE↓	REL↓	δ_1 ↑	RMSE↓	MAE↓	REL↓	δ_1 ↑
DepthLab	0.118	0.041	0.015	0.993	0.213	0.100	0.037	0.976	2.032	0.828	0.061	0.962
Marigold-DC	0.116	0.040	0.014	0.993	0.157	0.061	0.022	0.988	1.931	0.818	0.054	0.971
LDCM (Ours)	**0.094**	**0.028**	**0.009**	**0.996**	**0.131**	**0.045**	**0.016**	**0.992**	**1.240**	**0.292**	**0.016**	**0.993**
Method	KITTI-32-Lines				KITTI-16-Lines				AVERAGE			
	RMSE↓	MAE↓	REL↓	δ_1 ↑	RMSE↓	MAE↓	REL↓	δ_1 ↑	RMSE↓	MAE↓	REL↓	δ_1 ↑
DepthLab	2.250	0.893	0.064	0.959	2.748	0.932	0.066	0.953	1.150	0.424	0.052	0.957
Marigold-DC	2.155	0.875	0.057	0.968	2.546	0.981	0.062	0.963	1.078	0.411	0.042	0.972
LDCM (Ours)	**1.416**	**0.332**	**0.018**	**0.991**	**1.603**	**0.393**	**0.020**	**0.990**	**0.762**	**0.191**	**0.020**	**0.987**

D More Comparison Results with Diffusion-based methods

Here, we present additional comparisons with diffusion-based models—Marigold-DC Viola et al. (2024) and DepthLab Liu et al. (2024). Due to their prohibitively long inference times, we evaluate these methods primarily on three benchmarks with varying levels of sparse input: NYUv2 Silberman et al. (2012) (500 and 100 points), VOID Wong et al. (2020) (150, 500, and 1500 points), and KITTI Geiger et al. (2012) (64, 32, and 16 scan lines). As shown in Table 8, LDCM consistently outperforms both Marigold-DC and DepthLab across all settings.

Table 9: Ablation study on the training data. We report the relative error (REL) for depth completion.

Configuration	Depth Completion (REL ↓)				
	KITTI	iBims-1	DIODE	ETH3D	Average
w/ more real data	0.020	**0.017**	0.035	**0.018**	**0.022**
Ours	**0.019**	0.018	**0.033**	0.019	**0.022**

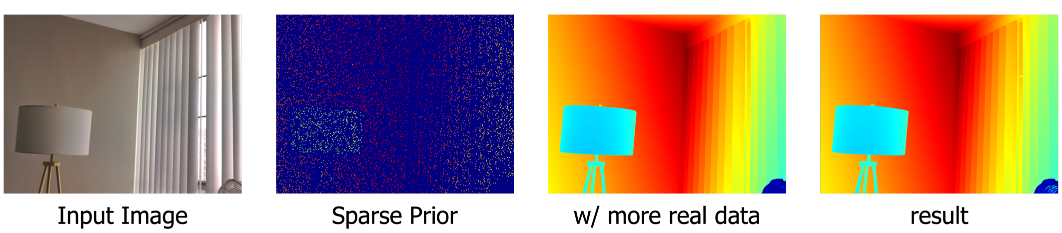

Figure 4: Qualitative comparison between the results from models using different training datasets.

E Ablation on the Training Data

Training Data. We perform an ablation study on the training data used to train the LDCM. In addition to the original datasets, we introduce an extra dataset: DrivingStereo Yang et al. (2019). The quantitative results are presented in Table 9. As shown, the inclusion of this additional data does not significantly affect metric performance. However, as illustrated in Fig. 4, incorporating more real-world data leads to visually less sharp predictions, likely due to imperfect supervision signals in the added dataset.

Table 10: **Quantitative comparison of depth completion methods on benchmark datasets.** All methods are evaluated under zero-shot settings. Methods marked with † produce relative depth, and metric depth is recovered by optimizing global scale and shift via least squares regression using the *same* sparse depth prior. The best and second-best results are highlighted.

Method	KITTI					iBims-1					DIODE Indoor				
	RMSE↓	MAE↓	REL↓	δ_1 ↑	Rk.↓	RMSE↓	MAE↓	REL↓	δ_1 ↑	Rk.↓	RMSE↓	MAE↓	REL↓	δ_1 ↑	Rk.↓
DepthAnythingV2†	4.007	1.890	0.092	0.916	5.318	0.349	0.179	0.043	0.975	5.614	0.386	0.189	0.045	0.976	4.909
DepthAnythingV2 w/ Poisson	2.448	0.953	0.051	0.959	2.955	0.231	0.098	0.027	0.976	3.136	0.195	0.091	0.026	0.967	2.795
VGGT†	4.219	2.518	0.158	0.783	6.955	0.348	0.194	0.053	0.957	6.727	0.425	0.294	0.096	0.920	6.750
VGGT w/ Poisson	2.627	1.112	0.065	0.937	4.205	0.241	0.104	0.028	0.975	4.318	0.217	0.111	0.037	0.957	4.341
MoGe V1†	3.050	1.821	0.125	0.887	5.341	0.238	0.120	0.035	0.981	4.159	0.272	0.175	0.064	0.950	5.250
MoGe V1 w/ Poisson	2.179	0.865	0.050	0.959	2.136	0.214	0.089	0.025	0.977	2.409	0.177	0.085	0.028	0.965	2.614
LDCM	**1.911**	**0.537**	**0.026**	**0.983**	**1.023**	**0.161**	**0.044**	**0.012**	**0.991**	**1.227**	**0.084**	**0.025**	**0.008**	**0.993**	**1.000**

Method	DIODE Outdoor					ETH3D					Average				
	RMSE↓	MAE↓	REL↓	δ_1 ↑	Rk.↓	RMSE↓	MAE↓	REL↓	δ_1 ↑	Rk.↓	RMSE↓	MAE↓	REL↓	δ_1 ↑	Rk.↓
DepthAnythingV2†	5.940	2.777	0.124	0.869	5.114	2.091	0.424	0.049	0.979	5.864	2.555	1.092	0.071	0.943	5.364
DepthAnythingV2 w/ Poisson	3.285	1.182	0.064	0.941	3.455	0.662	0.168	0.025	0.983	3.966	1.364	0.498	0.039	0.965	3.261
VGGT†	4.898	2.893	0.237	0.772	5.705	0.540	0.317	0.060	0.949	5.818	2.086	1.243	0.121	0.876	6.391
VGGT w/ Poisson	2.910	1.262	0.081	0.917	3.750	0.339	0.140	0.024	0.980	3.262	1.267	0.546	0.047	0.953	3.975
MoGe V1†	10.576	8.340	0.406	0.599	6.932	1.651	0.550	0.082	0.943	5.455	3.157	2.201	0.142	0.872	5.427
MoGe V1 w/ Poisson	2.340	0.910	0.053	0.950	2.000	0.319	0.118	0.021	0.986	2.262	1.046	0.413	0.035	0.967	2.284
LDCM	**1.969**	**0.529**	**0.031**	**0.970**	**1.000**	**0.187**	**0.048**	**0.008**	**0.997**	**1.000**	**0.862**	**0.237**	**0.017**	**0.987**	**1.050**

F Applying Poisson-based Alignment Strategy to Monocular Estimators

In Table 10, we apply the Poisson alignment strategy to relative geometry estimators to obtain dense depth maps. As shown in the table, this strategy effectively improves the metric accuracy of these approaches, demonstrating its effectiveness. Moreover, our LDCM maintains state-of-the-art performance.

G Inference Time

We report the per-stage inference times of our method, measured at a resolution of 480×640 on an NVIDIA L20 GPU. Our pipeline comprises four stages: Depth Anything Small (0.006 s), global alignment (0.006 s), Poisson-based alignment (0.020 s), and the subsequent refinement model (0.040 s), resulting in a total runtime of 0.072 s. For comparison, LWLR runs in 0.010 s under the same conditions. A detailed comparison with the inference times of several competing methods is provided in Table 11.

Table 11: Inference time (in seconds) of different methods at 480×640 resolution on an NVIDIA L20 GPU, with all inference performed in FP32 precision.

Method	OMNI-DC	PriorDA	DepthPro	VGGT	MoGe V2	DepthAnythingV2	LDCM (Ours)
Inference Time (s)	0.128	0.064	0.554	0.196	0.220	0.019	0.072

H More Qualitative Results

Fig. 6 and Fig. 7 presents a qualitative comparison between LDCM and state-of-the-art methods. Notably, LDCM produces sharper geometric structures and more accurate depth distributions, particularly in regions with complex geometry or extreme sparsity. The predictions from LDCM exhibit significantly clearer boundaries and finer details, demonstrating the effectiveness of our coarse-to-fine framework and structural prior integration. In Fig. 8, we provide more visualization results for depth map and point map.

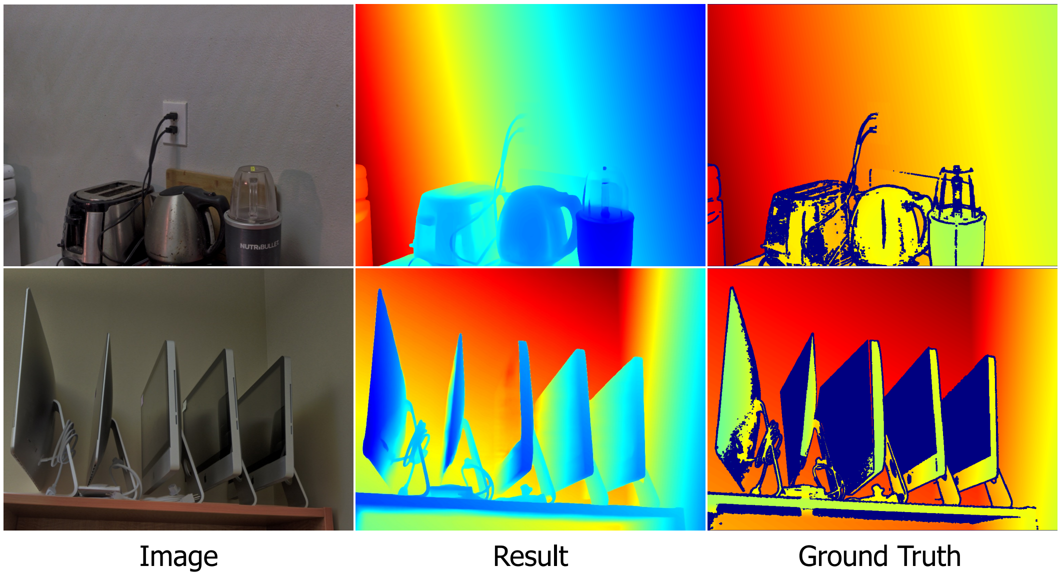

Figure 5: Example of two failure cases.

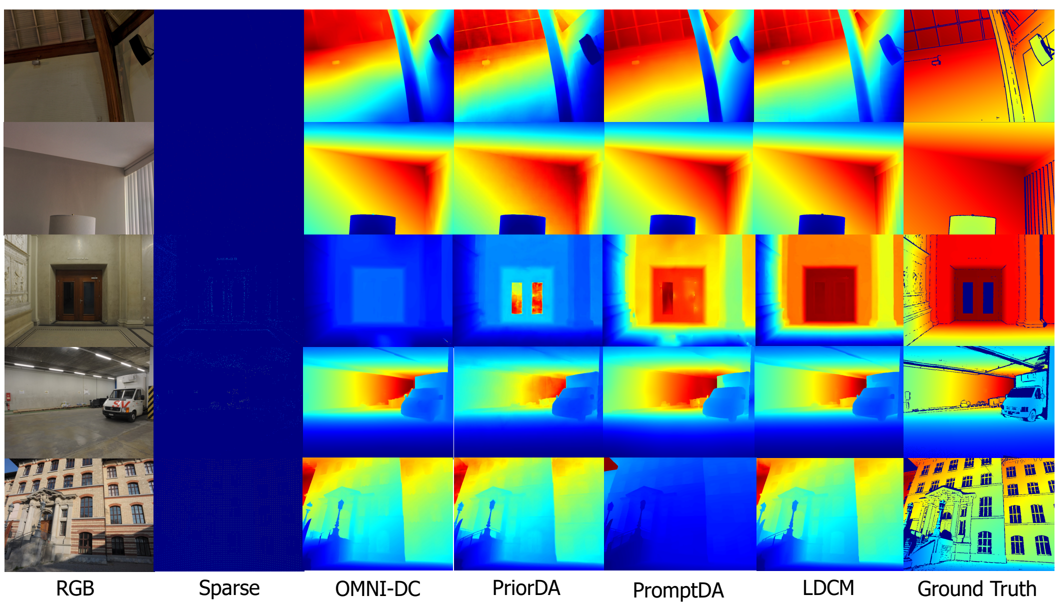

Figure 6: Visualization comparion with state-of-the-art methods.

I Noise Analysis

Fig. 9 presents an example with noisy input. When the sparse prior contains noise, the Poisson alignment strategy is adversely affected. However, the subsequent network effectively mitigates this issue and produces a high-quality result.

J Limtation and Future Work

Although LDCM achieves superior performance, accurately reconstructing transparent objects and reflective surfaces remains challenging, as illustrated by two failure cases in Fig. 5. This limitation

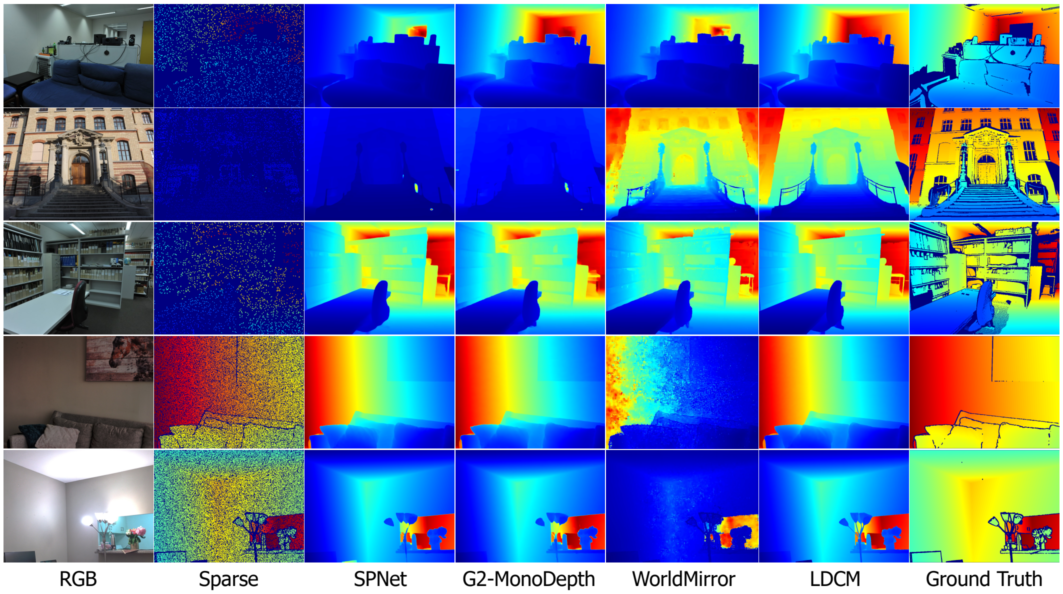

Figure 7: Visualization comparion with state-of-the-art methods.

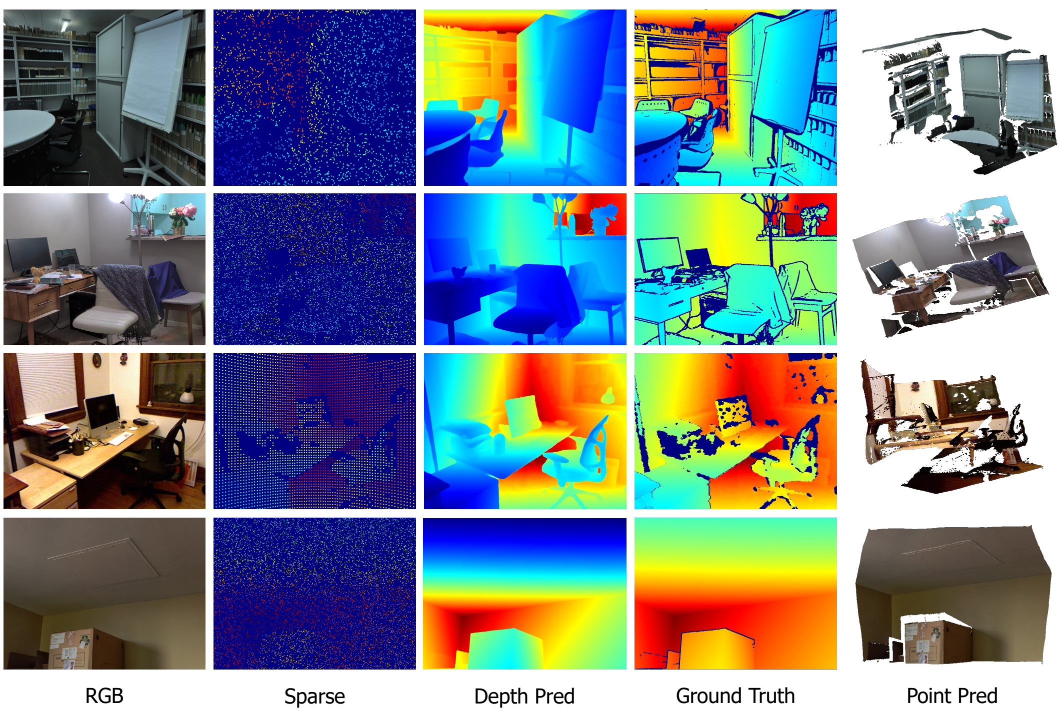

Figure 8: More visualization results for depth map and point map.

stems from the lack of large-scale datasets containing such materials, which are difficult to capture and annotate. In the future, we plan to investigate synthetic data simulation to augment training and improve robustness on these challenging scenarios. Additionally, while monocular video reconstruction is a promising application, achieving temporal consistency poses substantial challenges. Extending LDCM to process video sequences for consistent 3D geometry estimation over time is an important direction for future exploration.

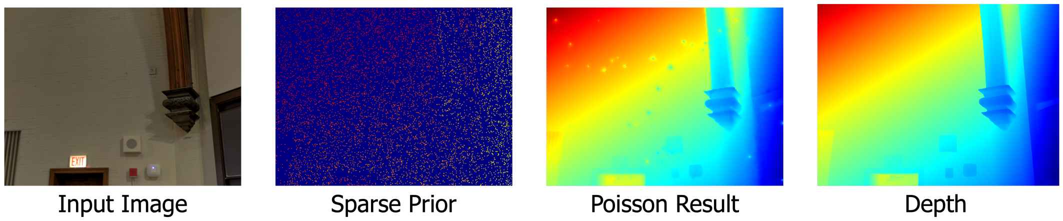

Figure 9: An example for noise input

K STATEMENT ON THE USE OF LLMS

Large language models (LLMs) were used only for linguistic refinement, such as improving grammar and phrasing. They played no role in shaping research concepts, designing experiments, or interpreting data. The authors authored all content, verified its accuracy and originality, and assume full responsibility for the manuscript.

Table 12: **Quantitative comparison of depth completion with baseline methods on the KITTI dataset Geiger et al. (2012); Uhrig et al. (2017).** Methods marked with † produce relative depth maps, where the metric depth is recovered by optimizing global scale and shift via least squares regression using the sparse depth prior. Methods marked with ‡ use scenario-specific configurations for indoor and outdoor scenes, respectively.The best and the second best results are highlighted.

method	Lidar-64-Lines					Lidar-32-Lines					Lidar-16-Lines				
	RMSE↓	MAE↓	REL↓	δ_1 ↑	Rk.↓	RMSE↓	MAE↓	REL↓	δ_1 ↑	Rk.↓	RMSE↓	MAE↓	REL↓	δ_1 ↑	Rk.↓
DepthPro	4.149	2.763	0.178	0.731	14.000	4.149	2.763	0.178	0.731	14.000	4.149	2.763	0.178	0.731	13.750
UniDepth V1	3.335	2.010	0.118	0.938	9.000	3.335	2.010	0.118	0.938	9.500	3.335	2.010	0.118	0.938	9.500
UniDepth V2	3.150	1.598	0.090	0.960	7.500	3.150	1.598	0.090	0.960	7.250	3.150	1.598	0.090	0.960	7.500
DepthAnythingV2†	3.902	1.826	0.088	0.923	9.250	3.903	1.824	0.088	0.923	8.750	3.902	1.824	0.088	0.923	9.000
VGGT†	4.122	2.417	0.148	0.804	12.000	4.126	2.415	0.147	0.806	13.000	4.134	2.431	0.149	0.802	12.500
MoGe V1†	3.822	2.450	0.159	0.869	11.500	3.299	1.997	0.131	0.899	10.250	2.977	1.720	0.113	0.915	8.500
MoGe V2	4.617	3.366	0.213	0.458	15.250	4.617	3.366	0.213	0.458	15.250	4.617	3.366	0.213	0.458	15.000
G2-MonoDepth‡	1.609	0.378	0.024	0.986	4.000	1.801	0.454	0.028	0.984	4.000	2.187	0.652	0.036	0.981	4.250
OMNI-DC	1.184	0.274	0.015	0.993	1.000	1.424	0.354	0.019	0.990	2.000	1.710	0.460	0.024	0.986	2.000
PriorDA	1.776	0.561	0.029	0.985	5.000	1.912	0.645	0.034	0.983	5.000	2.124	0.773	0.041	0.979	4.750
SPNet‡	1.547	0.369	0.023	0.987	3.000	1.774	0.418	0.026	0.985	3.000	2.069	0.531	0.031	0.982	3.000
PromptDA	2.409	0.857	0.043	0.973	6.000	2.490	0.886	0.043	0.972	6.000	2.682	0.993	0.050	0.966	6.000
WorldMirror†	3.740	2.245	0.159	0.793	11.500	4.076	2.078	0.121	0.883	11.250	5.017	2.543	0.134	0.832	13.000
MapAnything	12.431	6.241	0.318	0.621	15.750	12.621	6.357	0.322	0.616	15.750	12.856	6.551	0.331	0.606	15.750
Pow3R†	3.027	1.797	0.122	0.865	9.000	3.254	1.920	0.128	0.853	10.000	3.352	1.944	0.127	0.855	10.500
LDCM (Ours)	**1.240**	**0.292**	**0.016**	**0.993**	**1.750**	**1.416**	**0.332**	**0.018**	**0.991**	**1.000**	**1.603**	**0.393**	**0.020**	**0.990**	**1.000**

method	Lidar-8-Lines					Lidar-4-Lines					10%				
	RMSE↓	MAE↓	REL↓	δ_1 ↑	Rk.↓	RMSE↓	MAE↓	REL↓	δ_1 ↑	Rk.↓	RMSE↓	MAE↓	REL↓	δ_1 ↑	Rk.↓
DepthPro	4.149	2.763	0.178	0.731	13.250	4.149	2.763	0.178	0.731	13.250	4.149	2.763	0.178	0.731	14.000
UniDepth V1	3.335	2.010	0.118	0.938	9.500	3.335	2.010	0.118	0.938	8.500	3.335	2.010	0.118	0.938	9.250
UniDepth V2	3.150	1.598	0.090	0.960	7.500	3.150	1.598	0.090	0.960	5.000	3.150	1.598	0.090	0.960	7.500
DepthAnythingV2†	3.927	1.838	0.089	0.922	9.000	4.070	1.904	0.091	0.917	9.500	3.919	1.833	0.088	0.923	9.250
VGGT†	4.158	2.410	0.147	0.809	12.250	4.284	2.400	0.147	0.811	12.250	4.129	2.421	0.148	0.803	13.000
MoGe V1†	2.828	1.587	0.105	0.918	8.000	2.796	1.508	0.098	0.926	6.250	2.932	1.688	0.112	0.914	8.500
MoGe V2	4.617	3.366	0.213	0.458	15.000	4.617	3.366	0.213	0.458	15.000	4.617	3.366	0.213	0.458	15.250
G2-MonoDepth‡	2.658	0.877	0.046	0.972	4.500	3.847	1.572	0.077	0.930	7.500	1.849	0.490	0.028	0.985	3.750
OMNI-DC	2.116	0.629	0.031	0.981	2.000	3.305	1.114	0.050	0.958	3.000	1.759	0.443	0.025	0.985	2.250
PriorDA	2.404	0.936	0.049	0.973	4.500	3.300	1.320	0.063	0.954	4.250	1.980	0.640	0.032	0.982	5.000
SPNet‡	2.379	0.716	0.037	0.978	3.000	3.516	1.219	0.055	0.958	4.000	1.776	0.459	0.026	0.986	2.750
PromptDA	2.908	1.098	0.054	0.960	6.250	3.686	1.526	0.078	0.939	6.750	2.591	0.964	0.048	0.966	6.000
WorldMirror†	5.776	2.941	0.148	0.794	13.750	6.412	3.235	0.159	0.765	13.750	3.848	2.192	0.133	0.859	11.500
MapAnything	13.057	6.717	0.339	0.598	15.750	13.166	6.883	0.351	0.579	15.750	12.926	6.684	0.344	0.593	15.750
Pow3R†	3.448	1.977	0.128	0.854	10.500	3.648	1.961	0.123	0.864	10.000	3.491	2.043	0.132	0.855	11.000
LDCM (Ours)	**1.878**	**0.494**	**0.023**	**0.987**	**1.000**	**2.592**	**0.767**	**0.031**	**0.978**	**1.000**	**1.565**	**0.373**	**0.019**	**0.990**	**1.000**

method	5%					3%					1%				
	RMSE↓	MAE↓	REL↓	δ_1 ↑	Rk.↓	RMSE↓	MAE↓	REL↓	δ_1 ↑	Rk.↓	RMSE↓	MAE↓	REL↓	δ_1 ↑	Rk.↓
DepthPro	4.149	2.763	0.178	0.731	14.000	4.149	2.763	0.178	0.731	14.000	4.149	2.763	0.178	0.731	13.750
UniDepth V1	3.335	2.010	0.118	0.938	9.250	3.335	2.010	0.118	0.938	9.250	3.335	2.010	0.118	0.938	9.250
UniDepth V2	3.150	1.598	0.090	0.960	7.750	3.150	1.598	0.090	0.960	7.500	3.150	1.598	0.090	0.960	7.000
DepthAnythingV2†	3.924	1.835	0.088	0.922	9.250	3.940	1.843	0.089	0.922	9.500	3.996	1.866	0.090	0.920	9.500
VGGT†	4.136	2.428	0.149	0.802	13.000	4.146	2.435	0.150	0.801	13.000	4.185	2.458	0.151	0.797	13.250
MoGe V1†	2.803	1.569	0.104	0.922	8.000	2.748	1.517	0.100	0.925	7.750	2.757	1.512	0.099	0.922	7.500
MoGe V2	4.617	3.366	0.213	0.458	15.250	4.617	3.366	0.213	0.458	15.250	4.617	3.366	0.213	0.458	15.250
G2-MonoDepth‡	2.035	0.573	0.031	0.983	3.750	2.244	0.672	0.035	0.980	4.000	2.930	1.040	0.051	0.966	5.250
OMNI-DC	1.951	0.516	0.028	0.983	3.000	2.124	0.589	0.031	0.980	3.000	2.677	0.840	0.042	0.969	3.500
PriorDA	2.099	0.690	0.034	0.980	5.000	2.210	0.738	0.036	0.978	4.750	2.524	0.880	0.042	0.972	3.000
SPNet‡	1.897	0.513	0.027	0.986	2.000	2.053	0.577	0.029	0.984	2.000	2.534	0.773	0.037	0.977	2.250
PromptDA	2.762	1.070	0.055	0.961	6.000	2.874	1.117	0.056	0.959	6.500	3.245	1.341	0.068	0.946	6.750
WorldMirror†	3.820	2.123	0.125	0.868	11.250	3.835	2.128	0.125	0.867	11.250	3.903	2.160	0.127	0.860	11.250
MapAnything	12.980	6.726	0.345	0.594	15.750	13.106	6.986	0.368	0.573	15.750	13.334	7.326	0.388	0.550	15.750
Pow3R†	3.472	2.020	0.131	0.850	11.250	3.472	2.010	0.130	0.853	11.000	3.544	2.047	0.132	0.850	11.250
LDCM (Ours)	**1.691**	**0.420**	**0.021**	**0.989**	**1.000**	**1.821**	**0.468**	**0.022**	**0.988**	**1.000**	**2.160**	**0.610**	**0.027**	**0.983**	**1.000**

method	SIFT					ORB					Average				
	RMSE↓	MAE↓	REL↓	δ_1 ↑	Rk.↓	RMSE↓	MAE↓	REL↓	δ_1 ↑	Rk.↓	RMSE↓	MAE↓	REL↓	δ_1 ↑	Rk.↓
DepthPro	4.149	2.763	0.178	0.731	12.000	4.149	2.763	0.178	0.731	11.750	4.149	2.763	0.178	0.731	13.432
UniDepth V1	3.335	2.010	0.118	0.938	5.750	3.335	2.010	0.118	0.938	6.250	3.335	2.010	0.118	0.938	8.636
UniDepth V2	3.150	1.598	0.090	0.960	3.250	3.150	1.598	0.090	0.960	3.750	3.150	1.598	0.090	0.960	6.500
DepthAnythingV2†	4.295	2.080	0.102	0.896	8.000	4.299	2.116	0.108	0.886	9.000	4.007	1.890	0.092	0.916	9.091
VGGT†	4.516	2.949	0.199	0.691	14.000	4.473	2.933	0.204	0.682	13.750	4.219	2.518	0.158	0.783	12.909
MoGe V1†	3.274	2.194	0.170	0.792	8.500	3.315	2.289	0.184	0.760	9.500	3.050	1.821	0.125	0.887	8.568
MoGe V2	4.617	3.366	0.213	0.458	15.250	4.617	3.366	0.213	0.458	15.250	4.617	3.366	0.213	0.458	15.182
G2-MonoDepth‡	4.238	2.212	0.133	0.800	10.000	3.617	1.680	0.101	0.869	7.250	2.638	0.964	0.054	0.949	5.295
OMNI-DC	3.630	1.632	0.099	0.884	6.250	3.443	1.514	0.097	0.889	5.500	2.302	0.760	0.042	0.963	3.045
PriorDA	2.904	1.174	0.061	0.948	2.250	2.769	1.118	0.061	0.949	2.250	2.364	0.861	0.044	0.971	4.159
SPNet‡	3.358	1.482	0.085	0.891	4.500	3.107	1.265	0.075	0.911	3.500	2.365	0.757	0.041	0.966	3.000
PromptDA	3.882	1.990	0.120	0.887	7.250	3.909	2.027	0.126	0.872	8.500	3.040	1.261	0.067	0.946	6.545
WorldMirror†	4.166	2.558	0.165	0.769	10.750	4.239	2.551	0.166	0.770	10.750	4.439	2.432	0.142	0.824	11.818
MapAnything	13.101	7.111	0.374	0.561	15.750	13.133	7.046	0.372	0.577	15.750	12.974	6.784	0.350	0.588	15.750
Pow3R†	3.981	2.646	0.197	0.735	11.500	3.973	2.694	0.206	0.719	12.250	3.515	2.096	0.141	0.832	10.750
LDCM (Ours)	**2.579**	**0.910**	**0.043**	**0.963**	**1.000**	**2.478**	**0.846**	**0.042**	**0.962**	**1.000**	**1.911**	**0.537**	**0.026**	**0.983**	**1.068**

Table 13: **Quantitative comparison of depth completion with baseline methods on the indoor scenes of the DIODE dataset Vasiljevic et al. (2019).** Methods marked with † produce relative depth maps, where the metric depth is recovered by optimizing global scale and shift via least squares regression using the sparse depth prior. Methods marked with ‡ use scenario-specific configurations for indoor and outdoor scenes, respectively. The best and the second best results are highlighted.

Method	10% Noise					5%					3%				
	RMSE↓	MAE↓	REL↓	δ_1 ↑	Rk.↓	RMSE↓	MAE↓	REL↓	δ_1 ↑	Rk.↓	RMSE↓	MAE↓	REL↓	δ_1 ↑	Rk.↓
DepthPro	0.837	0.702	0.193	0.668	14.500	0.837	0.702	0.193	0.668	14.500	0.837	0.702	0.193	0.668	14.500
UniDepth V1	0.939	0.840	0.158	0.779	14.000	0.939	0.840	0.158	0.779	14.000	0.939	0.840	0.158	0.779	14.000
UniDepth V2	0.811	0.678	0.165	0.681	13.500	0.811	0.678	0.165	0.681	13.500	0.811	0.678	0.165	0.681	13.500
DepthAnythingV2†	0.383	0.185	0.041	0.979	8.500	0.387	0.181	0.040	0.979	8.750	0.388	0.181	0.040	0.979	8.750
VGGT†	0.392	0.262	0.078	0.928	11.750	0.391	0.261	0.078	0.929	11.750	0.391	0.261	0.078	0.929	11.750
MoGe V1†	0.243	0.144	0.045	0.956	8.750	0.239	0.140	0.043	0.958	8.250	0.239	0.140	0.043	0.958	8.000
MoGe V2	1.064	0.938	0.235	0.433	16.000	1.064	0.938	0.235	0.433	16.000	1.064	0.938	0.235	0.433	16.000
G2-MonoDepth‡	0.020	0.004	0.001	1.000	1.500	0.021	0.005	0.001	1.000	2.250	0.026	0.005	0.001	1.000	2.250
OMNI-DC	0.066	0.009	0.002	0.999	4.000	0.022	0.002	0.000	1.000	1.500	0.026	0.002	0.000	1.000	1.250
PriorDA	0.077	0.029	0.006	0.999	4.750	0.050	0.016	0.004	1.000	4.000	0.051	0.016	0.004	0.999	5.000
SPNet‡	0.019	0.003	0.001	1.000	1.000	0.018	0.003	0.001	1.000	1.500	0.021	0.003	0.001	1.000	1.500
PromptDA	0.099	0.049	0.014	0.998	6.000	0.092	0.047	0.013	0.997	6.000	0.095	0.047	0.013	0.998	6.000
WorldMirror†	0.323	0.195	0.062	0.958	10.250	0.380	0.231	0.069	0.946	10.500	0.376	0.220	0.066	0.948	10.500
MapAnything	0.535	0.129	0.030	0.977	8.500	0.508	0.133	0.027	0.984	8.250	0.552	0.156	0.031	0.982	8.500
Pow3R†	0.260	0.186	0.056	0.976	9.250	0.296	0.207	0.063	0.954	9.500	0.310	0.211	0.063	0.951	9.500
LDCM (Ours)	**0.023**	**0.005**	**0.001**	**1.000**	**2.000**	**0.025**	**0.004**	**0.001**	**1.000**	**2.500**	**0.028**	**0.004**	**0.001**	**1.000**	**2.500**

Method	1%					500					100				
	RMSE↓	MAE↓	REL↓	δ_1 ↑	Rk.↓	RMSE↓	MAE↓	REL↓	δ_1 ↑	Rk.↓	RMSE↓	MAE↓	REL↓	δ_1 ↑	Rk.↓
DepthPro	0.837	0.702	0.193	0.668	14.500	0.837	0.702	0.193	0.668	14.250	0.837	0.702	0.193	0.668	13.750
UniDepth V1	0.939	0.840	0.158	0.779	14.000	0.939	0.840	0.158	0.779	13.750	0.939	0.840	0.158	0.779	13.250
UniDepth V2	0.811	0.678	0.165	0.681	13.500	0.811	0.678	0.165	0.681	13.250	0.811	0.678	0.165	0.681	12.500
DepthAnythingV2†	0.391	0.182	0.040	0.979	8.000	0.410	0.189	0.041	0.978	8.500	0.428	0.193	0.041	0.978	7.500
VGGT†	0.391	0.261	0.078	0.928	11.500	0.392	0.262	0.078	0.928	10.750	0.399	0.261	0.078	0.931	9.750
MoGe V1†	0.239	0.140	0.043	0.958	7.750	0.240	0.141	0.044	0.956	7.750	0.244	0.141	0.043	0.959	6.250
MoGe V2	1.064	0.938	0.235	0.433	16.000	1.064	0.938	0.235	0.433	15.750	1.064	0.938	0.235	0.433	15.750
G2-MonoDepth‡	0.043	0.009	0.002	1.000	3.250	0.136	0.045	0.011	0.997	5.000	0.732	0.550	0.179	0.622	12.750
OMNI-DC	0.036	0.003	0.001	1.000	1.250	0.088	0.016	0.004	0.998	2.500	0.185	0.059	0.014	0.992	3.000
PriorDA	0.057	0.016	0.004	0.999	5.000	0.081	0.022	0.005	0.999	2.750	0.124	0.039	0.009	0.996	1.500
SPNet‡	0.034	0.005	0.001	1.000	1.250	0.101	0.020	0.004	0.998	3.000	0.200	0.067	0.016	0.992	3.750
PromptDA	0.105	0.051	0.014	0.997	6.000	0.166	0.077	0.022	0.991	6.000	0.246	0.115	0.031	0.982	5.250
WorldMirror†	0.343	0.193	0.057	0.954	9.750	0.326	0.183	0.054	0.955	8.750	0.330	0.180	0.052	0.957	7.500
MapAnything	0.635	0.224	0.045	0.974	10.000	1.149	0.609	0.135	0.879	13.000	1.248	0.771	0.153	0.791	13.000
Pow3R†	0.321	0.207	0.061	0.956	9.750	0.337	0.210	0.060	0.958	9.250	0.349	0.215	0.062	0.953	8.750
LDCM (Ours)	**0.038**	**0.005**	**0.001**	**1.000**	**1.750**	**0.079**	**0.012**	**0.002**	**0.999**	**1.000**	**0.154**	**0.034**	**0.006**	**0.996**	**1.250**

Method	SIFT					ORB					Virtual-Lidar-32-Lines				
	RMSE↓	MAE↓	REL↓	δ_1 ↑	Rk.↓	RMSE↓	MAE↓	REL↓	δ_1 ↑	Rk.↓	RMSE↓	MAE↓	REL↓	δ_1 ↑	Rk.↓
DepthPro	0.837	0.702	0.193	0.668	13.500	0.837	0.702	0.193	0.668	13.000	0.837	0.702	0.193	0.668	14.250
UniDepth V1	0.939	0.840	0.158	0.779	12.250	0.939	0.840	0.158	0.779	12.250	0.939	0.840	0.158	0.779	13.750
UniDepth V2	0.811	0.678	0.165	0.681	12.000	0.811	0.678	0.165	0.681	11.750	0.811	0.678	0.165	0.681	13.250
DepthAnythingV2†	0.365	0.221	0.072	0.961	3.250	0.343	0.205	0.060	0.961	3.000	0.388	0.181	0.040	0.979	8.000
VGGT†	0.571	0.447	0.183	0.881	9.750	0.577	0.438	0.174	0.877	8.500	0.391	0.261	0.078	0.928	11.000
MoGe V1†	0.411	0.329	0.161	0.919	6.750	0.413	0.328	0.155	0.913	5.250	0.240	0.140	0.043	0.957	7.500
MoGe V2	1.064	0.938	0.235	0.433	15.500	1.064	0.938	0.235	0.433	15.750	1.064	0.938	0.235	0.433	16.000
G2-MonoDepth‡	0.894	0.670	0.241	0.554	13.750	0.996	0.755	0.261	0.513	14.750	0.081	0.020	0.005	0.999	4.000
OMNI-DC	0.353	0.223	0.083	0.870	5.000	0.492	0.330	0.119	0.800	5.750	0.056	0.007	0.002	0.999	1.500
PriorDA	0.145	0.081	0.032	0.975	1.500	0.197	0.115	0.049	0.967	1.500	0.063	0.018	0.004	0.999	3.000
SPNet‡	0.473	0.318	0.125	0.768	7.750	0.552	0.375	0.140	0.746	7.500	0.071	0.011	0.002	0.999	2.500
PromptDA	0.365	0.252	0.095	0.877	5.500	0.608	0.419	0.149	0.795	8.500	0.124	0.058	0.018	0.995	6.000
WorldMirror†	0.532	0.411	0.187	0.897	9.000	0.648	0.502	0.214	0.874	10.000	0.330	0.185	0.054	0.954	9.000
MapAnything	1.105	0.670	0.157	0.812	11.250	1.032	0.578	0.140	0.854	9.750	1.057	0.560	0.147	0.879	12.750
Pow3R†	0.499	0.388	0.156	0.884	7.250	0.499	0.386	0.154	0.872	7.000	0.331	0.208	0.060	0.956	9.500
LDCM (Ours)	**0.149**	**0.072**	**0.027**	**0.973**	**1.500**	**0.208**	**0.104**	**0.037**	**0.963**	**1.500**	**0.053**	**0.007**	**0.001**	**0.999**	**1.000**

Method	Virtual-Lidar-16-Lines					Virtual-Lidar-8-Lines					Average				
	RMSE↓	MAE↓	REL↓	δ_1 ↑	Rk.↓	RMSE↓	MAE↓	REL↓	δ_1 ↑	Rk.↓	RMSE↓	MAE↓	REL↓	δ_1 ↑	Rk.↓
DepthPro	0.837	0.702	0.193	0.668	14.250	0.837	0.702	0.193	0.668	14.250	0.837	0.702	0.193	0.668	14.114
UniDepth V1	0.939	0.840	0.158	0.779	13.750	0.939	0.840	0.158	0.779	13.750	0.939	0.840	0.158	0.779	13.523
UniDepth V2	0.811	0.678	0.165	0.681	13.250	0.811	0.678	0.165	0.681	13.250	0.811	0.678	0.165	0.681	13.023
DepthAnythingV2†	0.382	0.180	0.040	0.979	8.000	0.382	0.179	0.039	0.979	8.000	0.386	0.189	0.045	0.976	7.295
VGGT†	0.392	0.261	0.078	0.928	11.000	0.393	0.264	0.079	0.928	11.000	0.425	0.294	0.096	0.920	10.773
MoGe V1†	0.240	0.140	0.043	0.957	7.500	0.241	0.142	0.044	0.954	7.500	0.272	0.175	0.064	0.950	7.386
MoGe V2	1.064	0.938	0.235	0.433	15.750	1.064	0.938	0.235	0.433	15.750	1.064	0.938	0.235	0.433	15.841
G2-MonoDepth‡	0.121	0.033	0.008	0.997	5.000	0.211	0.086	0.023	0.988	5.250	0.298	0.198	0.067	0.879	6.341
OMNI-DC	0.080	0.014	0.003	0.998	2.500	0.144	0.042	0.010	0.995	4.000	0.141	0.064	0.022	0.968	2.932
PriorDA	0.078	0.022	0.005	0.999	2.750	0.104	0.034	0.008	0.998	1.500	0.093	0.037	0.012	0.994	3.023
SPNet‡	0.094	0.017	0.004	0.998	3.250	0.143	0.038	0.009	0.996	3.000	0.157	0.078	0.028	0.954	3.273
PromptDA	0.146	0.066	0.018	0.994	6.000	0.190	0.087	0.024	0.988	5.500	0.203	0.115	0.037	0.965	6.068
WorldMirror†	0.327	0.182	0.053	0.956	8.750	0.331	0.188	0.056	0.951	9.000	0.386	0.243	0.084	0.941	9.364
MapAnything	1.077	0.606	0.149	0.870	13.000	1.099	0.600	0.126	0.890	13.000	0.909	0.458	0.104	0.899	11.000
Pow3R†	0.337	0.211	0.061	0.955	9.750	0.341	0.216	0.063	0.953	9.500	0.353	0.240	0.078	0.943	9.000
LDCM (Ours)	**0.067**	**0.011**	**0.002**	**0.999**	**1.000**	**0.104**	**0.022**	**0.005**	**0.998**	**1.000**	**0.084**	**0.025**	**0.008**	**0.993**	**1.545**

Table 14: **Quantitative comparison of depth completion with baseline methods on the outdoor scenes of the DIODE dataset Vasiljevic et al. (2019).** Methods marked with † produce relative depth maps, where the metric depth is recovered by optimizing global scale and shift via least squares regression using the sparse depth prior. Methods marked with ‡ use scenario-specific configurations for indoor and outdoor scenes, respectively. The best and the second best results are highlighted.

Method	Virtual-Lidar-64-Lines					Virtual-Lidar-32-Lines					Virtual-Lidar-16-Lines				
	RMSE↓	MAE↓	REL↓	δ_1 ↑	Rk.↓	RMSE↓	MAE↓	REL↓	δ_1 ↑	Rk.↓	RMSE↓	MAE↓	REL↓	δ_1 ↑	Rk.↓
DepthPro	9.539	7.635	0.403	0.177	14.750	9.539	7.635	0.403	0.177	15.250	9.539	7.635	0.403	0.177	15.000
UniDepth V1	5.782	3.841	0.189	0.661	12.000	5.782	3.841	0.189	0.661	11.750	5.782	3.841	0.189	0.661	11.750
UniDepth V2	11.145	8.936	0.515	0.526	15.750	11.145	8.936	0.515	0.526	15.750	11.145	8.936	0.515	0.526	15.750
DepthAnythingV2†	5.786	2.626	0.118	0.882	8.750	5.829	2.649	0.118	0.880	8.750	5.881	2.670	0.121	0.879	8.750
VGGT†	4.739	2.748	0.227	0.779	10.750	4.743	2.761	0.230	0.779	10.250	4.765	2.758	0.228	0.780	10.250
MoGe V1†	10.329	8.351	0.396	0.603	14.500	9.455	7.366	0.354	0.648	14.000	9.034	6.809	0.317	0.685	12.750
MoGe V2	4.807	3.352	0.182	0.680	10.750	4.807	3.352	0.182	0.680	10.500	4.807	3.352	0.182	0.680	10.750
G2-MonoDepth‡	1.938	0.489	0.039	0.975	4.000	2.275	0.629	0.052	0.967	4.500	2.719	0.882	0.069	0.950	5.000
OMNI-DC	1.899	0.424	0.033	0.977	3.000	2.196	0.532	0.042	0.970	3.250	2.659	0.738	0.056	0.960	3.750
PriorDA	1.970	0.674	0.041	0.969	5.000	2.097	0.716	0.044	0.966	4.000	2.278	0.796	0.050	0.961	2.500
SPNet‡	1.809	0.419	0.032	0.978	1.750	2.100	0.518	0.039	0.972	2.250	2.536	0.715	0.054	0.962	2.500
PromptDA	3.142	1.239	0.071	0.939	6.000	3.316	1.336	0.077	0.931	6.000	3.579	1.470	0.082	0.925	6.000
WorldMirror†	4.103	2.166	0.147	0.836	7.750	4.224	2.248	0.151	0.832	8.250	4.214	2.214	0.147	0.835	8.000
MapAnything	7.393	3.444	0.203	0.822	11.750	8.873	4.927	0.299	0.673	12.750	9.705	5.717	0.318	0.560	14.000
Pow3R†	3.859	2.169	0.179	0.834	8.250	3.910	2.193	0.179	0.835	7.750	3.957	2.193	0.178	0.835	7.750
LDCM (Ours)	**1.795**	**0.404**	**0.024**	**0.978**	**1.000**	**2.010**	**0.476**	**0.029**	**0.974**	**1.000**	**2.280**	**0.603**	**0.036**	**0.967**	**1.250**

Method	Virtual-Lidar-8-Lines					Virtual-Lidar-4-Lines					10% Noise				
	RMSE↓	MAE↓	REL↓	δ_1 ↑	Rk.↓	RMSE↓	MAE↓	REL↓	δ_1 ↑	Rk.↓	RMSE↓	MAE↓	REL↓	δ_1 ↑	Rk.↓
DepthPro	9.539	7.635	0.403	0.177	15.000	9.539	7.635	0.403	0.177	15.000	9.539	7.635	0.403	0.177	14.500
UniDepth V1	5.782	3.841	0.189	0.661	11.750	5.782	3.841	0.189	0.661	11.000	5.782	3.841	0.189	0.661	12.500
UniDepth V2	11.145	8.936	0.515	0.526	15.500	11.145	8.936	0.515	0.526	15.500	11.145	8.936	0.515	0.526	15.000
DepthAnythingV2†	5.911	2.746	0.123	0.875	8.750	6.421	2.974	0.138	0.855	6.250	5.778	2.655	0.119	0.881	9.500
VGGT†	4.836	2.792	0.227	0.780	10.500	5.463	3.182	0.263	0.773	10.000	4.741	2.753	0.225	0.789	11.000
MoGe V1†	7.903	5.351	0.270	0.744	12.500	7.833	4.104	0.241	0.798	11.500	12.694	10.609	0.512	0.488	15.500
MoGe V2	4.807	3.352	0.182	0.680	10.500	4.807	3.352	0.182	0.680	9.250	4.807	3.352	0.182	0.680	11.250
G2-MonoDepth‡	3.611	1.467	0.099	0.909	5.250	5.910	3.230	0.204	0.698	10.750	0.876	0.206	0.016	0.992	2.250
OMNI-DC	3.536	1.228	0.075	0.935	3.750	5.361	2.572	0.158	0.801	6.000	1.058	0.222	0.017	0.991	3.750
PriorDA	2.744	1.019	0.059	0.949	2.000	4.068	1.731	0.106	0.877	2.000	1.957	0.769	0.041	0.971	5.000
SPNet‡	3.286	1.148	0.079	0.939	3.250	4.652	2.188	0.168	0.813	5.000	0.850	0.192	0.014	0.993	1.000
PromptDA	4.106	1.780	0.096	0.908	6.000	5.690	3.010	0.167	0.788	8.000	2.933	1.207	0.068	0.939	6.000
WorldMirror†	4.360	2.294	0.150	0.830	8.250	4.724	2.444	0.151	0.829	4.250	3.049	1.525	0.112	0.891	7.250
MapAnything	10.595	6.288	0.308	0.520	14.500	10.993	6.991	0.346	0.343	14.500	5.845	2.077	0.122	0.884	9.750
Pow3R†	4.045	2.239	0.174	0.835	7.500	4.616	2.587	0.197	0.821	6.000	2.976	1.723	0.144	0.861	8.750
LDCM (Ours)	**2.679**	**0.823**	**0.045**	**0.954**	**1.000**	**3.418**	**1.300**	**0.072**	**0.913**	**1.000**	**1.052**	**0.222**	**0.014**	**0.992**	**2.250**

Method	5%					3%					1%				
	RMSE↓	MAE↓	REL↓	δ_1 ↑	Rk.↓	RMSE↓	MAE↓	REL↓	δ_1 ↑	Rk.↓	RMSE↓	MAE↓	REL↓	δ_1 ↑	Rk.↓
DepthPro	9.539	7.635	0.403	0.177	14.500	9.539	7.635	0.403	0.177	14.500	9.539	7.635	0.403	0.177	13.500
UniDepth V1	5.782	3.841	0.189	0.661	12.250	5.782	3.841	0.189	0.661	12.250	5.782	3.841	0.189	0.661	11.250
UniDepth V2	11.145	8.936	0.515	0.526	15.000	11.145	8.936	0.515	0.526	15.000	11.145	8.936	0.515	0.526	14.250
DepthAnythingV2†	5.891	2.667	0.119	0.881	9.750	5.896	2.666	0.119	0.881	9.250	5.924	2.680	0.119	0.881	8.250
VGGT†	4.732	2.756	0.228	0.781	11.000	4.732	2.759	0.229	0.781	11.000	4.734	2.758	0.229	0.781	10.000
MoGe V1†	12.548	10.462	0.502	0.496	15.500	12.131	10.042	0.480	0.519	15.500	11.346	9.323	0.441	0.558	14.250
MoGe V2	4.807	3.352	0.182	0.680	11.250	4.807	3.352	0.182	0.680	11.000	4.807	3.352	0.182	0.680	10.250
G2-MonoDepth‡	1.076	0.247	0.020	0.989	2.750	1.245	0.285	0.023	0.986	3.250	1.680	0.402	0.032	0.980	4.000
OMNI-DC	1.110	0.224	0.018	0.989	2.250	1.270	0.260	0.020	0.987	2.250	1.649	0.356	0.027	0.981	2.250
PriorDA	1.785	0.645	0.037	0.974	5.000	1.805	0.645	0.038	0.973	5.000	1.895	0.666	0.040	0.970	5.000
SPNet‡	1.029	0.227	0.017	0.990	1.500	1.187	0.258	0.020	0.988	1.250	1.566	0.349	0.027	0.982	1.250
PromptDA	2.941	1.210	0.070	0.937	6.000	2.981	1.206	0.070	0.938	6.000	3.090	1.233	0.073	0.935	6.000
WorldMirror†	3.510	1.836	0.127	0.860	8.250	3.844	2.047	0.141	0.840	8.250	6.659	2.731	0.159	0.860	9.250
MapAnything	5.868	2.073	0.116	0.895	8.750	6.099	2.226	0.125	0.888	9.250	3.796	2.152	0.180	0.833	8.000
Pow3R†	3.365	1.997	0.174	0.823	8.750	3.586	2.105	0.183	0.822	9.000	1.645	0.360	0.022	0.981	2.000
LDCM (Ours)	**1.209**	**0.255**	**0.016**	**0.989**	**2.750**	**1.348**	**0.285**	**0.018**	**0.987**	**2.500**	**1.645**	**0.360**	**0.022**	**0.981**	**2.000**

Method	SIFT					ORB					Average				
	RMSE↓	MAE↓	REL↓	δ_1 ↑	Rk.↓	RMSE↓	MAE↓	REL↓	δ_1 ↑	Rk.↓	RMSE↓	MAE↓	REL↓	δ_1 ↑	Rk.↓
DepthPro	9.539	7.635	0.403	0.177	14.500	9.539	7.635	0.403	0.177	14.500	9.539	7.635	0.403	0.177	14.636
UniDepth V1	5.782	3.841	0.189	0.661	11.750	5.782	3.841	0.189	0.661	11.500	5.782	3.841	0.189	0.661	11.795
UniDepth V2	11.145	8.936	0.515	0.526	15.250	11.145	8.936	0.515	0.526	15.000	11.145	8.936	0.515	0.526	15.250
DepthAnythingV2†	5.948	3.043	0.133	0.836	8.750	6.079	3.170	0.136	0.827	8.500	5.940	2.777	0.124	0.869	8.659
VGGT	5.102	3.192	0.256	0.739	11.000	5.296	3.368	0.267	0.728	10.750	4.898	2.893	0.237	0.772	10.591
MoGe V1†	11.377	9.519	0.472	0.535	15.250	11.684	9.807	0.485	0.518	15.500	10.576	8.340	0.406	0.599	14.250
MoGe V2	4.807	3.352	0.182	0.680	10.250	4.807	3.352	0.182	0.680	9.500	4.807	3.352	0.182	0.680	10.477
G2-MonoDepth‡	2.335	0.800	0.060	0.945	4.750	2.659	0.984	0.068	0.927	5.000	2.393	0.875	0.062	0.938	4.682
OMNI-DC	2.201	0.608	0.040	0.966	3.000	2.606	0.824	0.049	0.951	3.500	2.322	0.726	0.049	0.955	3.341
PriorDA	2.220	0.803	0.046	0.964	4.250	2.587	0.979	0.054	0.952	3.500	2.310	0.858	0.051	0.957	3.932
SPNet‡	1.983	0.549	0.038	0.970	1.750	2.223	0.678	0.044	0.961	1.750	2.111	0.658	0.048	0.959	2.114
PromptDA	3.705	1.572	0.083	0.915	6.000	4.159	1.911	0.102	0.882	6.000	3.604	1.561	0.087	0.912	6.182
WorldMirror†	4.426	2.477	0.166	0.802	7.750	5.995	3.501	0.209	0.696	11.250	4.464	2.317	0.151	0.828	8.045
MapAnything	7.718	3.593	0.208	0.797	11.500	7.540	3.316	0.183	0.821	9.750	7.675	3.891	0.219	0.731	11.318
Pow3R†	4.236	2.551	0.214	0.802	8.750	4.308	2.634	0.213	0.792	8.750	3.682	2.068	0.169	0.840	7.568
LDCM (Ours)	**1.984**	**0.491**	**0.028**	**0.974**	**1.250**	**2.234**	**0.603**	**0.034**	**0.965**	**1.250**	**1.969**	**0.529**	**0.031**	**0.970**	**1.568**

Table 15: **Quantitative comparison of depth completion with baseline methods on the iBims-1 dataset Koch et al. (2018).** Methods marked with † produce relative depth maps, where the metric depth is recovered by optimizing global scale and shift via least squares regression using the sparse depth prior. Methods marked with ‡ use scenario-specific configurations for indoor and outdoor scenes, respectively. The best and the second best results are highlighted.

Method	10% Noise					5%					3%				
	RMSE↓	MAE↓	REL↓	δ_1 ↑	Rk.↓	RMSE↓	MAE↓	REL↓	δ_1 ↑	Rk.↓	RMSE↓	MAE↓	REL↓	δ_1 ↑	Rk.↓
DepthPro	0.605	0.503	0.156	0.829	13.750	0.605	0.503	0.156	0.829	13.750	0.605	0.503	0.156	0.829	13.750
UniDepth V1	1.166	1.082	0.370	0.236	16.000	1.166	1.082	0.370	0.236	16.000	1.166	1.082	0.370	0.236	16.000
UniDepth V2	0.446	0.321	0.100	0.935	12.500	0.446	0.321	0.100	0.935	12.500	0.446	0.321	0.100	0.935	12.500
DepthAnythingV2†	0.332	0.169	0.041	0.980	8.750	0.347	0.172	0.041	0.978	9.250	0.348	0.172	0.041	0.978	9.250
VGGT†	0.339	0.178	0.048	0.965	10.750	0.337	0.176	0.047	0.964	10.500	0.337	0.176	0.047	0.964	10.750
MoGe V1†	0.234	0.117	0.034	0.985	7.000	0.231	0.110	0.031	0.985	7.000	0.231	0.110	0.031	0.985	7.000
MoGe V2	0.633	0.540	0.156	0.707	14.500	0.633	0.540	0.156	0.707	14.500	0.633	0.540	0.156	0.707	14.500
G2-MonoDepth‡	0.106	0.023	0.006	0.996	2.000	0.118	0.026	0.007	0.995	3.500	0.131	0.029	0.008	0.995	3.250
OMNI-DC	0.142	0.031	0.008	0.994	4.000	0.111	0.020	0.005	0.996	1.000	0.124	0.023	0.006	0.995	1.000
PriorDA	0.151	0.052	0.014	0.993	5.000	0.142	0.043	0.011	0.993	5.000	0.146	0.044	0.012	0.993	5.000
SPNet‡	0.102	0.020	0.005	0.996	1.000	0.112	0.022	0.006	0.996	1.750	0.126	0.025	0.006	0.995	1.750
PromptDA	0.191	0.077	0.022	0.988	6.000	0.192	0.076	0.021	0.988	6.000	0.196	0.079	0.022	0.987	6.000
WorldMirror†	0.285	0.174	0.052	0.976	10.000	0.298	0.169	0.047	0.978	9.000	0.305	0.160	0.043	0.975	8.500
MapAnything	0.934	0.317	0.086	0.917	13.000	0.921	0.303	0.080	0.925	13.000	0.925	0.312	0.082	0.925	13.000
Pow3R†	0.272	0.156	0.044	0.977	8.500	0.292	0.157	0.043	0.972	8.750	0.310	0.161	0.043	0.972	9.250
LDCM (Ours)	**0.113**	**0.022**	**0.006**	**0.996**	**2.000**	**0.120**	**0.023**	**0.006**	**0.995**	**3.000**	**0.127**	**0.024**	**0.006**	**0.995**	**1.750**

Method	1%					500					100				
	RMSE↓	MAE↓	REL↓	δ_1 ↑	Rk.↓	RMSE↓	MAE↓	REL↓	δ_1 ↑	Rk.↓	RMSE↓	MAE↓	REL↓	δ_1 ↑	Rk.↓
DepthPro	0.605	0.503	0.156	0.829	13.750	0.605	0.503	0.156	0.829	13.750	0.605	0.503	0.156	0.829	13.750
UniDepth V1	1.166	1.082	0.370	0.236	16.000	1.166	1.082	0.370	0.236	16.000	1.166	1.082	0.370	0.236	16.000
UniDepth V2	0.446	0.321	0.100	0.935	12.500	0.446	0.321	0.100	0.935	12.000	0.446	0.321	0.100	0.935	12.000
DepthAnythingV2†	0.352	0.173	0.041	0.978	9.250	0.381	0.179	0.042	0.978	9.250	0.381	0.183	0.042	0.976	8.500
VGGT†	0.337	0.177	0.047	0.964	10.750	0.338	0.181	0.048	0.961	10.250	0.341	0.183	0.049	0.959	9.500
MoGe V1†	0.231	0.110	0.031	0.985	7.000	0.232	0.111	0.032	0.985	6.500	0.236	0.112	0.032	0.984	4.000
MoGe V2	0.633	0.540	0.156	0.707	14.500	0.633	0.540	0.156	0.707	14.500	0.633	0.540	0.156	0.707	14.500
G2-MonoDepth‡	0.160	0.040	0.010	0.992	4.250	0.232	0.073	0.019	0.986	5.000	0.357	0.178	0.053	0.960	10.000
OMNI-DC	0.148	0.030	0.008	0.993	2.000	0.188	0.050	0.013	0.989	2.500	0.265	0.096	0.025	0.979	4.250
PriorDA	0.156	0.047	0.013	0.992	4.250	0.179	0.057	0.015	0.991	2.750	0.211	0.077	0.020	0.988	1.750
SPNet‡	0.156	0.034	0.008	0.993	2.500	0.211	0.055	0.014	0.988	3.500	0.270	0.092	0.023	0.981	3.750
PromptDA	0.205	0.084	0.023	0.988	6.000	0.237	0.101	0.027	0.986	6.000	0.338	0.153	0.040	0.975	6.250
WorldMirror†	0.326	0.160	0.042	0.971	8.750	0.342	0.168	0.043	0.971	9.250	0.347	0.172	0.044	0.968	8.750
MapAnything	0.923	0.317	0.083	0.924	13.000	0.992	0.407	0.123	0.893	13.500	1.057	0.454	0.125	0.900	13.500
Pow3R†	0.332	0.164	0.042	0.972	9.000	0.343	0.166	0.043	0.972	9.000	0.346	0.167	0.042	0.969	7.500
LDCM (Ours)	**0.142**	**0.029**	**0.007**	**0.994**	**1.000**	**0.169**	**0.041**	**0.011**	**0.991**	**1.000**	**0.202**	**0.061**	**0.015**	**0.988**	**1.000**

Method	SIFT					ORB					Virtual-Lidar-32-Lines				
	RMSE↓	MAE↓	REL↓	δ_1 ↑	Rk.↓	RMSE↓	MAE↓	REL↓	δ_1 ↑	Rk.↓	RMSE↓	MAE↓	REL↓	δ_1 ↑	Rk.↓
DepthPro	0.605	0.503	0.156	0.829	13.750	0.605	0.503	0.156	0.829	13.750	0.605	0.503	0.156	0.829	13.750
UniDepth V1	1.166	1.082	0.370	0.236	16.000	1.166	1.082	0.370	0.236	16.000	1.166	1.082	0.370	0.236	16.000
UniDepth V2	0.446	0.321	0.100	0.935	11.250	0.446	0.321	0.100	0.935	9.750	0.446	0.321	0.100	0.935	12.250
DepthAnythingV2†	0.321	0.185	0.048	0.972	5.750	0.334	0.198	0.052	0.963	4.750	0.373	0.206	0.049	0.969	10.500
VGGT†	0.388	0.256	0.073	0.933	10.750	0.399	0.270	0.077	0.930	8.750	0.337	0.178	0.048	0.963	10.250
MoGe V1†	0.257	0.151	0.048	0.967	4.750	0.270	0.165	0.053	0.957	4.500	0.231	0.110	0.031	0.985	6.500
MoGe V2	0.633	0.540	0.156	0.707	14.500	0.633	0.540	0.156	0.707	14.500	0.633	0.540	0.156	0.707	14.500
G2-MonoDepth‡	0.338	0.197	0.065	0.923	9.000	0.376	0.230	0.076	0.903	8.000	0.193	0.057	0.015	0.990	3.000
OMNI-DC	0.260	0.119	0.036	0.960	4.750	0.313	0.166	0.054	0.925	6.250	0.160	0.036	0.010	0.992	1.000
PriorDA	0.180	0.076	0.022	0.989	2.000	0.216	0.103	0.032	0.982	2.000	0.201	0.088	0.021	0.983	5.500
SPNet‡	0.224	0.096	0.028	0.981	3.000	0.264	0.129	0.041	0.961	3.250	0.173	0.040	0.010	0.992	1.500
PromptDA	0.317	0.182	0.053	0.948	6.500	0.394	0.244	0.072	0.903	8.250	0.209	0.086	0.024	0.986	5.250
WorldMirror†	0.382	0.236	0.066	0.940	8.750	0.567	0.380	0.103	0.897	12.000	0.336	0.161	0.041	0.972	8.000
MapAnything	0.977	0.408	0.115	0.901	13.500	1.002	0.427	0.122	0.896	13.500	0.973	0.365	0.098	0.912	13.250
Pow3R†	0.394	0.254	0.069	0.934	10.250	0.411	0.274	0.078	0.935	9.000	0.336	0.170	0.044	0.969	8.750
LDCM (Ours)	**0.170**	**0.053**	**0.015**	**0.991**	**1.000**	**0.186**	**0.067**	**0.020**	**0.989**	**1.000**	**0.196**	**0.076**	**0.018**	**0.983**	**4.500**

Method	Virtual-Lidar-16-Lines					Virtual-Lidar-8-Lines					Average				
	RMSE↓	MAE↓	REL↓	δ_1 ↑	Rk.↓	RMSE↓	MAE↓	REL↓	δ_1 ↑	Rk.↓	RMSE↓	MAE↓	REL↓	δ_1 ↑	Rk.↓
DepthPro	0.605	0.503	0.156	0.829	13.750	0.605	0.503	0.156	0.829	13.750	0.605	0.503	0.156	0.829	13.750
UniDepth V1	1.166	1.082	0.370	0.236	16.000	1.166	1.082	0.370	0.236	16.000	1.166	1.082	0.370	0.236	16.000
UniDepth V2	0.446	0.321	0.100	0.935	12.000	0.446	0.321	0.100	0.935	12.000	0.446	0.321	0.100	0.935	11.932
DepthAnythingV2†	0.333	0.166	0.040	0.978	8.250	0.336	0.166	0.040	0.979	7.750	0.349	0.179	0.043	0.975	8.295
VGGT†	0.338	0.179	0.048	0.963	10.750	0.339	0.180	0.048	0.962	10.500	0.348	0.194	0.053	0.957	10.318
MoGe V1†	0.232	0.111	0.032	0.985	7.000	0.233	0.111	0.032	0.984	5.250	0.238	0.120	0.035	0.981	6.045
MoGe V2	0.633	0.540	0.156	0.707	14.500	0.633	0.540	0.156	0.707	14.500	0.633	0.540	0.156	0.707	14.500
G2-MonoDepth‡	0.216	0.070	0.018	0.987	5.250	0.273	0.109	0.029	0.978	6.250	0.227	0.094	0.028	0.973	5.409
OMNI-DC	0.176	0.046	0.012	0.990	2.500	0.225	0.075	0.021	0.984	3.000	0.192	0.063	0.018	0.982	2.932
PriorDA	0.169	0.056	0.015	0.991	3.000	0.187	0.070	0.019	0.990	2.000	0.176	0.065	0.018	0.990	3.477
SPNet‡	0.198	0.052	0.013	0.989	3.500	0.241	0.080	0.021	0.984	3.750	0.189	0.059	0.016	0.987	2.659
PromptDA	0.217	0.090	0.025	0.988	5.750	0.242	0.109	0.030	0.984	5.000	0.249	0.116	0.033	0.975	6.091
WorldMirror†	0.337	0.162	0.042	0.971	8.750	0.342	0.168	0.043	0.970	9.500	0.352	0.192	0.051	0.963	9.205
MapAnything	0.972	0.394	0.113	0.901	13.500	0.975	0.410	0.117	0.910	13.500	0.968	0.374	0.104	0.909	13.295
Pow3R†	0.342	0.169	0.043	0.971	10.000	0.343	0.170	0.044	0.971	10.000	0.338	0.183	0.049	0.965	9.091
LDCM (Ours)	**0.165**	**0.039**	**0.010**	**0.992**	**1.000**	**0.181**	**0.050**	**0.013**	**0.991**	**1.000**	**0.161**	**0.044**	**0.012**	**0.991**	**1.659**

Table 16: **Quantitative comparison of depth completion with baseline methods on the indoor scenes of the ETH3D dataset Schops et al. (2017).** Methods marked with † produce relative depth maps, where the metric depth is recovered by optimizing global scale and shift via least squares regression using the sparse depth prior. Methods marked with ‡ use scenario-specific configurations for indoor and outdoor scenes, respectively. The best and the second best results are highlighted.

Method	10% Noise					5%					3%				
	RMSE↓	MAE↓	REL↓	δ_1 ↑	Rk.↓	RMSE↓	MAE↓	REL↓	δ_1 ↑	Rk.↓	RMSE↓	MAE↓	REL↓	δ_1 ↑	Rk.↓
DepthPro	0.831	0.670	0.192	0.705	14.750	0.831	0.670	0.192	0.705	14.500	0.831	0.670	0.192	0.705	14.500
UniDepth V1	2.549	2.330	0.695	0.071	16.000	2.549	2.330	0.695	0.071	16.000	2.549	2.330	0.695	0.071	16.000
UniDepth V2	0.660	0.562	0.169	0.799	13.250	0.660	0.562	0.169	0.799	13.250	0.660	0.562	0.169	0.799	13.250
DepthAnythingV2†	0.808	0.203	0.037	0.989	10.000	1.017	0.220	0.038	0.988	10.500	1.002	0.220	0.038	0.988	10.750
VGGT†	0.391	0.199	0.049	0.966	10.250	0.386	0.201	0.050	0.959	11.000	0.386	0.202	0.050	0.959	10.500
MoGe V1†	0.214	0.122	0.031	0.995	7.000	0.204	0.114	0.028	0.995	7.000	0.204	0.114	0.028	0.994	7.000
MoGe V2	0.542	0.419	0.117	0.784	12.750	0.542	0.419	0.117	0.784	12.750	0.542	0.419	0.117	0.784	12.750
G2-MonoDepth‡	0.055	0.011	0.002	1.000	2.000	0.062	0.012	0.002	1.000	2.750	0.076	0.014	0.003	1.000	3.000
OMNI-DC	0.116	0.017	0.003	0.999	4.250	0.052	0.006	0.001	1.000	1.250	0.063	0.008	0.002	1.000	1.250
PriorDA	0.110	0.040	0.008	0.999	4.500	0.090	0.026	0.006	0.999	5.000	0.093	0.027	0.006	0.999	4.750
SPNet‡	0.076	0.010	0.001	1.000	1.750	0.080	0.010	0.001	1.000	2.250	0.101	0.013	0.002	1.000	2.500
PromptDA	0.173	0.076	0.018	0.996	6.000	0.148	0.067	0.017	0.996	6.000	0.159	0.071	0.019	0.995	6.000
WorldMirror†	0.328	0.197	0.050	0.984	9.500	0.280	0.154	0.038	0.992	8.000	0.261	0.141	0.035	0.991	8.000
MapAnything	1.076	0.272	0.055	0.951	12.750	1.039	0.248	0.046	0.962	12.250	1.083	0.271	0.051	0.958	12.750
Pow3R†	0.323	0.192	0.044	0.980	8.750	0.309	0.180	0.043	0.975	9.500	0.286	0.159	0.038	0.980	9.250
LDCM (Ours)	**0.046**	**0.009**	**0.002**	**1.000**	**1.250**	**0.051**	**0.009**	**0.002**	**1.000**	**1.750**	**0.058**	**0.009**	**0.002**	**1.000**	**1.250**

Method	1%					500					100				
	RMSE↓	MAE↓	REL↓	δ_1 ↑	Rk.↓	RMSE↓	MAE↓	REL↓	δ_1 ↑	Rk.↓	RMSE↓	MAE↓	REL↓	δ_1 ↑	Rk.↓
DepthPro	0.831	0.670	0.192	0.705	14.500	0.831	0.670	0.192	0.705	14.500	0.831	0.670	0.192	0.705	14.250
UniDepth V1	2.549	2.330	0.695	0.071	16.000	2.549	2.330	0.695	0.071	16.000	2.549	2.330	0.695	0.071	16.000
UniDepth V2	0.660	0.562	0.169	0.799	13.250	0.660	0.562	0.169	0.799	13.250	0.660	0.562	0.169	0.799	13.000
DepthAnythingV2†	1.016	0.221	0.038	0.987	11.000	1.016	0.220	0.038	0.987	11.000	1.006	0.222	0.038	0.987	10.250
VGGT†	0.387	0.203	0.050	0.959	10.500	0.389	0.200	0.050	0.962	10.500	0.398	0.198	0.048	0.965	10.250
MoGe V1†	0.205	0.114	0.028	0.994	7.000	0.206	0.114	0.028	0.995	6.000	0.214	0.118	0.029	0.995	3.750
MoGe V2	0.542	0.419	0.117	0.784	12.750	0.542	0.419	0.117	0.784	12.250	0.542	0.419	0.117	0.784	12.250
G2-MonoDepth‡	0.118	0.024	0.005	0.999	3.250	0.215	0.061	0.012	0.997	5.000	0.443	0.190	0.045	0.972	9.750
OMNI-DC	0.089	0.012	0.002	0.999	1.250	0.153	0.031	0.006	0.998	2.500	0.309	0.089	0.017	0.992	4.750
PriorDA	0.103	0.029	0.006	0.999	3.500	0.133	0.037	0.007	0.999	2.500	0.222	0.064	0.012	0.997	2.250
SPNet‡	0.145	0.020	0.003	0.999	3.000	0.223	0.039	0.006	0.998	3.750	0.323	0.085	0.015	0.994	4.250
PromptDA	0.188	0.078	0.019	0.995	6.000	0.268	0.106	0.025	0.990	7.000	0.396	0.154	0.033	0.987	7.500
WorldMirror†	0.241	0.125	0.031	0.992	8.000	0.234	0.121	0.029	0.992	7.500	0.246	0.127	0.031	0.992	5.250
MapAnything	1.162	0.333	0.068	0.945	12.750	1.390	0.549	0.144	0.873	13.250	1.676	0.702	0.149	0.876	13.750
Pow3R†	0.279	0.146	0.034	0.984	9.250	0.287	0.145	0.034	0.985	9.250	0.298	0.150	0.035	0.982	7.250
LDCM (Ours)	**0.074**	**0.012**	**0.002**	**0.999**	**1.000**	**0.106**	**0.021**	**0.004**	**0.999**	**1.000**	**0.157**	**0.041**	**0.008**	**0.998**	**1.000**

Method	SIFT					ORB					Virtual-Lidar-32-Lines				
	RMSE↓	MAE↓	REL↓	δ_1 ↑	Rk.↓	RMSE↓	MAE↓	REL↓	δ_1 ↑	Rk.↓	RMSE↓	MAE↓	REL↓	δ_1 ↑	Rk.↓
DepthPro	0.831	0.670	0.192	0.705	14.750	0.831	0.670	0.192	0.705	14.750	0.831	0.670	0.192	0.705	14.500
UniDepth V1	2.549	2.330	0.695	0.071	16.000	2.549	2.330	0.695	0.071	16.000	2.549	2.330	0.695	0.071	16.000
UniDepth V2	0.660	0.562	0.169	0.799	13.500	0.660	0.562	0.169	0.799	13.500	0.660	0.562	0.169	0.799	13.250
DepthAnythingV2†	0.436	0.179	0.040	0.990	6.500	0.396	0.183	0.042	0.990	5.000	0.918	0.206	0.037	0.989	10.750
VGGT†	0.416	0.242	0.068	0.937	10.000	0.441	0.277	0.084	0.911	10.500	0.387	0.209	0.053	0.953	10.750
MoGe V1†	0.228	0.141	0.040	0.978	4.500	0.250	0.164	0.048	0.965	4.750	0.205	0.115	0.029	0.993	7.000
MoGe V2	0.542	0.419	0.117	0.784	12.500	0.542	0.419	0.117	0.784	12.750	0.542	0.419	0.117	0.784	12.500
G2-MonoDepth‡	0.435	0.234	0.076	0.910	10.500	0.440	0.237	0.077	0.914	9.250	0.158	0.048	0.009	0.998	4.750
OMNI-DC	0.248	0.114	0.035	0.966	5.000	0.284	0.144	0.045	0.954	5.000	0.107	0.017	0.003	0.999	1.500
PriorDA	0.189	0.084	0.028	0.984	2.250	0.227	0.108	0.033	0.980	2.250	0.111	0.030	0.006	0.999	3.000
SPNet‡	0.287	0.108	0.031	0.981	4.000	0.308	0.127	0.036	0.974	3.750	0.164	0.026	0.004	0.999	3.000
PromptDA	0.352	0.205	0.055	0.951	8.750	0.367	0.221	0.061	0.938	7.750	0.182	0.076	0.018	0.997	6.000
WorldMirror†	0.279	0.171	0.046	0.978	6.000	0.494	0.319	0.081	0.936	10.250	0.233	0.122	0.030	0.992	8.000
MapAnything	1.427	0.545	0.129	0.889	13.250	1.353	0.485	0.114	0.907	13.000	1.330	0.460	0.108	0.910	13.000
Pow3R†	0.311	0.174	0.045	0.975	7.000	0.341	0.209	0.055	0.961	6.500	0.283	0.151	0.036	0.979	9.250
LDCM (Ours)	**0.127**	**0.045**	**0.012**	**0.995**	**1.000**	**0.139**	**0.056**	**0.016**	**0.996**	**1.000**	**0.087**	**0.014**	**0.003**	**0.999**	**1.000**

Method	Virtual-Lidar-16-Lines					Virtual-Lidar-8-Lines					Average				
	RMSE↓	MAE↓	REL↓	δ_1 ↑	Rk.↓	RMSE↓	MAE↓	REL↓	δ_1 ↑	Rk.↓	RMSE↓	MAE↓	REL↓	δ_1 ↑	Rk.↓
DepthPro	0.831	0.670	0.192	0.705	14.500	0.831	0.670	0.192	0.705	14.500	0.831	0.670	0.192	0.705	14.545
UniDepth V1	2.549	2.330	0.695	0.071	16.000	2.549	2.330	0.695	0.071	16.000	2.549	2.330	0.695	0.071	16.000
UniDepth V2	0.660	0.562	0.169	0.799	13.250	0.660	0.562	0.169	0.799	13.250	0.660	0.562	0.169	0.799	13.273
DepthAnythingV2†	0.924	0.206	0.037	0.989	10.750	0.889	0.203	0.037	0.988	10.500	0.857	0.208	0.038	0.988	9.727
VGGT†	0.387	0.207	0.053	0.954	10.750	0.393	0.218	0.056	0.949	10.750	0.396	0.214	0.056	0.952	10.523
MoGe V1†	0.206	0.117	0.029	0.993	6.750	0.209	0.121	0.030	0.990	5.250	0.213	0.123	0.032	0.990	6.000
MoGe V2	0.542	0.419	0.117	0.784	12.250	0.542	0.419	0.117	0.784	12.500	0.542	0.419	0.117	0.784	12.545
G2-MonoDepth‡	0.202	0.060	0.012	0.997	4.750	0.315	0.126	0.027	0.990	6.500	0.229	0.092	0.025	0.980	5.591
OMNI-DC	0.139	0.028	0.006	0.998	2.500	0.223	0.061	0.013	0.995	3.000	0.162	0.048	0.012	0.991	2.932
PriorDA	0.129	0.039	0.008	0.999	2.500	0.166	0.059	0.013	0.997	2.000	0.143	0.049	0.012	0.996	3.136
SPNet‡	0.202	0.041	0.007	0.998	3.500	0.285	0.094	0.019	0.994	4.500	0.199	0.052	0.011	0.994	3.295
PromptDA	0.233	0.090	0.021	0.994	6.250	0.289	0.120	0.028	0.990	5.750	0.250	0.115	0.029	0.984	6.636
WorldMirror†	0.234	0.122	0.030	0.992	8.000	0.242	0.131	0.032	0.988	7.250	0.279	0.157	0.039	0.984	7.795
MapAnything	1.323	0.520	0.133	0.890	13.250	1.325	0.487	0.115	0.908	13.000	1.289	0.443	0.101	0.915	13.000
Pow3R†	0.291	0.148	0.034	0.982	9.250	0.289	0.156	0.036	0.978	8.750	0.300	0.165	0.039	0.978	8.545
LDCM (Ours)	**0.104**	**0.020**	**0.004**	**0.999**	**1.000**	**0.136**	**0.034**	**0.007**	**0.998**	**1.000**	**0.099**	**0.025**	**0.006**	**0.998**	**1.114**

Table 17: **Quantitative comparison of depth completion with baseline methods on the outdoor scenes of the ETH3D dataset Schops et al. (2017).** Methods marked with † produce relative depth maps, where the metric depth is recovered by optimizing global scale and shift via least squares regression using the sparse depth prior. Methods marked with ‡ use scenario-specific configurations for indoor and outdoor scenes, respectively. The best and the second best results are highlighted.

Method	Virtual-Lidar-64-Lines					Virtual-Lidar-32-Lines					Virtual-Lidar-16-Lines				
	RMSE↓	MAE↓	REL↓	δ_1 ↑	Rk.↓	RMSE↓	MAE↓	REL↓	δ_1 ↑	Rk.↓	RMSE↓	MAE↓	REL↓	δ_1 ↑	Rk.↓
DepthPro	5.567	4.454	0.411	0.248	15.500	5.567	4.454	0.411	0.248	15.500	5.567	4.454	0.411	0.248	15.500
UniDepth V1	4.414	4.009	0.463	0.160	15.500	4.414	4.009	0.463	0.160	15.500	4.414	4.009	0.463	0.160	15.500
UniDepth V2	2.600	1.775	0.230	0.652	13.500	2.600	1.775	0.230	0.652	13.500	2.600	1.775	0.230	0.652	13.250
DepthAnythingV2†	3.443	0.648	0.058	0.972	10.000	3.361	0.641	0.057	0.973	10.000	3.757	0.673	0.059	0.972	10.000
VGGT†	0.650	0.383	0.056	0.957	9.000	0.651	0.382	0.056	0.957	9.000	0.653	0.384	0.056	0.957	8.500
MoGe V1†	2.554	1.190	0.143	0.876	12.500	2.561	0.801	0.124	0.899	11.250	3.301	0.752	0.111	0.921	11.500
MoGe V2	1.152	0.819	0.111	0.893	11.250	1.152	0.819	0.111	0.893	11.250	1.152	0.819	0.111	0.893	11.250
G2-MonoDepth‡	0.308	0.068	0.011	0.996	4.500	0.442	0.111	0.017	0.992	4.750	0.610	0.175	0.027	0.985	4.750
OMNI-DC	0.234	0.035	0.004	0.997	2.000	0.281	0.050	0.006	0.997	2.000	0.354	0.085	0.010	0.995	2.250
PriorDA	0.267	0.083	0.010	0.996	4.000	0.291	0.090	0.011	0.996	3.500	0.334	0.111	0.014	0.995	2.500
SPNet‡	0.289	0.042	0.005	0.998	2.750	0.474	0.070	0.008	0.996	3.500	0.671	0.123	0.015	0.993	5.000
PromptDA	0.935	0.355	0.044	0.964	7.250	0.972	0.365	0.045	0.961	7.750	1.030	0.371	0.041	0.970	7.500
WorldMirror†	0.584	0.327	0.048	0.963	6.750	0.631	0.352	0.050	0.958	7.250	0.647	0.362	0.052	0.955	7.750
MapAnything	2.781	0.994	0.109	0.897	11.750	2.804	1.092	0.126	0.885	13.000	2.814	1.191	0.148	0.865	12.750
Pow3R†	0.637	0.361	0.053	0.958	8.000	0.636	0.344	0.050	0.964	6.750	0.634	0.337	0.050	0.962	6.500
LDCM (Ours)	**0.204**	**0.033**	**0.004**	**0.998**	**1.000**	**0.246**	**0.042**	**0.005**	**0.998**	**1.000**	**0.294**	**0.059**	**0.007**	**0.997**	**1.000**

Method	Virtual-Lidar-8-Lines					Virtual-Lidar-4-Lines					10% Noise				
	RMSE↓	MAE↓	REL↓	δ_1 ↑	Rk.↓	RMSE↓	MAE↓	REL↓	δ_1 ↑	Rk.↓	RMSE↓	MAE↓	REL↓	δ_1 ↑	Rk.↓
DepthPro	5.567	4.454	0.411	0.248	15.500	5.567	4.454	0.411	0.248	15.500	5.567	4.454	0.411	0.248	15.500
UniDepth V1	4.414	4.009	0.463	0.160	15.500	4.414	4.009	0.463	0.160	15.250	4.414	4.009	0.463	0.160	15.500
UniDepth V2	2.600	1.775	0.230	0.652	13.250	2.600	1.775	0.230	0.652	13.250	2.600	1.775	0.230	0.652	13.750
DepthAnythingV2†	3.392	0.642	0.059	0.971	9.250	3.319	0.608	0.063	0.963	6.000	3.052	0.620	0.057	0.972	10.000
VGGT†	0.670	0.393	0.058	0.953	7.000	0.742	0.463	0.074	0.926	4.500	0.661	0.387	0.054	0.965	7.000
MoGe V1†	3.993	0.707	0.097	0.941	11.500	4.979	0.539	0.097	0.948	8.000	2.184	1.702	0.183	0.838	12.500
MoGe V2	1.152	0.819	0.111	0.893	11.250	1.152	0.819	0.111	0.893	8.750	1.152	0.819	0.111	0.893	11.500
G2-MonoDepth‡	1.005	0.409	0.057	0.954	7.000	1.862	1.117	0.171	0.774	11.750	0.128	0.031	0.004	0.999	3.250
OMNI-DC	0.594	0.221	0.025	0.983	3.000	1.282	0.751	0.095	0.888	8.500	0.177	0.028	0.003	0.999	3.000
PriorDA	0.489	0.181	0.022	0.989	2.000	1.071	0.559	0.090	0.896	6.250	0.280	0.113	0.012	0.997	5.000
SPNet‡	1.104	0.327	0.045	0.970	5.250	2.088	0.898	0.134	0.856	11.000	0.110	0.019	0.002	1.000	1.000
PromptDA	1.311	0.492	0.057	0.952	8.500	1.372	0.749	0.092	0.902	7.500	0.912	0.423	0.049	0.962	8.250
WorldMirror†	0.715	0.406	0.057	0.941	7.250	0.732	0.436	0.071	0.919	4.000	0.694	0.404	0.056	0.972	7.250
MapAnything	2.917	1.231	0.145	0.867	12.750	3.036	1.401	0.153	0.866	12.000	2.189	0.653	0.079	0.921	11.250
Pow3R†	0.645	0.333	0.050	0.962	5.000	0.712	0.390	0.063	0.933	2.500	0.658	0.415	0.056	0.960	8.000
LDCM (Ours)	**0.420**	**0.107**	**0.012**	**0.994**	**1.000**	**0.551**	**0.229**	**0.029**	**0.986**	**1.000**	**0.116**	**0.023**	**0.002**	**0.999**	**1.750**

Method	5%					3%					1%				
	RMSE↓	MAE↓	REL↓	δ_1 ↑	Rk.↓	RMSE↓	MAE↓	REL↓	δ_1 ↑	Rk.↓	RMSE↓	MAE↓	REL↓	δ_1 ↑	Rk.↓
DepthPro	5.567	4.454	0.411	0.248	15.500	5.567	4.454	0.411	0.248	15.500	5.567	4.454	0.411	0.248	15.500
UniDepth V1	4.414	4.009	0.463	0.160	15.500	4.414	4.009	0.463	0.160	15.500	4.414	4.009	0.463	0.160	15.500
UniDepth V2	2.600	1.775	0.230	0.652	13.750	2.600	1.775	0.230	0.652	13.750	2.600	1.775	0.230	0.652	13.750
DepthAnythingV2†	3.707	0.672	0.059	0.971	10.250	3.746	0.673	0.060	0.971	10.250	3.769	0.668	0.060	0.971	10.000
VGGT†	0.649	0.382	0.056	0.959	7.750	0.649	0.382	0.056	0.959	7.250	0.650	0.382	0.055	0.959	8.250
MoGe V1†	2.057	1.574	0.177	0.838	12.500	2.151	1.342	0.157	0.858	12.500	2.139	0.940	0.134	0.884	12.500
MoGe V2	1.152	0.819	0.111	0.893	11.500	1.152	0.819	0.111	0.893	11.500	1.152	0.819	0.111	0.893	11.500
G2-MonoDepth‡	0.156	0.036	0.005	0.999	3.250	0.202	0.044	0.006	0.998	3.750	0.367	0.079	0.012	0.995	4.500
OMNI-DC	0.155	0.020	0.002	0.999	1.500	0.190	0.025	0.003	0.998	2.000	0.255	0.041	0.005	0.997	2.000
PriorDA	0.242	0.079	0.009	0.997	5.000	0.253	0.080	0.009	0.997	5.000	0.281	0.086	0.010	0.996	4.000
SPNet‡	0.143	0.022	0.003	0.999	1.500	0.182	0.028	0.003	0.999	1.750	0.383	0.052	0.006	0.997	3.250
PromptDA	0.817	0.307	0.038	0.966	7.000	0.837	0.311	0.039	0.968	7.000	0.956	0.344	0.043	0.966	7.000
WorldMirror†	0.773	0.415	0.055	0.962	8.000	0.761	0.418	0.056	0.953	8.750	0.699	0.386	0.053	0.953	8.750
MapAnything	2.116	0.593	0.067	0.934	11.000	2.243	0.661	0.074	0.927	11.000	2.451	0.817	0.094	0.911	11.250
Pow3R†	0.644	0.391	0.056	0.955	8.000	0.650	0.383	0.054	0.958	7.750	0.634	0.346	0.051	0.963	7.000
LDCM (Ours)	**0.146**	**0.025**	**0.003**	**0.999**	**2.000**	**0.168**	**0.027**	**0.003**	**0.999**	**1.250**	**0.225**	**0.037**	**0.004**	**0.998**	**1.000**

Method	SIFT					ORB					Average				
	RMSE↓	MAE↓	REL↓	δ_1 ↑	Rk.↓	RMSE↓	MAE↓	REL↓	δ_1 ↑	Rk.↓	RMSE↓	MAE↓	REL↓	δ_1 ↑	Rk.↓
DepthPro	5.567	4.454	0.411	0.248	15.500	5.567	4.454	0.411	0.248	15.500	5.567	4.454	0.411	0.248	15.500
UniDepth V1	4.414	4.009	0.463	0.160	15.250	4.414	4.009	0.463	0.160	15.500	4.414	4.009	0.463	0.160	15.455
UniDepth V2	2.600	1.775	0.230	0.652	13.250	2.600	1.775	0.230	0.652	13.500	2.600	1.775	0.230	0.652	13.500
DepthAnythingV2†	2.613	0.597	0.060	0.964	8.250	2.415	0.603	0.062	0.954	7.500	3.325	0.640	0.059	0.969	9.227
VGGT†	0.727	0.486	0.080	0.913	8.500	0.823	0.582	0.101	0.897	7.750	0.684	0.419	0.064	0.946	7.682
MoGe V1†	4.949	0.572	0.106	0.946	10.500	3.109	0.622	0.116	0.894	11.250	3.089	0.976	0.131	0.895	11.500
MoGe V2	1.152	0.819	0.111	0.893	11.500	1.152	0.819	0.111	0.893	10.000	1.152	0.819	0.111	0.893	11.023
G2-MonoDepth‡	0.924	0.398	0.077	0.918	8.000	0.885	0.404	0.077	0.920	6.250	0.626	0.261	0.042	0.957	5.614
OMNI-DC	0.487	0.177	0.026	0.978	2.750	0.594	0.232	0.033	0.968	3.250	0.418	0.151	0.019	0.982	2.932
PriorDA	0.421	0.172	0.026	0.980	2.000	0.510	0.218	0.033	0.975	2.000	0.404	0.161	0.022	0.983	3.750
SPNet‡	0.826	0.221	0.034	0.974	4.750	0.761	0.231	0.037	0.971	3.750	0.639	0.185	0.027	0.978	3.955
PromptDA	1.076	0.492	0.062	0.938	7.750	1.184	0.583	0.076	0.905	7.750	1.037	0.436	0.053	0.950	7.568
WorldMirror†	0.730	0.460	0.072	0.920	7.500	1.491	0.935	0.123	0.836	11.750	0.769	0.446	0.063	0.939	7.727
MapAnything	2.796	1.145	0.143	0.869	13.000	2.617	0.989	0.124	0.884	12.750	2.615	0.979	0.115	0.893	12.045
Pow3R†	0.686	0.414	0.068	0.933	6.250	0.727	0.474	0.080	0.906	6.250	0.660	0.381	0.057	0.950	6.545
LDCM (Ours)	**0.316**	**0.089**	**0.012**	**0.995**	**1.000**	**0.333**	**0.101**	**0.013**	**0.992**	**1.000**	**0.274**	**0.070**	**0.009**	**0.996**	**1.182**

Table 18: **Quantitative comparison of point map estimation with baseline methods on the KITTI dataset Geiger et al. (2012); Uhrig et al. (2017).** Methods marked with ‡ use scenario-specific configurations for indoor and outdoor scenes, respectively. The best and the second-best results are highlighted.

Method	Lidar-64-Lines					Lidar-32-Lines					Lidar-16-Lines				
	MAE^p ↓	RMSE^p ↓	REL^p ↓	δ_1^p ↑	Rk.↓	MAE^p ↓	RMSE^p ↓	REL^p ↓	δ_1^p ↑	Rk.↓	MAE^p ↓	RMSE^p ↓	REL^p ↓	δ_1^p ↑	Rk.↓
UniDepth V1	2.207	3.540	0.120	0.954	7.750	2.207	3.540	0.120	0.954	7.750	2.207	3.540	0.120	0.954	7.750
UniDepth V2	1.813	3.540	0.096	0.961	7.000	1.813	3.540	0.096	0.961	7.000	1.813	3.540	0.096	0.961	7.000
MoGe V2	3.536	4.899	0.208	0.484	9.000	3.536	4.899	0.208	0.484	9.000	3.536	4.899	0.208	0.484	9.000
G2-MonoDepth‡	1.224	2.183	0.079	0.984	4.000	1.267	2.346	0.080	0.983	3.750	1.386	2.665	0.083	0.979	4.000
OMNI-DC	1.134	1.777	0.071	0.992	2.000	1.198	1.983	0.074	0.988	2.000	1.278	2.231	0.078	0.984	2.000
PriorDA	1.333	2.285	0.080	0.982	5.000	1.394	2.409	0.083	0.979	5.000	1.495	2.607	0.088	0.974	4.750
SPNet‡	1.200	2.113	0.077	0.986	3.000	1.253	2.332	0.080	0.984	3.000	1.341	2.597	0.083	0.980	3.000
PromptDA	1.537	2.826	0.088	0.972	6.000	1.559	2.910	0.088	0.970	6.000	1.659	3.148	0.094	0.963	6.000
LDCM (ours)	**0.851**	**1.656**	**0.049**	**0.993**	**1.000**	**0.881**	**1.812**	**0.051**	**0.991**	**1.000**	**0.934**	**2.017**	**0.052**	**0.989**	**1.000**

Method	Lidar-8-Lines					Lidar-4-Lines					10%				
	MAE^p ↓	RMSE^p ↓	REL^p ↓	δ_1^p ↑	Rk.↓	MAE^p ↓	RMSE^p ↓	REL^p ↓	δ_1^p ↑	Rk.↓	MAE^p ↓	RMSE^p ↓	REL^p ↓	δ_1^p ↑	Rk.↓
UniDepth V1	2.207	3.540	0.120	0.954	7.750	2.207	3.540	0.120	0.954	5.500	2.207	3.540	0.120	0.954	7.750
UniDepth V2	1.813	3.540	0.096	0.961	6.500	1.813	3.540	0.096	0.961	2.000	1.813	3.540	0.096	0.961	6.750
MoGe V2	3.536	4.899	0.208	0.484	9.000	3.536	4.899	0.208	0.484	9.000	3.536	4.899	0.208	0.484	9.000
G2-MonoDepth‡	1.599	3.125	0.092	0.969	4.250	2.195	4.272	0.116	0.922	7.000	1.283	2.366	0.079	0.983	3.500
OMNI-DC	1.408	2.592	0.083	0.978	2.000	1.821	3.760	0.096	0.953	3.750	1.274	2.298	0.079	0.983	2.750
PriorDA	1.623	2.867	0.094	0.966	4.750	1.936	3.706	0.103	0.945	5.000	1.398	2.472	0.083	0.978	5.000
SPNet‡	1.465	2.857	0.086	0.977	3.000	1.878	3.946	0.097	0.955	4.250	1.256	2.309	0.078	0.985	2.250
PromptDA	1.744	3.413	0.096	0.956	6.250	2.187	4.467	0.118	0.932	7.000	1.660	3.133	0.094	0.960	6.250
LDCM (ours)	**1.022**	**2.301**	**0.054**	**0.987**	**1.000**	**1.309**	**3.212**	**0.062**	**0.974**	**1.000**	**0.917**	**1.953**	**0.052**	**0.990**	**1.000**

Method	5%					3%					1%				
	MAE^p ↓	RMSE^p ↓	REL^p ↓	δ_1^p ↑	Rk.↓	MAE^p ↓	RMSE^p ↓	REL^p ↓	δ_1^p ↑	Rk.↓	MAE^p ↓	RMSE^p ↓	REL^p ↓	δ_1^p ↑	Rk.↓
UniDepth V1	2.207	3.540	0.120	0.954	7.750	2.207	3.540	0.120	0.954	7.500	2.207	3.540	0.120	0.954	7.250
UniDepth V2	1.813	3.540	0.096	0.961	6.500	1.813	3.540	0.096	0.961	6.500	1.813	3.540	0.096	0.961	6.000
MoGe V2	3.536	4.899	0.208	0.484	9.000	3.536	4.899	0.208	0.484	9.000	3.536	4.899	0.208	0.484	9.000
G2-MonoDepth‡	1.333	2.519	0.080	0.982	3.500	1.401	2.712	0.082	0.978	3.750	1.679	3.352	0.092	0.963	4.750
OMNI-DC	1.329	2.464	0.081	0.981	3.500	1.388	2.638	0.083	0.978	3.250	1.603	3.196	0.092	0.965	4.000
PriorDA	1.436	2.575	0.084	0.976	5.000	1.476	2.677	0.085	0.974	4.750	1.594	2.998	0.090	0.967	2.750
SPNet‡	1.304	2.454	0.079	0.984	2.000	1.353	2.596	0.081	0.982	2.000	1.512	3.015	0.086	0.975	2.250
PromptDA	1.779	3.312	0.102	0.956	6.500	1.806	3.424	0.102	0.953	6.750	2.082	4.041	0.117	0.934	7.500
LDCM (ours)	**0.958**	**2.088**	**0.053**	**0.988**	**1.000**	**0.881**	**2.129**	**0.047**	**0.987**	**1.000**	**1.007**	**2.483**	**0.051**	**0.983**	**1.000**

Method	SIFT					ORB					Average				
	MAE^p ↓	RMSE^p ↓	REL^p ↓	δ_1^p ↑	Rk.↓	MAE^p ↓	RMSE^p ↓	REL^p ↓	δ_1^p ↑	Rk.↓	MAE^p ↓	RMSE^p ↓	REL^p ↓	δ_1^p ↑	Rk.↓
UniDepth V1	2.207	3.540	0.120	0.954	3.750	2.207	3.540	0.120	0.954	4.000	2.207	3.540	0.120	0.954	6.773
UniDepth V2	1.813	3.540	0.096	0.961	2.000	1.813	3.540	0.096	0.961	2.250	1.813	3.540	0.096	0.961	5.409
MoGe V2	3.536	4.899	0.208	0.484	9.000	3.536	4.899	0.208	0.484	9.000	3.536	4.899	0.208	0.484	9.000
G2-MonoDepth‡	2.736	4.677	0.158	0.795	8.000	2.261	4.085	0.133	0.864	6.750	1.669	3.118	0.098	0.946	4.841
OMNI-DC	2.316	4.173	0.139	0.875	6.000	2.210	4.001	0.136	0.882	6.250	1.542	2.828	0.092	0.960	3.409
PriorDA	1.830	3.358	0.103	0.938	3.000	1.792	3.245	0.104	0.935	2.750	1.573	2.836	0.091	0.965	4.341
SPNet‡	2.096	3.845	0.120	0.888	4.500	1.921	3.631	0.113	0.908	4.500	1.507	2.881	0.089	0.964	3.068
PromptDA	2.609	4.581	0.154	0.868	7.000	2.642	4.475	0.159	0.852	8.000	1.933	3.612	0.110	0.938	6.659
LDCM (ours)	**1.290**	**2.918**	**0.064**	**0.959**	**1.250**	**1.247**	**2.820**	**0.065**	**0.956**	**1.250**	**1.027**	**2.308**	**0.055**	**0.982**	**1.045**

Table 19: **Quantitative comparison of point map estimation with baseline methods on the indoor scenes of the DIODE dataset Vasiljevic et al. (2019).** Methods marked with ‡ use scenario-specific configurations for indoor and outdoor scenes, respectively. The best and the second-best results are highlighted.

Method	10% Noise					5%					3%				
	MAE^p ↓	RMSE^p ↓	REL^p ↓	δ_1^p ↑	Rk.↓	MAE^p ↓	RMSE^p ↓	REL^p ↓	δ_1^p ↑	Rk.↓	MAE^p ↓	RMSE^p ↓	REL^p ↓	δ_1^p ↑	Rk.↓
UniDepth V1	0.911	1.017	0.159	0.779	7.500	0.911	1.017	0.159	0.779	7.500	0.911	1.017	0.159	0.779	7.500
UniDepth V2	0.730	0.872	0.164	0.694	7.500	0.730	0.872	0.164	0.694	7.500	0.730	0.872	0.164	0.694	7.500
MoGe V2	1.048	1.185	0.242	0.410	9.000	1.048	1.185	0.242	0.410	9.000	1.048	1.185	0.242	0.410	9.000
G2-MonoDepth‡	0.118	0.136	0.027	1.000	1.750	0.118	0.137	0.027	1.000	2.250	0.118	0.140	0.028	1.000	2.750
OMNI-DC	0.122	0.163	0.028	0.999	4.000	0.118	0.137	0.027	1.000	2.250	0.118	0.139	0.027	1.000	2.000
PriorDA	0.132	0.179	0.029	0.999	4.750	0.123	0.155	0.028	0.999	5.000	0.123	0.156	0.028	0.999	4.750
SPNet‡	0.118	0.138	0.027	1.000	2.000	0.117	0.135	0.027	1.000	1.750	0.118	0.136	0.027	1.000	1.750
PromptDA	0.138	0.189	0.033	0.997	6.000	0.133	0.180	0.032	0.996	6.000	0.133	0.183	0.031	0.997	6.000
LDCM (ours)	**0.107**	**0.127**	**0.021**	**1.000**	**1.000**	**0.107**	**0.128**	**0.021**	**1.000**	**1.000**	**0.107**	**0.130**	**0.021**	**1.000**	**1.000**

Method	1%					500					100				
	MAE^p ↓	RMSE^p ↓	REL^p ↓	δ_1^p ↑	Rk.↓	MAE^p ↓	RMSE^p ↓	REL^p ↓	δ_1^p ↑	Rk.↓	MAE^p ↓	RMSE^p ↓	REL^p ↓	δ_1^p ↑	Rk.↓
UniDepth V1	0.911	1.017	0.159	0.779	7.500	0.911	1.017	0.159	0.779	7.500	0.911	1.017	0.159	0.779	7.000
UniDepth V2	0.730	0.872	0.164	0.694	7.500	0.730	0.872	0.164	0.694	7.500	0.730	0.872	0.164	0.694	7.000
MoGe V2	1.048	1.185	0.242	0.410	9.000	1.048	1.185	0.242	0.410	9.000	1.048	1.185	0.242	0.410	9.000
G2-MonoDepth‡	0.120	0.149	0.028	0.999	3.250	0.144	0.220	0.034	0.996	5.000	0.651	0.843	0.191	0.598	7.000
OMNI-DC	0.118	0.145	0.028	0.999	2.500	0.127	0.184	0.029	0.998	2.500	0.161	0.275	0.036	0.991	4.000
PriorDA	0.123	0.159	0.028	0.999	3.750	0.128	0.179	0.029	0.999	2.250	0.140	0.217	0.031	0.996	1.500
SPNet‡	0.118	0.140	0.027	0.999	2.000	0.127	0.187	0.029	0.998	2.750	0.156	0.268	0.035	0.992	3.000
PromptDA	0.136	0.191	0.032	0.995	6.000	0.167	0.263	0.042	0.989	6.000	0.228	0.428	0.061	0.978	5.000
LDCM (ours)	**0.107**	**0.134**	**0.021**	**1.000**	**1.000**	**0.111**	**0.167**	**0.022**	**0.999**	**1.000**	**0.128**	**0.235**	**0.024**	**0.996**	**1.250**

Method	SIFT					ORB					Virtual-Lidar-32-Lines				
	MAE^p ↓	RMSE^p ↓	REL^p ↓	δ_1^p ↑	Rk.↓	MAE^p ↓	RMSE^p ↓	REL^p ↓	δ_1^p ↑	Rk.↓	MAE^p ↓	RMSE^p ↓	REL^p ↓	δ_1^p ↑	Rk.↓
UniDepth V1	0.911	1.017	0.159	0.779	7.000	0.911	1.017	0.159	0.779	6.500	0.911	1.017	0.159	0.779	7.500
UniDepth V2	0.730	0.872	0.164	0.694	6.500	0.730	0.872	0.164	0.694	6.500	0.730	0.872	0.164	0.694	7.500
MoGe V2	1.048	1.185	0.242	0.410	8.750	1.048	1.185	0.242	0.410	8.750	1.048	1.185	0.242	0.410	9.000
G2-MonoDepth‡	0.777	1.000	0.251	0.545	7.750	0.866	1.111	0.270	0.504	8.000	0.127	0.178	0.029	0.998	4.750
OMNI-DC	0.313	0.429	0.099	0.867	3.250	0.448	0.616	0.135	0.790	4.250	0.121	0.158	0.028	0.999	1.750
PriorDA	0.174	0.232	0.050	0.975	1.500	0.205	0.280	0.066	0.967	1.500	0.124	0.164	0.029	0.999	3.250
SPNet‡	0.350	0.478	0.117	0.818	5.000	0.398	0.554	0.132	0.794	3.000	0.121	0.163	0.028	0.999	2.000
PromptDA	0.336	0.448	0.108	0.874	3.750	0.511	0.708	0.160	0.791	5.000	0.144	0.211	0.036	0.993	6.000
LDCM (ours)	**0.172**	**0.243**	**0.045**	**0.964**	**1.500**	**0.201**	**0.300**	**0.053**	**0.952**	**1.500**	**0.108**	**0.144**	**0.021**	**0.999**	**1.000**

Method	Virtual-Lidar-16-Lines					Virtual-Lidar-8-Lines					Average				
	MAE^p ↓	RMSE^p ↓	REL^p ↓	δ_1^p ↑	Rk.↓	MAE^p ↓	RMSE^p ↓	REL^p ↓	δ_1^p ↑	Rk.↓	MAE^p ↓	RMSE^p ↓	REL^p ↓	δ_1^p ↑	Rk.↓
UniDepth V1	0.911	1.017	0.159	0.779	7.500	0.911	1.017	0.159	0.779	7.500	0.911	1.017	0.159	0.779	7.318
UniDepth V2	0.730	0.872	0.164	0.694	7.500	0.730	0.872	0.164	0.694	7.500	0.730	0.872	0.164	0.694	7.273
MoGe V2	1.048	1.185	0.242	0.410	9.000	1.048	1.185	0.242	0.410	9.000	1.048	1.185	0.242	0.410	8.955
G2-MonoDepth‡	0.136	0.211	0.031	0.997	5.000	0.175	0.285	0.042	0.987	5.750	0.305	0.401	0.087	0.875	4.841
OMNI-DC	0.126	0.176	0.029	0.998	2.250	0.145	0.229	0.034	0.994	4.000	0.174	0.241	0.045	0.967	2.977
PriorDA	0.127	0.177	0.029	0.999	2.500	0.136	0.197	0.031	0.998	1.250	0.140	0.190	0.034	0.994	2.909
SPNet‡	0.126	0.182	0.029	0.998	2.750	0.139	0.220	0.032	0.996	3.000	0.172	0.236	0.046	0.963	2.636
PromptDA	0.150	0.232	0.036	0.993	6.000	0.170	0.275	0.041	0.987	5.000	0.204	0.301	0.056	0.963	5.523
LDCM (ours)	**0.110**	**0.155**	**0.021**	**0.999**	**1.000**	**0.137**	**0.202**	**0.028**	**0.998**	**1.500**	**0.127**	**0.179**	**0.027**	**0.992**	**1.159**

Table 20: **Quantitative comparison of point map estimation with baseline methods on the outdoor scenes of the DIODE dataset Vasiljevic et al. (2019).** Methods marked with ‡ use scenario-specific configurations for indoor and outdoor scenes, respectively. The best and the second-best results are highlighted.

Method	Virtual-Lidar-64-Lines					Virtual-Lidar-32-Lines					Virtual-Lidar-16-Lines				
	MAE^p ↓	RMSE^p ↓	REL^p ↓	δ_1^p ↑	Rk.↓	MAE^p ↓	RMSE^p ↓	REL^p ↓	δ_1^p ↑	Rk.↓	MAE^p ↓	RMSE^p ↓	REL^p ↓	δ_1^p ↑	Rk.↓
UniDepth V1	4.280	6.372	0.196	0.644	7.500	4.280	6.372	0.196	0.644	7.500	4.280	6.372	0.196	0.644	7.500
UniDepth V2	9.686	12.049	0.521	0.505	9.000	9.686	12.049	0.521	0.505	9.000	9.686	12.049	0.521	0.505	9.000
MoGe V2	4.041	5.505	0.205	0.626	7.500	4.041	5.505	0.205	0.626	7.500	4.041	5.505	0.205	0.626	7.500
G2-MonoDepth	1.867	3.009	0.105	0.962	4.250	1.983	3.309	0.116	0.953	4.500	2.188	3.726	0.130	0.933	5.000
OMNI-DC	1.838	2.970	0.101	0.965	3.000	1.927	3.230	0.108	0.958	3.500	2.102	3.673	0.120	0.946	3.750
PriorDA	1.980	3.071	0.104	0.953	4.750	2.018	3.184	0.106	0.950	4.000	2.087	3.349	0.111	0.944	2.750
SPNet	1.806	2.857	0.099	0.966	2.000	1.885	3.113	0.105	0.960	2.000	2.052	3.547	0.117	0.950	2.500
PromptDA	2.392	4.186	0.123	0.923	6.000	2.484	4.427	0.128	0.916	6.000	2.607	4.638	0.133	0.907	6.000
LDCM (ours)	**1.508**	**2.581**	**0.084**	**0.977**	**1.000**	**1.563**	**2.755**	**0.088**	**0.973**	**1.000**	**1.667**	**3.022**	**0.093**	**0.965**	**1.000**

Method	Virtual-Lidar-8-Lines					Virtual-Lidar-4-Lines					10% Noise				
	MAE^p ↓	RMSE^p ↓	REL^p ↓	δ_1^p ↑	Rk.↓	MAE^p ↓	RMSE^p ↓	REL^p ↓	δ_1^p ↑	Rk.↓	MAE^p ↓	RMSE^p ↓	REL^p ↓	δ_1^p ↑	Rk.↓
UniDepth V1	4.280	6.372	0.196	0.644	7.500	4.280	6.372	0.196	0.644	6.250	4.280	6.372	0.196	0.644	7.500
UniDepth V2	9.686	12.049	0.521	0.505	9.000	9.686	12.049	0.521	0.505	9.000	9.686	12.049	0.521	0.505	9.000
MoGe V2	4.041	5.505	0.205	0.626	7.500	4.041	5.505	0.205	0.626	5.750	4.041	5.505	0.205	0.626	7.500
G2-MonoDepth	2.659	4.565	0.152	0.887	5.250	4.215	6.818	0.237	0.658	7.000	1.645	2.195	0.087	0.980	2.750
OMNI-DC	2.503	4.513	0.133	0.916	3.750	3.689	6.325	0.200	0.769	4.500	1.661	2.301	0.087	0.980	3.500
PriorDA	2.272	3.798	0.118	0.929	2.000	2.921	5.112	0.155	0.857	2.000	2.035	3.117	0.102	0.951	5.000
SPNet	2.359	4.143	0.134	0.923	3.250	3.125	5.372	0.194	0.827	3.000	1.638	2.207	0.085	0.981	2.250
PromptDA	2.896	5.216	0.144	0.886	5.750	4.086	6.913	0.208	0.762	6.500	2.385	3.954	0.119	0.920	6.000
LDCM (ours)	**1.850**	**3.456**	**0.099**	**0.953**	**1.000**	**2.313**	**4.361**	**0.119**	**0.905**	**1.000**	**1.345**	**2.032**	**0.076**	**0.991**	**1.000**

Method	5%					3%					1%				
	MAE^p ↓	RMSE^p ↓	REL^p ↓	δ_1^p ↑	Rk.↓	MAE^p ↓	RMSE^p ↓	REL^p ↓	δ_1^p ↑	Rk.↓	MAE^p ↓	RMSE^p ↓	REL^p ↓	δ_1^p ↑	Rk.↓
UniDepth V1	4.280	6.372	0.196	0.644	7.500	4.280	6.372	0.196	0.644	7.500	4.280	6.372	0.196	0.644	7.500
UniDepth V2	9.686	12.049	0.521	0.505	9.000	9.686	12.049	0.521	0.505	9.000	9.686	12.049	0.521	0.505	9.000
MoGe V2	4.041	5.505	0.205	0.626	7.500	4.041	5.505	0.205	0.626	7.500	4.041	5.505	0.205	0.626	7.500
G2-MonoDepth	1.671	2.313	0.089	0.977	3.750	1.702	2.437	0.092	0.975	3.750	1.798	2.796	0.099	0.967	4.000
OMNI-DC	1.670	2.335	0.088	0.978	3.250	1.698	2.450	0.091	0.976	3.250	1.777	2.754	0.096	0.969	3.000
PriorDA	1.950	2.933	0.101	0.955	5.000	1.951	2.947	0.101	0.955	5.000	1.973	3.029	0.103	0.953	5.000
SPNet	1.655	2.265	0.087	0.979	2.000	1.679	2.362	0.089	0.977	2.000	1.750	2.650	0.095	0.971	2.000
PromptDA	2.336	3.900	0.119	0.923	6.000	2.356	3.962	0.120	0.923	6.000	2.444	4.183	0.127	0.919	6.000
LDCM (ours)	**1.366**	**2.098**	**0.077**	**0.988**	**1.000**	**1.394**	**2.202**	**0.079**	**0.986**	**1.000**	**1.462**	**2.436**	**0.082**	**0.980**	**1.000**

Method	SIFT					ORB					Average				
	MAE^p ↓	RMSE^p ↓	REL^p ↓	δ_1^p ↑	Rk.↓	MAE^p ↓	RMSE^p ↓	REL^p ↓	δ_1^p ↑	Rk.↓	MAE^p ↓	RMSE^p ↓	REL^p ↓	δ_1^p ↑	Rk.↓
UniDepth V1	4.280	6.372	0.196	0.644	7.500	4.280	6.372	0.196	0.644	7.500	4.280	6.372	0.196	0.644	7.386
UniDepth V2	9.686	12.049	0.521	0.505	9.000	9.686	12.049	0.521	0.505	9.000	9.686	12.049	0.521	0.505	9.000
MoGe V2	4.041	5.505	0.205	0.626	7.500	4.041	5.505	0.205	0.626	7.500	4.041	5.505	0.205	0.626	7.341
G2-MonoDepth	2.120	3.399	0.121	0.924	5.000	2.291	3.734	0.126	0.903	5.000	2.194	3.482	0.123	0.920	4.568
OMNI-DC	1.971	3.284	0.104	0.952	3.000	2.146	3.692	0.110	0.933	3.000	2.089	3.412	0.113	0.940	3.409
PriorDA	2.078	3.326	0.106	0.944	4.000	2.232	3.698	0.113	0.927	4.000	2.136	3.415	0.111	0.938	3.955
SPNet	1.883	2.993	0.102	0.956	2.000	1.962	3.215	0.104	0.946	2.000	1.981	3.157	0.110	0.949	2.273
PromptDA	2.699	4.737	0.132	0.894	6.000	3.043	5.181	0.150	0.856	6.000	2.703	4.663	0.137	0.894	6.023
LDCM (ours)	**1.551**	**2.734**	**0.086**	**0.974**	**1.000**	**1.642**	**2.996**	**0.090**	**0.962**	**1.000**	**1.606**	**2.788**	**0.088**	**0.969**	**1.000**

Table 21: **Quantitative comparison of point map estimation with baseline methods on the iBims-1 dataset Koch et al. (2018).** Methods marked with ‡ use scenario-specific configurations for indoor and outdoor scenes, respectively. The best and the second-best results are highlighted.

Method	10% Noise					5%					3%				
	MAE^p ↓	$RMSE^p$ ↓	REL^p ↓	δ_1^p ↑	Rk.↓	MAE^p ↓	$RMSE^p$ ↓	REL^p ↓	δ_1^p ↑	Rk.↓	MAE^p ↓	$RMSE^p$ ↓	REL^p ↓	δ_1^p ↑	Rk.↓
UniDepth V1	1.154	1.239	0.370	0.239	9.000	1.154	1.239	0.370	0.239	9.000	1.154	1.239	0.370	0.239	9.000
UniDepth V2	0.365	0.489	0.107	0.932	7.000	0.365	0.489	0.107	0.932	7.000	0.365	0.489	0.107	0.932	7.000
MoGe V2	0.574	0.667	0.156	0.740	8.000	0.574	0.667	0.156	0.740	8.000	0.574	0.667	0.156	0.740	8.000
G2-MonoDepth‡	0.131	0.181	0.036	0.995	3.000	0.133	0.191	0.036	0.994	3.500	0.136	0.201	0.037	0.994	3.500
OMNI-DC	0.137	0.209	0.037	0.993	4.000	0.131	0.186	0.036	0.995	2.250	0.133	0.197	0.037	0.994	3.000
PriorDA	0.145	0.213	0.040	0.993	4.750	0.142	0.210	0.039	0.992	5.000	0.143	0.213	0.039	0.992	5.000
SPNet‡	0.128	0.175	0.035	0.996	1.750	0.130	0.181	0.036	0.995	1.750	0.132	0.189	0.036	0.995	1.750
PromptDA	0.163	0.257	0.045	0.988	6.000	0.165	0.261	0.045	0.987	6.000	0.166	0.263	0.045	0.988	6.000
LDCM (ours)	**0.075**	**0.151**	**0.021**	**0.996**	**1.000**	**0.076**	**0.158**	**0.022**	**0.995**	**1.000**	**0.078**	**0.164**	**0.022**	**0.995**	**1.000**

Method	1%					500					100				
	MAE^p ↓	$RMSE^p$ ↓	REL^p ↓	δ_1^p ↑	Rk.↓	MAE^p ↓	$RMSE^p$ ↓	REL^p ↓	δ_1^p ↑	Rk.↓	MAE^p ↓	$RMSE^p$ ↓	REL^p ↓	δ_1^p ↑	Rk.↓
UniDepth V1	1.154	1.239	0.370	0.239	9.000	1.154	1.239	0.370	0.239	9.000	1.154	1.239	0.370	0.239	9.000
UniDepth V2	0.365	0.489	0.107	0.932	7.000	0.365	0.489	0.107	0.932	7.000	0.365	0.489	0.107	0.932	7.000
MoGe V2	0.574	0.667	0.156	0.740	8.000	0.574	0.667	0.156	0.740	8.000	0.574	0.667	0.156	0.740	8.000
G2-MonoDepth‡	0.143	0.226	0.039	0.991	4.250	0.166	0.274	0.044	0.985	5.000	0.249	0.392	0.069	0.958	6.000
OMNI-DC	0.138	0.214	0.038	0.992	2.500	0.152	0.247	0.042	0.988	3.000	0.187	0.310	0.051	0.977	4.000
PriorDA	0.146	0.221	0.040	0.991	4.500	0.153	0.236	0.042	0.990	2.750	0.168	0.281	0.045	0.987	2.000
SPNet‡	0.138	0.213	0.037	0.992	2.000	0.151	0.253	0.041	0.988	2.750	0.176	0.311	0.046	0.982	3.250
PromptDA	0.172	0.275	0.046	0.987	6.000	0.186	0.300	0.049	0.985	5.750	0.216	0.352	0.057	0.980	4.750
LDCM (ours)	**0.082**	**0.177**	**0.023**	**0.994**	**1.000**	**0.094**	**0.204**	**0.026**	**0.991**	**1.000**	**0.112**	**0.241**	**0.030**	**0.988**	**1.000**

Method	SIFT					ORB					Virtual-Lidar-32-Lines				
	MAE^p ↓	$RMSE^p$ ↓	REL^p ↓	δ_1^p ↑	Rk.↓	MAE^p ↓	$RMSE^p$ ↓	REL^p ↓	δ_1^p ↑	Rk.↓	MAE^p ↓	$RMSE^p$ ↓	REL^p ↓	δ_1^p ↑	Rk.↓
UniDepth V1	1.154	1.239	0.370	0.239	9.000	1.154	1.239	0.370	0.239	9.000	1.154	1.239	0.370	0.239	9.000
UniDepth V2	0.365	0.489	0.107	0.932	6.750	0.365	0.489	0.107	0.932	6.250	0.365	0.489	0.107	0.932	7.000
MoGe V2	0.574	0.667	0.156	0.740	8.000	0.574	0.667	0.156	0.740	8.000	0.574	0.667	0.156	0.740	8.000
G2-MonoDepth‡	0.273	0.396	0.082	0.920	6.250	0.303	0.432	0.092	0.900	5.750	0.154	0.255	0.041	0.989	4.000
OMNI-DC	0.210	0.324	0.059	0.958	4.000	0.251	0.375	0.074	0.925	4.250	0.143	0.227	0.039	0.991	2.750
PriorDA	0.164	0.242	0.046	0.988	2.000	0.184	0.273	0.053	0.981	2.000	0.188	0.270	0.048	0.982	5.750
SPNet‡	0.170	0.259	0.048	0.985	3.000	0.192	0.290	0.056	0.971	3.000	0.142	0.226	0.038	0.991	2.000
PromptDA	0.258	0.378	0.072	0.947	5.000	0.315	0.453	0.088	0.903	5.750	0.174	0.277	0.047	0.986	5.250
LDCM (ours)	**0.103**	**0.208**	**0.029**	**0.990**	**1.000**	**0.119**	**0.230**	**0.034**	**0.986**	**1.000**	**0.085**	**0.185**	**0.024**	**0.993**	**1.000**

Method	Virtual-Lidar-16-Lines					Virtual-Lidar-8-Lines					Average				
	MAE^p ↓	$RMSE^p$ ↓	REL^p ↓	δ_1^p ↑	Rk.↓	MAE^p ↓	$RMSE^p$ ↓	REL^p ↓	δ_1^p ↑	Rk.↓	MAE^p ↓	$RMSE^p$ ↓	REL^p ↓	δ_1^p ↑	Rk.↓
UniDepth V1	1.154	1.239	0.370	0.239	9.000	1.154	1.239	0.370	0.239	9.000	1.154	1.239	0.370	0.239	9.000
UniDepth V2	0.365	0.489	0.107	0.932	7.000	0.365	0.489	0.107	0.932	7.000	0.365	0.489	0.107	0.932	6.909
MoGe V2	0.574	0.667	0.156	0.740	8.000	0.574	0.667	0.156	0.740	8.000	0.574	0.667	0.156	0.740	8.000
G2-MonoDepth‡	0.165	0.277	0.044	0.986	5.250	0.197	0.328	0.052	0.977	5.750	0.186	0.287	0.052	0.972	4.750
OMNI-DC	0.150	0.240	0.041	0.989	2.750	0.173	0.284	0.048	0.982	4.250	0.164	0.256	0.046	0.980	3.341
PriorDA	0.152	0.233	0.041	0.990	2.750	0.162	0.248	0.044	0.988	2.000	0.159	0.240	0.043	0.989	3.500
SPNet‡	0.150	0.248	0.040	0.989	2.750	0.168	0.280	0.045	0.985	3.000	0.152	0.239	0.042	0.988	2.455
PromptDA	0.177	0.282	0.047	0.987	5.750	0.193	0.305	0.052	0.983	4.750	0.199	0.309	0.054	0.975	5.545
LDCM (ours)	**0.091**	**0.198**	**0.025**	**0.992**	**1.000**	**0.101**	**0.215**	**0.028**	**0.990**	**1.000**	**0.092**	**0.194**	**0.026**	**0.992**	**1.000**

Table 22: **Quantitative comparison of point map estimation with baseline methods on the indoor scenes of the ETH3D dataset Schops et al. (2017).** Methods marked with ‡ use scenario-specific configurations for indoor and outdoor scenes, respectively. The best and the second-best results are highlighted.

Method	10% Noise					5%					3%				
	MAE^p ↓	RMSE^p ↓	REL^p ↓	δ_1^p ↑	Rk.↓	MAE^p ↓	RMSE^p ↓	REL^p ↓	δ_1^p ↑	Rk.↓	MAE^p ↓	RMSE^p ↓	REL^p ↓	δ_1^p ↑	Rk.↓
UniDepth V1	2.429	2.649	0.641	0.066	9.000	2.429	2.649	0.641	0.066	9.000	2.429	2.649	0.641	0.066	9.000
UniDepth V2	0.624	0.726	0.166	0.825	8.000	0.624	0.726	0.166	0.825	8.000	0.624	0.726	0.166	0.825	8.000
MoGe V2	0.500	0.620	0.123	0.839	7.000	0.500	0.620	0.123	0.839	7.000	0.500	0.620	0.123	0.839	7.000
G2-MonoDepth‡	0.361	0.412	0.088	0.956	2.750	0.362	0.416	0.088	0.956	4.000	0.363	0.421	0.089	0.956	4.500
OMNI-DC	0.367	0.436	0.089	0.954	5.250	0.361	0.413	0.088	0.956	3.000	0.361	0.417	0.088	0.956	3.000
PriorDA	0.371	0.438	0.089	0.956	5.000	0.365	0.427	0.089	0.956	5.250	0.365	0.429	0.089	0.956	5.000
SPNet‡	0.361	0.414	0.088	0.956	3.000	0.361	0.413	0.088	0.956	3.000	0.361	0.419	0.088	0.956	3.250
PromptDA	0.331	0.417	0.078	0.968	2.500	0.319	0.397	0.078	0.967	2.000	0.321	0.404	0.078	0.967	2.000
LDCM (ours)	**0.256**	**0.300**	**0.070**	**0.999**	**1.000**	**0.255**	**0.300**	**0.070**	**0.999**	**1.000**	**0.255**	**0.302**	**0.070**	**0.999**	**1.000**

Method	1%					500					100				
	MAE^p ↓	RMSE^p ↓	REL^p ↓	δ_1^p ↑	Rk.↓	MAE^p ↓	RMSE^p ↓	REL^p ↓	δ_1^p ↑	Rk.↓	MAE^p ↓	RMSE^p ↓	REL^p ↓	δ_1^p ↑	Rk.↓
UniDepth V1	2.429	2.649	0.641	0.066	9.000	2.429	2.649	0.641	0.066	9.000	2.429	2.649	0.641	0.066	9.000
UniDepth V2	0.624	0.726	0.166	0.825	8.000	0.624	0.726	0.166	0.825	8.000	0.624	0.726	0.166	0.825	8.000
MoGe V2	0.500	0.620	0.123	0.839	7.000	0.500	0.620	0.123	0.839	7.000	0.500	0.620	0.123	0.839	6.750
G2-MonoDepth‡	0.367	0.440	0.089	0.955	5.000	0.388	0.511	0.092	0.952	6.000	0.468	0.662	0.109	0.915	6.250
OMNI-DC	0.363	0.428	0.089	0.956	3.000	0.372	0.460	0.090	0.954	3.500	0.407	0.566	0.095	0.947	4.750
PriorDA	0.367	0.435	0.089	0.956	3.750	0.371	0.449	0.090	0.955	2.750	0.385	0.486	0.092	0.952	2.500
SPNet‡	0.365	0.439	0.089	0.956	3.750	0.375	0.484	0.090	0.954	4.000	0.399	0.559	0.093	0.950	3.750
PromptDA	0.328	0.423	0.079	0.966	2.000	0.348	0.485	0.082	0.963	2.750	0.396	0.608	0.088	0.955	3.000
LDCM (ours)	**0.257**	**0.311**	**0.070**	**0.998**	**1.000**	**0.263**	**0.334**	**0.071**	**0.998**	**1.000**	**0.279**	**0.382**	**0.073**	**0.996**	**1.000**

Method	SIFT					ORB					Virtual-Lidar-32-Lines				
	MAE^p ↓	RMSE^p ↓	REL^p ↓	δ_1^p ↑	Rk.↓	MAE^p ↓	RMSE^p ↓	REL^p ↓	δ_1^p ↑	Rk.↓	MAE^p ↓	RMSE^p ↓	REL^p ↓	δ_1^p ↑	Rk.↓
UniDepth V1	2.429	2.649	0.641	0.066	9.000	2.429	2.649	0.641	0.066	9.000	2.429	2.649	0.641	0.066	9.000
UniDepth V2	0.624	0.726	0.166	0.825	8.000	0.624	0.726	0.166	0.825	8.000	0.624	0.726	0.166	0.825	8.000
MoGe V2	0.500	0.620	0.123	0.839	6.250	0.500	0.620	0.123	0.839	6.250	0.500	0.620	0.123	0.839	7.000
G2-MonoDepth‡	0.517	0.675	0.136	0.844	6.750	0.520	0.695	0.135	0.853	6.750	0.376	0.460	0.091	0.953	6.000
OMNI-DC	0.429	0.532	0.107	0.904	4.500	0.447	0.567	0.112	0.890	4.250	0.365	0.437	0.089	0.955	3.250
PriorDA	0.394	0.477	0.099	0.939	2.000	0.408	0.511	0.101	0.936	2.000	0.367	0.438	0.089	0.956	3.500
SPNet‡	0.408	0.515	0.100	0.924	3.000	0.419	0.539	0.102	0.922	3.000	0.367	0.450	0.089	0.955	4.000
PromptDA	0.436	0.557	0.106	0.909	4.500	0.455	0.582	0.112	0.893	4.500	0.326	0.420	0.078	0.968	2.000
LDCM (ours)	**0.279**	**0.350**	**0.075**	**0.991**	**1.000**	**0.285**	**0.360**	**0.077**	**0.986**	**1.000**	**0.258**	**0.319**	**0.070**	**0.998**	**1.000**

Method	Virtual-Lidar-16-Lines					Virtual-Lidar-8-Lines					Average				
	MAE^p ↓	RMSE^p ↓	REL^p ↓	δ_1^p ↑	Rk.↓	MAE^p ↓	RMSE^p ↓	REL^p ↓	δ_1^p ↑	Rk.↓	MAE^p ↓	RMSE^p ↓	REL^p ↓	δ_1^p ↑	Rk.↓
UniDepth V1	2.429	2.649	0.641	0.066	9.000	2.429	2.649	0.641	0.066	9.000	2.429	2.649	0.641	0.066	9.000
UniDepth V2	0.624	0.726	0.166	0.825	8.000	0.624	0.726	0.166	0.825	8.000	0.624	0.726	0.166	0.825	8.000
MoGe V2	0.500	0.620	0.123	0.839	7.000	0.500	0.620	0.123	0.839	7.000	0.500	0.620	0.123	0.839	6.841
G2-MonoDepth‡	0.383	0.487	0.092	0.952	6.000	0.421	0.563	0.098	0.943	6.000	0.411	0.522	0.101	0.930	5.455
OMNI-DC	0.370	0.451	0.090	0.955	3.000	0.389	0.505	0.093	0.950	4.000	0.385	0.474	0.094	0.943	3.773
PriorDA	0.371	0.447	0.090	0.955	3.000	0.379	0.465	0.091	0.952	2.750	0.377	0.455	0.092	0.952	3.409
SPNet‡	0.373	0.469	0.090	0.954	4.500	0.399	0.523	0.094	0.948	5.000	0.381	0.475	0.092	0.948	3.659
PromptDA	0.338	0.459	0.080	0.965	2.500	0.360	0.500	0.085	0.959	2.250	0.360	0.477	0.086	0.953	2.727
LDCM (ours)	**0.263**	**0.332**	**0.071**	**0.998**	**1.000**	**0.272**	**0.354**	**0.072**	**0.996**	**1.000**	**0.266**	**0.331**	**0.072**	**0.996**	**1.000**

Table 23: **Quantitative comparison of point map estimation with baseline methods on the outdoor scenes of the ETH3D dataset Schops et al. (2017).** Methods marked with ‡ use scenario-specific configurations for indoor and outdoor scenes, respectively. The best and the second-best results are highlighted.

Method	Virtual-Lidar-64-Lines					Virtual-Lidar-32-Lines					Virtual-Lidar-16-Lines				
	MAE^p ↓	RMSE^p ↓	REL^p ↓	δ_1^p ↑	Rk.↓	MAE^p ↓	RMSE^p ↓	REL^p ↓	δ_1^p ↑	Rk.↓	MAE^p ↓	RMSE^p ↓	REL^p ↓	δ_1^p ↑	Rk.↓
UniDepth V1	4.653	5.100	0.461	0.145	9.000	4.653	5.100	0.461	0.145	9.000	4.653	5.100	0.461	0.145	9.000
UniDepth V2	1.879	2.844	0.216	0.712	8.000	1.879	2.844	0.216	0.712	8.000	1.879	2.844	0.216	0.712	8.000
MoGe V2	0.931	1.206	0.115	0.890	6.750	0.931	1.206	0.115	0.890	6.750	0.931	1.206	0.115	0.890	6.500
G2-MonoDepth‡	0.638	0.843	0.088	0.929	4.250	0.665	0.943	0.092	0.924	4.750	0.713	1.091	0.098	0.916	5.250
OMNI-DC	0.626	0.793	0.086	0.931	2.000	0.634	0.823	0.087	0.930	2.250	0.655	0.871	0.089	0.927	2.250
PriorDA	0.641	0.804	0.087	0.929	3.750	0.646	0.818	0.088	0.929	2.750	0.657	0.846	0.089	0.927	2.250
SPNet‡	0.631	0.893	0.087	0.931	3.250	0.653	1.069	0.089	0.929	4.000	0.704	1.354	0.096	0.925	5.000
PromptDA	0.756	1.329	0.094	0.923	6.250	0.762	1.365	0.094	0.921	6.250	0.772	1.431	0.092	0.927	4.750
LDCM (ours)	**0.393**	**0.510**	**0.041**	**0.998**	**1.000**	**0.402**	**0.539**	**0.042**	**0.998**	**1.000**	**0.414**	**0.572**	**0.043**	**0.997**	**1.000**

Method	Virtual-Lidar-8-Lines					Virtual-Lidar-4-Lines					10% Noise				
	MAE^p ↓	RMSE^p ↓	REL^p ↓	δ_1^p ↑	Rk.↓	MAE^p ↓	RMSE^p ↓	REL^p ↓	δ_1^p ↑	Rk.↓	MAE^p ↓	RMSE^p ↓	REL^p ↓	δ_1^p ↑	Rk.↓
UniDepth V1	4.653	5.100	0.461	0.145	9.000	4.653	5.100	0.461	0.145	9.000	4.653	5.100	0.461	0.145	9.000
UniDepth V2	1.879	2.844	0.216	0.712	8.000	1.879	2.844	0.216	0.712	8.000	1.879	2.844	0.216	0.712	8.000
MoGe V2	0.931	1.206	0.115	0.890	5.500	0.931	1.206	0.115	0.890	2.000	0.931	1.206	0.115	0.890	7.000
G2-MonoDepth‡	0.907	1.448	0.118	0.876	6.250	1.541	2.283	0.201	0.724	6.750	0.618	0.732	0.085	0.932	3.000
OMNI-DC	0.757	1.067	0.098	0.913	3.000	1.209	1.726	0.143	0.820	5.000	0.623	0.758	0.085	0.931	3.750
PriorDA	0.705	0.957	0.093	0.921	2.000	1.030	1.479	0.140	0.850	3.500	0.657	0.817	0.088	0.930	5.000
SPNet‡	0.858	1.816	0.116	0.902	5.500	1.222	2.483	0.160	0.823	6.000	0.613	0.725	0.084	0.933	2.000
PromptDA	0.872	1.711	0.103	0.913	4.500	1.137	1.783	0.131	0.863	3.750	0.715	1.180	0.088	0.929	5.750
LDCM (ours)	**0.451**	**0.676**	**0.046**	**0.994**	**1.000**	**0.552**	**0.821**	**0.058**	**0.982**	**1.000**	**0.394**	**0.476**	**0.040**	**0.999**	**1.000**

Method	5%					3%					1%				
	MAE^p ↓	RMSE^p ↓	REL^p ↓	δ_1^p ↑	Rk.↓	MAE^p ↓	RMSE^p ↓	REL^p ↓	δ_1^p ↑	Rk.↓	MAE^p ↓	RMSE^p ↓	REL^p ↓	δ_1^p ↑	Rk.↓
UniDepth V1	4.653	5.100	0.461	0.145	9.000	4.653	5.100	0.461	0.145	9.000	4.653	5.100	0.461	0.145	9.000
UniDepth V2	1.879	2.844	0.216	0.712	8.000	1.879	2.844	0.216	0.712	8.000	1.879	2.844	0.216	0.712	8.000
MoGe V2	0.931	1.206	0.115	0.890	7.000	0.931	1.206	0.115	0.890	6.750	0.931	1.206	0.115	0.890	6.750
G2-MonoDepth‡	0.621	0.748	0.085	0.932	2.750	0.626	0.776	0.086	0.931	3.750	0.648	0.894	0.089	0.927	4.500
OMNI-DC	0.617	0.746	0.085	0.932	2.000	0.619	0.761	0.085	0.932	2.000	0.629	0.805	0.086	0.930	2.000
PriorDA	0.638	0.789	0.087	0.930	5.000	0.639	0.795	0.087	0.930	4.750	0.644	0.814	0.088	0.929	3.250
SPNet‡	0.617	0.760	0.085	0.932	2.500	0.621	0.801	0.085	0.932	3.000	0.644	0.994	0.089	0.930	3.500
PromptDA	0.707	1.202	0.089	0.929	6.000	0.733	1.253	0.091	0.926	6.250	0.771	1.358	0.095	0.921	6.250
LDCM (ours)	**0.394**	**0.486**	**0.040**	**0.999**	**1.000**	**0.396**	**0.498**	**0.040**	**0.999**	**1.000**	**0.405**	**0.539**	**0.041**	**0.998**	**1.000**

Method	SIFT					ORB					Average				
	MAE^p ↓	RMSE^p ↓	REL^p ↓	δ_1^p ↑	Rk.↓	MAE^p ↓	RMSE^p ↓	REL^p ↓	δ_1^p ↑	Rk.↓	MAE^p ↓	RMSE^p ↓	REL^p ↓	δ_1^p ↑	Rk.↓
UniDepth V1	4.653	5.100	0.461	0.145	9.000	4.653	5.100	0.461	0.145	9.000	4.653	5.100	0.461	0.145	9.000
UniDepth V2	1.879	2.844	0.216	0.712	8.000	1.879	2.844	0.216	0.712	8.000	1.879	2.844	0.216	0.712	8.000
MoGe V2	0.931	1.206	0.115	0.890	5.750	0.931	1.206	0.115	0.890	5.000	0.931	1.206	0.115	0.890	5.977
G2-MonoDepth‡	0.876	1.346	0.129	0.848	6.250	0.885	1.318	0.130	0.857	6.000	0.794	1.129	0.109	0.891	4.864
OMNI-DC	0.717	0.973	0.097	0.914	3.000	0.765	1.080	0.101	0.902	3.500	0.714	0.946	0.095	0.915	2.795
PriorDA	0.688	0.890	0.094	0.920	2.000	0.730	0.979	0.099	0.912	2.000	0.698	0.908	0.095	0.919	3.295
SPNet‡	0.754	1.453	0.106	0.909	4.500	0.743	1.321	0.102	0.910	4.000	0.733	1.243	0.100	0.914	3.932
PromptDA	0.871	1.454	0.106	0.899	5.250	0.963	1.576	0.119	0.865	6.500	0.824	1.422	0.100	0.911	5.591
LDCM (ours)	**0.444**	**0.615**	**0.046**	**0.993**	**1.000**	**0.454**	**0.644**	**0.047**	**0.990**	**1.000**	**0.427**	**0.580**	**0.044**	**0.995**	**1.000**

Table 24: **Quantitative comparison of affine-invariant point map estimation with baseline methods on the KITTI dataset Geiger et al. (2012); Uhrig et al. (2017).** The best and the second-best results are highlighted.

Method	Lidar-64-Lines			Lidar-32-Lines			Lidar-16-Lines			Lidar-8-Lines		
	$REL^p \downarrow$	$\delta_1^p \uparrow$	Rk.↓	$REL^p \downarrow$	$\delta_1^p \uparrow$	Rk.↓	$REL^p \downarrow$	$\delta_1^p \uparrow$	Rk.↓	$REL^p \downarrow$	$\delta_1^p \uparrow$	Rk.↓
VGGT	0.147	0.823	5.000	0.147	0.823	4.500	0.147	0.823	4.500	0.147	0.823	4.500
MoGe V2	0.056	0.968	2.000	0.056	0.968	2.000	0.056	0.968	2.000	0.056	0.968	2.000
WorldMirror	0.095	0.920	3.000	0.103	0.900	3.000	0.118	0.865	3.000	0.129	0.838	3.500
MapAnything	0.362	0.347	6.000	0.364	0.345	6.000	0.364	0.346	6.000	0.366	0.345	6.000
Pow3R	0.140	0.886	4.000	0.147	0.870	4.000	0.151	0.858	4.500	0.153	0.848	4.000
LDCM	**0.031**	**0.993**	**1.000**	**0.033**	**0.991**	**1.000**	**0.034**	**0.989**	**1.000**	**0.036**	**0.987**	**1.000**
Method	Lidar-4-Lines			10%			5%			3%		
	$REL^p \downarrow$	$\delta_1^p \uparrow$	Rk.↓	$REL^p \downarrow$	$\delta_1^p \uparrow$	Rk.↓	$REL^p \downarrow$	$\delta_1^p \uparrow$	Rk.↓	$REL^p \downarrow$	$\delta_1^p \uparrow$	Rk.↓
VGGT	0.147	0.823	4.000	0.147	0.823	4.500	0.147	0.823	4.500	0.147	0.823	4.500
MoGe V2	0.056	0.968	2.000	0.056	0.968	2.000	0.056	0.968	2.000	0.056	0.968	2.000
WorldMirror	0.136	0.821	4.000	0.102	0.900	3.000	0.100	0.901	3.000	0.100	0.902	3.000
MapAnything	0.367	0.344	6.000	0.365	0.345	6.000	0.365	0.345	6.000	0.367	0.341	6.000
Pow3R	0.154	0.844	4.000	0.154	0.847	4.500	0.155	0.843	4.500	0.155	0.841	4.500
LDCM	**0.043**	**0.976**	**1.000**	**0.034**	**0.990**	**1.000**	**0.035**	**0.989**	**1.000**	**0.036**	**0.987**	**1.000**
Method	1%			SIFT			ORB			Average		
	$REL^p \downarrow$	$\delta_1^p \uparrow$	Rk.↓	$REL^p \downarrow$	$\delta_1^p \uparrow$	Rk.↓	$REL^p \downarrow$	$\delta_1^p \uparrow$	Rk.↓	$REL^p \downarrow$	$\delta_1^p \uparrow$	Rk.↓
VGGT	0.147	0.823	4.500	0.147	0.823	4.500	0.147	0.823	4.500	0.147	0.823	4.500
MoGe V2	0.056	0.968	2.000	0.056	0.968	1.500	0.056	0.968	1.500	0.056	0.968	1.909
WorldMirror	0.100	0.902	3.000	0.100	0.902	3.000	0.102	0.897	3.000	0.108	0.886	3.136
MapAnything	0.370	0.338	6.000	0.367	0.344	6.000	0.367	0.343	6.000	0.366	0.344	6.000
Pow3R	0.155	0.839	4.500	0.155	0.839	4.500	0.155	0.840	4.500	0.152	0.850	4.318
LDCM	**0.040**	**0.983**	**1.000**	**0.054**	**0.961**	**1.500**	**0.051**	**0.963**	**1.500**	**0.039**	**0.983**	**1.091**

Table 25: **Quantitative comparison of affine-invariant point map estimation with baseline methods on the indoor scenes of the DIODE dataset Vasiljevic et al. (2019).** The best and the second-best results are highlighted.

Method	10% Noise			5%			3%			1%		
	$REL^p \downarrow$	$\delta_1^p \uparrow$	Rk.↓	$REL^p \downarrow$	$\delta_1^p \uparrow$	Rk.↓	$REL^p \downarrow$	$\delta_1^p \uparrow$	Rk.↓	$REL^p \downarrow$	$\delta_1^p \uparrow$	Rk.↓
VGGT	0.107	0.926	5.000	0.107	0.926	5.000	0.107	0.926	5.000	0.107	0.926	4.500
MoGe V2	0.052	0.972	2.000	0.052	0.972	2.000	0.052	0.972	2.000	0.052	0.972	2.000
WorldMirror	0.079	0.951	3.500	0.072	0.952	3.500	0.070	0.953	3.000	0.071	0.953	3.000
MapAnything	0.169	0.762	6.000	0.168	0.762	6.000	0.168	0.762	6.000	0.169	0.763	6.000
Pow3R	0.099	0.960	3.500	0.104	0.954	3.500	0.106	0.951	4.000	0.108	0.946	4.500
LDCM	**0.009**	**1.000**	**1.000**	**0.009**	**1.000**	**1.000**	**0.009**	**1.000**	**1.000**	**0.009**	**0.999**	**1.000**
Method	500			100			SIFT			ORB		
	$REL^p \downarrow$	$\delta_1^p \uparrow$	Rk.↓	$REL^p \downarrow$	$\delta_1^p \uparrow$	Rk.↓	$REL^p \downarrow$	$\delta_1^p \uparrow$	Rk.↓	$REL^p \downarrow$	$\delta_1^p \uparrow$	Rk.↓
VGGT	0.107	0.926	4.500	0.107	0.926	4.500	0.107	0.926	4.500	0.107	0.926	4.500
MoGe V2	0.052	0.972	2.000	0.052	0.972	2.000	0.052	0.972	2.000	0.052	0.972	1.500
WorldMirror	0.072	0.955	3.000	0.073	0.955	3.000	0.073	0.956	3.000	0.078	0.945	3.000
MapAnything	0.175	0.753	6.000	0.173	0.758	6.000	0.176	0.753	6.000	0.175	0.758	6.000
Pow3R	0.110	0.944	4.500	0.110	0.943	4.500	0.109	0.944	4.500	0.109	0.944	4.500
LDCM	**0.010**	**0.999**	**1.000**	**0.012**	**0.996**	**1.000**	**0.029**	**0.979**	**1.000**	**0.036**	**0.972**	**1.000**
Method	Virtual-Lidar-32-Lines			Virtual-Lidar-16-Lines			Virtual-Lidar-8-Lines			Average		
	$REL^p \downarrow$	$\delta_1^p \uparrow$	Rk.↓	$REL^p \downarrow$	$\delta_1^p \uparrow$	Rk.↓	$REL^p \downarrow$	$\delta_1^p \uparrow$	Rk.↓	$REL^p \downarrow$	$\delta_1^p \uparrow$	Rk.↓
VGGT	0.107	0.926	4.500	0.107	0.926	4.500	0.107	0.926	4.500	0.107	0.926	4.636
MoGe V2	0.052	0.972	2.000	0.052	0.972	2.000	0.052	0.972	2.000	0.052	0.972	1.955
WorldMirror	0.072	0.955	3.000	0.072	0.955	3.000	0.073	0.955	3.000	0.073	0.953	3.091
MapAnything	0.175	0.753	6.000	0.173	0.758	6.000	0.173	0.759	6.000	0.172	0.758	6.000
Pow3R	0.109	0.945	4.500	0.109	0.943	4.500	0.110	0.944	4.500	0.108	0.947	4.273
LDCM	**0.010**	**0.999**	**1.000**	**0.010**	**0.999**	**1.000**	**0.011**	**0.997**	**1.000**	**0.014**	**0.995**	**1.000**

Table 26: **Quantitative comparison of affine-invariant point map estimation with baseline methods on the outdoor scenes of the DIODE dataset Vasiljevic et al. (2019).** The best and the second-best results are highlighted.

Method	Virtual-Lidar-64-Lines			Virtual-Lidar-32-Lines			Virtual-Lidar-16-Lines			Virtual-Lidar-8-Lines		
	$\mathrm{REL}^p \downarrow$	$\delta_1^p \uparrow$	Rk.↓	$\mathrm{REL}^p \downarrow$	$\delta_1^p \uparrow$	Rk.↓	$\mathrm{REL}^p \downarrow$	$\delta_1^p \uparrow$	Rk.↓	$\mathrm{REL}^p \downarrow$	$\delta_1^p \uparrow$	Rk.↓
VGGT	0.215	0.700	5.000	0.215	0.700	5.000	0.215	0.700	5.000	0.215	0.700	5.000
MoGe V2	0.124	0.841	2.000	0.124	0.841	2.000	0.124	0.841	2.000	0.124	0.841	2.000
WorldMirror	0.156	0.786	3.000	0.156	0.788	3.000	0.154	0.792	3.000	0.155	0.792	3.000
MapAnything	0.299	0.506	6.000	0.310	0.481	6.000	0.309	0.489	6.000	0.317	0.487	6.000
Pow3R	0.200	0.745	4.000	0.200	0.747	4.000	0.201	0.743	4.000	0.201	0.745	4.000
LDCM	**0.072**	**0.965**	**1.000**	**0.079**	**0.950**	**1.000**	**0.090**	**0.920**	**1.000**	**0.097**	**0.903**	**1.000**

Method	Virtual-Lidar-4-Lines			10% Noise			5%			3%		
	$\mathrm{REL}^p \downarrow$	$\delta_1^p \uparrow$	Rk.↓	$\mathrm{REL}^p \downarrow$	$\delta_1^p \uparrow$	Rk.↓	$\mathrm{REL}^p \downarrow$	$\delta_1^p \uparrow$	Rk.↓	$\mathrm{REL}^p \downarrow$	$\delta_1^p \uparrow$	Rk.↓
VGGT	0.215	0.700	5.000	0.215	0.700	5.000	0.215	0.700	5.000	0.215	0.700	5.000
MoGe V2	0.124	0.841	2.000	0.124	0.841	2.000	0.124	0.841	2.000	0.124	0.841	2.000
WorldMirror	0.154	0.793	3.000	0.140	0.822	3.000	0.151	0.799	3.000	0.157	0.782	3.000
MapAnything	0.311	0.500	6.000	0.296	0.500	6.000	0.291	0.510	6.000	0.291	0.517	6.000
Pow3R	0.201	0.745	4.000	0.181	0.770	4.000	0.190	0.756	4.000	0.194	0.752	4.000
LDCM	**0.117**	**0.856**	**1.000**	**0.059**	**0.988**	**1.000**	**0.061**	**0.985**	**1.000**	**0.063**	**0.981**	**1.000**

Method	1%			SIFT			ORB			Average		
	$\mathrm{REL}^p \downarrow$	$\delta_1^p \uparrow$	Rk.↓	$\mathrm{REL}^p \downarrow$	$\delta_1^p \uparrow$	Rk.↓	$\mathrm{REL}^p \downarrow$	$\delta_1^p \uparrow$	Rk.↓	$\mathrm{REL}^p \downarrow$	$\delta_1^p \uparrow$	Rk.↓
VGGT	0.215	0.700	5.000	0.215	0.700	5.000	0.215	0.700	5.000	0.215	0.700	5.000
MoGe V2	0.124	0.841	2.000	0.124	0.841	2.000	0.124	0.841	2.000	0.124	0.841	2.000
WorldMirror	0.158	0.781	3.000	0.157	0.784	3.000	0.170	0.750	3.500	0.155	0.788	3.045
MapAnything	0.293	0.515	6.000	0.301	0.505	6.000	0.302	0.505	6.000	0.302	0.501	6.000
Pow3R	0.199	0.747	4.000	0.200	0.748	4.000	0.197	0.751	3.500	0.197	0.750	3.955
LDCM	**0.068**	**0.971**	**1.000**	**0.071**	**0.966**	**1.000**	**0.073**	**0.957**	**1.000**	**0.077**	**0.949**	**1.000**

Table 27: **Quantitative comparison of affine-invariant point map estimation with baseline methods on the iBims dataset Koch et al. (2018).** The best and the second-best results are highlighted.

Method	10% Noise			5%			3%			1%		
	$\mathrm{REL}^p \downarrow$	$\delta_1^p \uparrow$	Rk.↓	$\mathrm{REL}^p \downarrow$	$\delta_1^p \uparrow$	Rk.↓	$\mathrm{REL}^p \downarrow$	$\delta_1^p \uparrow$	Rk.↓	$\mathrm{REL}^p \downarrow$	$\delta_1^p \uparrow$	Rk.↓
VGGT	0.048	0.967	4.000	0.048	0.967	4.000	0.048	0.967	3.500	0.048	0.967	3.500
MoGe V2	0.046	0.972	2.500	0.046	0.972	2.500	0.046	0.972	2.500	0.046	0.972	2.500
WorldMirror	0.044	0.972	2.000	0.043	0.968	2.500	0.043	0.965	3.000	0.042	0.963	3.500
MapAnything	0.233	0.612	6.000	0.231	0.616	6.000	0.231	0.614	6.000	0.230	0.618	6.000
Pow3R	0.077	0.952	5.000	0.068	0.962	5.000	0.064	0.965	4.500	0.061	0.967	4.000
LDCM	**0.013**	**0.996**	**1.000**	**0.013**	**0.995**	**1.000**	**0.014**	**0.995**	**1.000**	**0.015**	**0.994**	**1.000**

Method	500			100			SIFT			ORB		
	$\mathrm{REL}^p \downarrow$	$\delta_1^p \uparrow$	Rk.↓	$\mathrm{REL}^p \downarrow$	$\delta_1^p \uparrow$	Rk.↓	$\mathrm{REL}^p \downarrow$	$\delta_1^p \uparrow$	Rk.↓	$\mathrm{REL}^p \downarrow$	$\delta_1^p \uparrow$	Rk.↓
VGGT	0.048	0.967	4.500	0.048	0.967	4.500	0.048	0.967	4.000	0.048	0.967	3.000
MoGe V2	0.046	0.972	2.500	0.046	0.972	2.500	0.046	0.972	2.500	0.046	0.972	2.000
WorldMirror	0.042	0.968	2.500	0.042	0.968	2.500	0.042	0.967	3.000	0.060	0.946	4.500
MapAnything	0.235	0.597	6.000	0.234	0.602	6.000	0.232	0.614	6.000	0.234	0.613	6.000
Pow3R	0.061	0.968	4.000	0.061	0.968	4.000	0.062	0.968	4.000	0.062	0.967	4.000
LDCM	**0.018**	**0.991**	**1.000**	**0.022**	**0.987**	**1.000**	**0.020**	**0.990**	**1.000**	**0.024**	**0.989**	**1.000**

Method	Virtual-Lidar-32-Lines			Virtual-Lidar-16-Lines			Virtual-Lidar-8-Lines			Average		
	$\mathrm{REL}^p \downarrow$	$\delta_1^p \uparrow$	Rk.↓	$\mathrm{REL}^p \downarrow$	$\delta_1^p \uparrow$	Rk.↓	$\mathrm{REL}^p \downarrow$	$\delta_1^p \uparrow$	Rk.↓	$\mathrm{REL}^p \downarrow$	$\delta_1^p \uparrow$	Rk.↓
VGGT	0.048	0.967	3.500	0.048	0.967	4.000	0.048	0.967	4.500	0.048	0.967	3.909
MoGe V2	0.046	0.972	2.500	0.046	0.972	2.500	0.046	0.972	2.500	0.046	0.972	2.455
WorldMirror	0.042	0.967	2.500	0.042	0.967	3.000	0.042	0.968	2.500	0.044	0.965	2.864
MapAnything	0.233	0.610	6.000	0.233	0.609	6.000	0.232	0.613	6.000	0.233	0.611	6.000
Pow3R	0.062	0.966	5.000	0.061	0.968	4.000	0.061	0.968	4.000	0.064	0.965	4.318
LDCM	**0.015**	**0.993**	**1.000**	**0.017**	**0.991**	**1.000**	**0.020**	**0.990**	**1.000**	**0.017**	**0.992**	**1.000**

Table 28: **Quantitative comparison of affine-invariant point map estimation with baseline methods on the indoor scenes of the ETH3D dataset Schops et al. (2017).** The best and the second-best results are highlighted.

Method	10% Noise			5%			3%			1%		
	REL$^p \downarrow$	$\delta_1^p \uparrow$	Rk.$\downarrow$	REL$^p \downarrow$	$\delta_1^p \uparrow$	Rk.$\downarrow$	REL$^p \downarrow$	$\delta_1^p \uparrow$	Rk.$\downarrow$	REL$^p \downarrow$	$\delta_1^p \uparrow$	Rk.$\downarrow$
VGGT	0.045	0.988	2.000	0.045	0.988	3.500	0.045	0.988	3.500	0.045	0.988	3.500
MoGe V2	0.041	0.986	2.500	0.041	0.986	3.000	0.041	0.986	3.500	0.041	0.986	3.000
WorldMirror	0.048	0.986	4.000	0.042	0.989	2.500	0.040	0.990	1.500	0.041	0.992	1.500
MapAnything	0.255	0.559	6.000	0.252	0.562	6.000	0.252	0.562	6.000	0.254	0.560	6.000
Pow3R	0.070	0.987	4.000	0.068	0.990	3.500	0.069	0.990	3.500	0.070	0.990	4.000
LDCM	**0.047**	**0.994**	**2.000**	**0.047**	**0.994**	**2.500**	**0.047**	**0.994**	**2.500**	**0.047**	**0.994**	**2.500**

Method	500			100			SIFT			ORB		
	REL$^p \downarrow$	$\delta_1^p \uparrow$	Rk.$\downarrow$	REL$^p \downarrow$	$\delta_1^p \uparrow$	Rk.$\downarrow$	REL$^p \downarrow$	$\delta_1^p \uparrow$	Rk.$\downarrow$	REL$^p \downarrow$	$\delta_1^p \uparrow$	Rk.$\downarrow$
VGGT	0.045	0.988	3.000	0.045	0.988	3.000	0.045	0.988	3.000	0.045	0.988	2.500
MoGe V2	0.041	0.986	3.000	0.041	0.986	3.000	0.041	0.986	3.000	0.041	0.986	2.500
WorldMirror	0.043	0.991	2.000	0.043	0.990	2.000	0.043	0.990	2.000	0.048	0.980	4.000
MapAnything	0.261	0.545	6.000	0.259	0.549	6.000	0.258	0.549	6.000	0.257	0.554	6.000
Pow3R	0.073	0.988	4.000	0.073	0.988	4.000	0.073	0.988	4.000	0.073	0.989	3.500
LDCM	**0.047**	**0.993**	**2.500**	**0.048**	**0.992**	**2.500**	**0.049**	**0.993**	**2.500**	**0.050**	**0.992**	**2.500**

Method	Virtual-Lidar-32-Lines			Virtual-Lidar-16-Lines			Virtual-Lidar-8-Lines			Average		
	REL$^p \downarrow$	$\delta_1^p \uparrow$	Rk.$\downarrow$	REL$^p \downarrow$	$\delta_1^p \uparrow$	Rk.$\downarrow$	REL$^p \downarrow$	$\delta_1^p \uparrow$	Rk.$\downarrow$	REL$^p \downarrow$	$\delta_1^p \uparrow$	Rk.$\downarrow$
VGGT	0.045	0.988	3.500	0.045	0.988	3.000	0.045	0.988	3.500	0.045	0.988	3.091
MoGe V2	0.041	0.986	3.000	0.041	0.986	3.000	0.041	0.986	3.000	0.041	0.986	2.955
WorldMirror	0.041	0.991	1.500	0.042	0.991	2.000	0.043	0.990	2.000	0.043	0.989	2.273
MapAnything	0.259	0.551	6.000	0.257	0.554	6.000	0.256	0.552	6.000	0.256	0.554	6.000
Pow3R	0.071	0.989	4.000	0.072	0.988	4.000	0.073	0.989	4.000	0.071	0.989	3.864
LDCM	**0.047**	**0.994**	**2.500**	**0.047**	**0.993**	**2.500**	**0.048**	**0.992**	**2.500**	**0.048**	**0.993**	**2.455**

Table 29: **Quantitative comparison of affine-invariant point map estimation with baseline methods on the outdoor scenes of the ETH3D dataset Schops et al. (2017).** The best and the second-best results are highlighted.

Method	Virtual-Lidar-64-Lines			Virtual-Lidar-32-Lines			Virtual-Lidar-16-Lines			Virtual-Lidar-8-Lines		
	REL$^p \downarrow$	$\delta_1^p \uparrow$	Rk.$\downarrow$	REL$^p \downarrow$	$\delta_1^p \uparrow$	Rk.$\downarrow$	REL$^p \downarrow$	$\delta_1^p \uparrow$	Rk.$\downarrow$	REL$^p \downarrow$	$\delta_1^p \uparrow$	Rk.$\downarrow$
VGGT	0.061	0.967	4.500	0.061	0.967	4.500	0.061	0.967	4.500	0.061	0.967	4.500
MoGe V2	0.046	0.974	2.500	0.046	0.974	2.500	0.046	0.974	2.500	0.046	0.974	2.500
WorldMirror	0.048	0.970	3.500	0.048	0.969	3.500	0.048	0.971	3.500	0.050	0.969	3.500
MapAnything	0.273	0.542	6.000	0.277	0.535	6.000	0.276	0.540	6.000	0.275	0.543	6.000
Pow3R	0.076	0.977	3.500	0.075	0.978	3.500	0.075	0.978	3.500	0.075	0.980	3.500
LDCM	**0.027**	**0.997**	**1.000**	**0.028**	**0.997**	**1.000**	**0.029**	**0.996**	**1.000**	**0.032**	**0.993**	**1.000**

Method	Virtual-Lidar-4-Lines			10% Noise			5%			3%		
	REL$^p \downarrow$	$\delta_1^p \uparrow$	Rk.$\downarrow$	REL$^p \downarrow$	$\delta_1^p \uparrow$	Rk.$\downarrow$	REL$^p \downarrow$	$\delta_1^p \uparrow$	Rk.$\downarrow$	REL$^p \downarrow$	$\delta_1^p \uparrow$	Rk.$\downarrow$
VGGT	0.061	0.967	4.500	0.061	0.967	3.500	0.061	0.967	3.500	0.061	0.967	3.500
MoGe V2	0.046	0.974	2.500	0.046	0.974	2.000	0.046	0.974	2.000	0.046	0.974	2.000
WorldMirror	0.048	0.973	3.500	0.058	0.961	3.500	0.061	0.953	4.000	0.063	0.951	4.500
MapAnything	0.276	0.546	6.000	0.271	0.545	6.000	0.268	0.549	6.000	0.268	0.553	6.000
Pow3R	0.075	0.980	3.500	0.082	0.960	5.000	0.079	0.969	4.000	0.078	0.972	4.000
LDCM	**0.040**	**0.985**	**1.000**	**0.026**	**0.998**	**1.000**	**0.027**	**0.998**	**1.000**	**0.027**	**0.998**	**1.000**

Method	1%			SIFT			ORB			Average		
	REL$^p \downarrow$	$\delta_1^p \uparrow$	Rk.$\downarrow$	REL$^p \downarrow$	$\delta_1^p \uparrow$	Rk.$\downarrow$	REL$^p \downarrow$	$\delta_1^p \uparrow$	Rk.$\downarrow$	REL$^p \downarrow$	$\delta_1^p \uparrow$	Rk.$\downarrow$
VGGT	0.061	0.967	4.000	0.061	0.967	4.500	0.061	0.967	3.500	0.061	0.967	4.091
MoGe V2	0.046	0.974	2.500	0.046	0.974	2.500	0.046	0.974	2.000	0.046	0.974	2.318
WorldMirror	0.054	0.961	4.000	0.050	0.969	3.500	0.077	0.931	4.500	0.055	0.962	3.773
MapAnything	0.271	0.548	6.000	0.276	0.543	6.000	0.275	0.545	6.000	0.273	0.544	6.000
Pow3R	0.076	0.975	3.500	0.076	0.977	3.500	0.077	0.973	3.500	0.077	0.974	3.727
LDCM	**0.027**	**0.997**	**1.000**	**0.031**	**0.994**	**1.000**	**0.030**	**0.994**	**1.000**	**0.029**	**0.995**	**1.000**